

Using mass spectrometry-based proteomics to improve the understanding of multiple sclerosis treatments

Ragnhild Reehorst Lereim

Thesis for the degree of Philosophiae Doctor (PhD)
University of Bergen, Norway
2021

UNIVERSITY OF BERGEN



Using mass spectrometry-based proteomics to improve the understanding of multiple sclerosis treatments

Ragnhild Reehorst Lereim



Thesis for the degree of Philosophiae Doctor (PhD)
at the University of Bergen

Date of defense: 23.06.2021

© Copyright Ragnhild Reehorst Lereim

The material in this publication is covered by the provisions of the Copyright Act.

Year: 2021

Title: Using mass spectrometry-based proteomics to improve the understanding of multiple sclerosis treatments

Name: Ragnhild Reehorst Lereim

Print: Skipnes Kommunikasjon / University of Bergen

Scientific environment

The candidate has been affiliated to the Department of Biomedicine at the University of Bergen, Norway. The work presented in this thesis was performed at the Proteomics Unit at the University of Bergen (PROBE). The main supervisor of the work was Assoc. Prof. Dr. Harald Barsnes, with Prof. Dr. Frode S. Berven, Dr. Astrid Guldbrandsen and Dr. Eystein Oveland as co-supervisors.

The work is part of the Multiple Sclerosis Project in collaboration with the Multiple Sclerosis Competence Centre at Haukeland University Hospital. The Multiple Sclerosis Project was funded by the Kristian Gerhard Jebsen Foundation.

The PhD fellowship was granted by the University of Bergen.

Acknowledgements

First of all, I would like to express my deepest gratitude to my main supervisor Dr. Harald Barsnes. You have been a source of great scientific insights these years, and have lead me through the work in this thesis. Thank you for including me on your team, and for always finding the time to discuss science – your dedication is a great source of inspiration to me. Thank you to my co-supervisors Prof. Frode Berven, Dr. Astrid Guldbrandsen and Dr. Eystein Oveland. Frode, you have an overview of the field that is impressive, and I am truly inspired by your ability to always consider the glass half-full. Astrid, thank you for your help in planning experiments and in the writing process, you have really guided me through this PhD both scientifically and otherwise. Finally, Eystein, your standard operation procedures provide firm footing in a field that can be overwhelming at times. Thank you all for your input and support during this time.

I would also like to thank the Multiple Sclerosis Competence Centre, in particular Prof. MD Kjell-Morten Myhr, Dr. MD Øyvind Torkildsen, Dr. MD Stig Wergeland and Dr. Agnes Elisabeth Nystad for your help in manuscript writing and biological interpretation. This work has greatly benefitted from your excellent input! Furthermore, thanks to all the others at the Multiple Sclerosis Competence Centre for interesting seminars and discussions.

Thanks to all the people at the Proteomics Unit (PROBE) past and present, for a great scientific and social environment. Thanks to Olav Mjaavatten for your help with mass spectrometry analysis, lab-work, guidance and patience – I have learned so much from you these years. Thanks to Bram for many discussions about statistics and help with programming, as well as interesting talks by the coffee machine. Thanks to Yehia and Carlos for the many smiles we have shared. Furthermore, thanks to Even Birkeland for help with mass spectrometry analysis and inspiring discussions. Thanks to Anne, Rebecca, Maria and Frode S for scientific input and great seminars. Thanks to Mari, for your patience and excellence! And Elise, thank you for the scientific input, your great sense of humour, and for providing a break in stressful times. I have looked forward to going to work during these years thanks to all of you.

Thanks to the “master group”, namely Ronja, Line, Anne and Silje. Having friends that can understand the ups and downs that comes with this line of work is invaluable, but in honesty, I have valued not talking about work with you the most.

Finally, I would like to thank my friends and family who have supported me during these years. Thanks to Tina, Thea and Lene – I hope we will see more of each other in the future, but I have valued greatly that we have kept in touch even though we seldomly are in the same place. Thanks to my mom and dad that have always encouraged creativity and curiosity. Thanks to my sister Margrete, for your interest in my work and extensive support. And Ingeborg and Sigurd, you always make me smile, and allow me to return to childhood no matter how old I am.

And to Daniel, thank you for all your support and understanding, it is invaluable and beyond words. Last, but definitely not least (but definitely smallest), Håvard, you add meaning to this work.

Oslo, April 2021,

Ragnhild Reehorst Lereim

Table of contents

SCIENTIFIC ENVIRONMENT	3
ACKNOWLEDGEMENTS.....	4
TABLE OF CONTENTS	6
ABBREVIATIONS	9
ABSTRACT	11
LIST OF PUBLICATIONS	12
1. INTRODUCTION	13
1.1 MULTIPLE SCLEROSIS	13
1.1.1 <i>Epidemiology and etiology of multiple sclerosis</i>	13
1.1.2 <i>Disease development and diagnosis</i>	14
1.1.3 <i>Disease categories</i>	15
1.1.4 <i>Treatment options</i>	15
1.2 MULTIPLE SCLEROSIS ANIMAL MODELS	18
1.2.1 <i>Cuprizone</i>	18
1.3 PROTEINS.....	19
1.3.1 <i>Proteins and proteomes</i>	19
1.4 CEREBROSPINAL FLUID	20
1.4.1 <i>Biology</i>	20
1.4.2 <i>Cerebrospinal fluid proteins</i>	21
1.5 BIOMARKERS	21
1.5.1 <i>Biomarker discovery, verification and validation</i>	22
1.5.2 <i>Sample material and biomarker discovery</i>	22
1.5.3 <i>Cerebrospinal fluid biomarkers in multiple sclerosis</i>	23
1.5.4 <i>Proteomic studies of the cuprizone animal model</i>	25
1.5.5 <i>Natalizumab monitoring treatment biomarkers from proteomics</i>	25
1.6 MASS SPECTROMETRY-BASED PROTEOMICS	26
1.6.1 <i>Liquid chromatography</i>	27
1.6.2 <i>Mass spectrometry</i>	28
1.6.3 <i>Quantitative proteomics</i>	32
1.6.4 <i>Sample preparation</i>	38
1.7 IMMUNOHISTOCHEMISTRY	42
1.8 BIOINFORMATICS IN QUANTITATIVE PROTEOMICS	43
1.8.1 <i>Identification and quantification</i>	43
1.8.2 <i>Functional analysis and data visualization</i>	45

1.8.3	Databases for protein biomarkers	47
2.	AIMS OF THE STUDY	49
3.	SUMMARY OF PAPERS	50
4.	METHODOLOGICAL CONSIDERATIONS	52
4.1	BRAIN AREA SELECTION	52
4.2	PATIENT SELECTION	52
4.2.1	Removal of outliers	53
4.2.2	Pooling of samples	54
4.3	QUANTITATIVE PROTEOMICS	55
4.3.1	Reproducibility	55
4.3.2	Tandem mass tag	55
4.3.3	Sample fractionation	57
4.3.4	Selecting a label-free discovery approach	57
4.3.5	Technical variation in label-free discovery	57
4.3.6	Individual differences in treatment response	58
4.4	PRM ASSAY BUILDING	59
4.4.1	PRM versus ELISA	59
4.4.2	PRM method	59
4.4.3	Choice of internal standards	60
4.4.4	Peptide tests and cut-offs for PRM-assays	60
4.4.5	Linear area, LOD and LOQ	61
4.4.6	CSF-PR in determining disease-relevance	62
5.	DISCUSSION	64
5.1	MONITORING DISEASE PROCESSES IN MULTIPLE SCLEROSIS	64
5.1.1	Effects of Fingolimod on remyelination	64
5.1.2	Effects of Natalizumab on inflammation, neurological processes and metabolism	65
5.1.3	Monitoring multiple sclerosis by mass spectrometry-based proteomics	66
5.1.4	Protein changes across neurological diseases	67
5.2	VERIFICATION STRATEGY	68
5.2.1	Database dependencies for biomarker selection	68
5.2.2	A rectangular biomarker verification strategy	68
5.2.3	Quantification of low-abundant biomarkers	69
5.3	SIGNAL OR NOISE	70
5.3.1	Technical vs biological variation	70
5.3.2	Absolute relative quantification	72
6.	CONCLUSION	74

7. FUTURE PERSPECTIVES.....75

REFERENCES.....76

Abbreviations

AD	Alzheimer's disease
ALS	Amyotrophic lateral sclerosis
AUC	Area under the curve
CDMS	Clinical definite Multiple sclerosis
CHI3L1	Chitinase 3-like protein 1
CHI3L2	Chitinase 3-like protein 2
CHIT	Chitotriosidase
CID	Collision induced dissociation
CIS	Clinically isolated symptom
CJD	Creutzfeldt-Jacob disease
CNS	Central nervous system
CSF	Cerebrospinal fluid
CV	Coefficient of variation
DDA	Data-dependent acquisition
DIA	Data-independent acquisition
EAE	Experimental autoimmune encephalomyelitis
ELISA	Enzyme-linked immunosorbent assay
ESI	Electrospray ionization
ETD	Electron-transfer dissociation
GFAP	Glial fibrillary acidic protein
GO	Gene Ontology
HCD	Higher-energy collision induced dissociation
HPLC	High-performance liquid chromatography
HPP	Human proteome project
HSCT	autologous hematopoietic stem cell transplantation
IGHM	Immunoglobulin heavy constant mu
IHC	Immunohistochemistry
iTraq	Isobaric tag for relative and absolute quantitation
JCV	John Cunningham virus
K	Lysine (amino acid)
LC	Liquid chromatography
LFB	Luxol fast blue
LOD	Level of detection
LOQ	Level of quantification
m/z	Mass-to-charge ratio
MAG	Myelin-associated glycoprotein
MALDI	Matrix assisted laser desorption ionization
MM	Mixed mode (chromatography)
MOBP	Myelin-associated oligodendrocyte basic protein
MRI	Magnetic resonance imaging
MRM	Multiple reaction monitoring
MS	Mass spectrometry
MS/MS	Tandem mass spectrometry
MS1	Mass spectrometry scan (prior to peptide fragmentation)
MS2	Tandem mass spectrometry scan (following peptide fragmentation)

MScI	Multiple sclerosis
NF-H	Neurofilament heavy
NF-L	Neurofilament light
OCBs	Oligoclonal bands
OND	Other neurological disorders
PD	Parkinson's disease
PLP	Proteolipid protein
PML	Progressive multifocal leukoencephalopathy
PMS	Progressive multiple sclerosis
PPMS	Primary progressive multiple sclerosis
PRM	Parallel reaction monitoring
PSM	Peptide-spectrum match
R	Arginine (amino acid) OR Programming language
RRMS	Relapsing-remitting multiple sclerosis
S1PR	Sphingosine-1-phosphate receptors
SCX	Strong cation exchange
SIL	Stable isotope Labeling
SILAC	Stable Isotope Labeling by/with Amino acids in Cell culture
SIM	Selected ion monitoring
SPMS	Secondary progressive multiple sclerosis
SRM	Single reaction monitoring
SWATH	Sequential Window Acquisition of all Theoretical Mass Spectra
TMT	Tandem mass tag
TOF	Time-of-flight
ULQ	Upper level of quantification
XIC	Extracted ion chromatogram

Abstract

In this work, the effects of multiple sclerosis (MScl) treatments were investigated by quantitative proteomics. First, the effects of the anti-inflammatory drug Fingolimod was studied to see if the drug affected central nervous system (CNS) repair in a non-inflammatory MScl mouse model. Next, the cerebrospinal fluid (CSF) proteome was investigated to learn more about the treatment response and mechanism of action in the CNS of MScl patients treated with the anti-inflammatory drug Natalizumab.

Proteomic analysis identified over 6000 proteins in the frontal right hemisphere of the mouse model. Abundance changes of these proteins were measured during de- and remyelination and confirmed the global proteome effects of the disease model known from previous studies. The analysis showed no benefit of Fingolimod on myelination, which was also supported by histological analyses of brain sections in the corpus callosum. However, the proteomic approach did detect a novel reduction in one of the drug receptors known to be expressed in several cells in the brain.

CSF samples from MScl patients in Czech cohort with a relapsing-remitting (RRMS) disease course was sampled at the beginning of, and after approximately two years of treatment. Proteomic changes during treatment were then related to disease processes in RRMS by comparison to online datasets in CSF-PR. The findings confirmed the known anti-inflammatory effect of Natalizumab, but also revealed previously unknown effects of the treatment on neurological proteins and metabolism.

Finally, targeted proteomics assays were created based on biomarker candidates from existing literature, with the long-term goal of defining a biomarker panel for clinical use. Proteins linked to known disease processes were selected based on, *e.g.*, peptide uniqueness, inter- and intra-day stability and optimal digestion time, in order to design robust assays that can be compared over time.

List of publications

Nystad AE, **Lereim RR**, Wergeland S, Oveland E, Myhr KM, Bø L, Torkildsen Ø: Fingolimod downregulates brain sphingosine-1-phosphate receptor 1 levels but does not promote remyelination or neuroprotection in the cuprizone model. *J Neuroimmunol.* 2020 Feb 15;339:577091.

Guldbrandsen A, **Lereim RR**, Jacobsen M, Garberg H, Kroksveen AC, Barsnes H, Berven FS. (2020): Development of robust targeted proteomics assays for cerebrospinal fluid biomarkers in multiple sclerosis, *Clin Proteomics.* 2020 Sep 18;17:33.

Lereim RR, Nytrova P, Myhr KM, Barsnes H, Berven FS: Evidence from cerebrospinal fluid proteomics suggests that natalizumab promote anti-inflammatory and repair effects in multiple sclerosis. Unpublished work in manuscript form.

1. Introduction

1.1 Multiple sclerosis

Multiple sclerosis (MScl) is a chronic disease of the central nervous system (CNS) that causes neurological disability in young adults ¹. It was first illustrated by the Scottish pathologist Robert Carswell in 1838 ², and further characterized and defined by the French neurologist Jean-Martin Charcot in 1886 ³. The disease generally refers to the multiple scars or plaques visible in the brains and spinal cord of those affected by the disease. It does not have a single underlying cause, but is rather a result of both genetic and environmental factors ¹, and although much research has been conducted since the discovery of MScl, there is still uncertainty about many aspects of the disease.

1.1.1 Epidemiology and etiology of multiple sclerosis

MScl is the most common disabling disease to affect young adults besides trauma. The disease affects women more frequently than men, and the disease prevalence increases with increasing distance from the equator ¹. Globally, the estimated number of people with MScl is 2.3 million, with the highest prevalence in Europe and North America ⁴. Norway has a prevalence of 203 per 100 000 inhabitants, one of the highest reported worldwide ⁵. The average disease duration is 30 years, during which MScl patients have an increased risk of developing comorbidities such as depression, anxiety, fatigue, suicide and certain autoimmune diseases, thus greatly affecting the quality of life (as reviewed in ⁶). MScl patients in Norway is expected to have their lifespan shortened by an average of seven years compared to the general population ⁷.

MScl is in part hereditary, as shown by increased occurrence of the disease within families ¹, for example, a meta-study from 2015 estimated 50% joint heritability between twins ⁸. This hereditary component is mainly due to genetic variation of immune system components such as the major histocompatibility complex ⁹ and the genes IL7R and IL2RA ¹⁰, however additional genetic variants have also been found ¹¹.

This genetic factor could explain the global distribution of MScl, although immigration in childhood from low-risk to high-risk areas also increases the disease prevalence of the immigrants to that of their new country^{12, 13}, a factor that cannot be explained by genetics alone. Some argue that this could be caused by reduced sun exposure in the high latitude areas, as low vitamin D levels has been linked to increased MScl susceptibility^{14, 15}, and furthermore the hygiene hypothesis speculate that low exposure to infections during childhood in high latitude areas might lead to unfortunate immune responses later in life and increase the risk of developing MScl^{16, 17}. Specific infections, in particular the Epstein-Barr virus infection, commonly known as mononucleosis and usually appearing in early adolescence, increases the risk of developing MScl, possibly due to molecular mimicry to myelin¹⁸. Additional MScl risk factors include obesity and smoking¹.

1.1.2 Disease development and diagnosis

MScl as drawn by Robert Carswell in 1838 illustrates the characteristic scars or plaques that can be seen in the post-mortem spinal cord and brain of MScl patients. This scarring is due to damage of myelin sheets and axons in the CNS¹. Myelin sheets function as electrical insulators that allow the nerve signal to rapidly transmit down the axon, allowing normal neurological function. Damage of the myelin sheet leads to a disturbance in nerve cell signal conduction in the area of the brain or spinal cord where it occurs, and can manifest in the patient as a variety of symptoms depending on the site of demyelination and the extent of inflammation¹. This damage is believed to be caused by the patient's own immune cells, but how this immune response is initialized is however debated^{1, 19, 20}. Myelin damage early in the disease course can manifest as an acute episode called a clinically isolated symptom (CIS). However, patients experiencing CIS do not always develop clinical definite MScl (CDMS), and the conversion rate varies between 40% to 85% in published studies²¹⁻²³. In any case, the damage in the CNS shows up as scarring or plaques in the white matter of the CNS, visible by magnetic resonance imaging (MRI). For those that do develop MScl, this scarring increases, and accumulation of damage can lead to escalation of disability and neurodegeneration over time¹.

The International Panel on Diagnosis of Multiple Sclerosis released the McDonald criteria for diagnosing MScl in 2001²⁴, later revised^{25, 26}. The criteria include a combination of MScl plaques or lesions in the CNS as seen by MRI, as well as clinical history and observations of oligoclonal bands in the cerebrospinal fluid from the patients – indicating ongoing inflammation in the CNS. There is currently no single test that can be used to diagnose MScl.

1.1.3 Disease categories

The majority of patients with CDMS have relapsing-remitting MScl (RRMS), a disease course characterized by neurological relapses, driven mainly by inflammatory activity and demyelination, and remission during which the symptoms commonly disappear either partially or fully due to the restricted ability of the CNS to self-repair. The remaining patients have a more progressive development of disability mainly due to noninflammatory mechanisms referred to as progressive MScl (PMS). In addition, there is primary progressive MScl (PPMS), which is progressive from disease onset that affects less than 10% of patients, and secondary progressive MScl (SPMS), which usually follows RRMS as the periods of remission becomes scarcer and the disability progression is continuous²⁷.

1.1.4 Treatment options

There is currently no available cure for MScl, albeit in recent years autologous hematopoietic stem cell transplantation (HSCT) has proven promise as a possible cure of the disease, where studies show suppression of disease development for 4-5 years in 70-80% of the patients²⁸. A recent study of thirty patients receiving HSCT in Norway between 2015 and 2018 reported no mortality, however other severe side effects were found, including autoimmune thyroid disease and symptoms of ovarian failure²⁹. This treatment is therefore currently only recommended for aggressive and highly active refractory RRMS, as it is still considered experimental, and more large-scale studies are needed^{28, 30}.

The first drug used in the treatment of MScl was interferon beta³¹, shown to delay the transition between CIS and CDMS³². In recent years, there has been an increase in the

number of drugs available to treat MScl (as reviewed in ^{30,33}) (**Figure 1**). The majority of the available drugs work by reducing the immunological damage to the CNS by preventing relapses and are authorized to treat RRMS. As each drug is accompanied by side effects, risk stratification of possible adverse events is important in guiding treatment decisions prior to drug administration ^{30,33}.

Modestly effective	Moderately effective	Highly effective	Experimental treatments
Teriflunomide Glatiramer acetate Interferon	Fingolimod Siponimod ¹ Ozanimod Dimethyl fumarate Diroximel fumarate ¹ Cladribine ^{1*}	Ocrelizumab ^{1,2} Ofatumumab Natalizumab Alemtuzumab* Mitoxantrone*	“Off-label” treatments Experimental treatment Autologous hematopoietic stem cell transplantation

Figure 1: Treatment options for RRMS in multiple sclerosis. ¹ Can treat SPMS, ² can treat PPMS, * seldomly used due to adverse side effects. Figure based on ^{30,33}.

Early treatment by more effective therapies such as Fingolimod, Natalizumab or Alemtuzumab decreases the risk of developing SPMS compared to, for example, interferon beta ³⁴, and thus patients are commonly treated by such therapies early in the disease course. Due to the number of available treatment options and the heterogenous disease development, there is a strong need for clinical markers to better guide treatment decisions and facilitate drug switching. The two treatments of most importance to this work are outlined below.

Natalizumab

Natalizumab is a monoclonal antibody that targets the surface molecules, more specifically the $\alpha4\beta1$ integrin ³⁵, on leucocytes, thereby inhibiting both the recruitment of immune cells across the blood-brain barrier ³⁶ and the activity of immune cells in the CNS ³⁷. As Natalizumab hinders the migration of leucocytes to sites of inflammation in general, it is also used to treat Crohn’s disease, an inflammatory bowel disease ³⁸. Natalizumab treatment of RRMS patients has been shown to reduce the mean annual relapse rate by 68% after one year, and the number of active lesions by 92% over two years compared to placebo ³⁹.

The successful reduction of immune activity by Natalizumab can lead to opportunistic infections of the common John Cunningham virus (JCV), potentially leading to progressive multifocal leukoencephalopathy (PML) and, in some instances, death ⁴⁰. For this reason, the Natalizumab-containing drug Tysabri was withdrawn from the market in 2005. However, the drug was re-approved in 2006, arguably because of the drug's effectiveness on aggressive RRMS ⁴¹. Patients are now commonly screened for JCV infection prior to, and during Natalizumab treatment ³³. JCV negative patients seldom develop PML, but in positive patients, the risk of developing PML increases after two years of treatment ³³.

In-line with the reduction in immune cell recruitment, immunological proteins are also reduced in the cerebrospinal fluid (CSF) of patients undergoing Natalizumab therapy ⁴², while a second study have found a change in neurological proteins ⁴³. Due to inconsistent findings, the effect on neurological proteins is considered secondary to the effect of immune modulation ^{42,44}, and additional studies are still needed to investigate the overall effects of Natalizumab in order to identify potential individual differences in drug response and possibly enable early drug switching.

Fingolimod

Fingolimod is another treatment of RRMS. Phosphorylated Fingolimod is an agonist for the sphingosine-1-phosphate receptors (S1PRs), facilitating its downregulation and subsequent sequestration of lymphocytes within lymph nodes ⁴⁵, and hindering their migration to the CNS. Fingolimod has been shown to reduce the annual relapse rate by approximately 50%, and the disability progression by approximately 30% ^{46,47}. Even though the drug is primarily known to affect lymphocyte homing, several cell types in the CNS express S1PRs, including microglia ⁴⁸, astrocytes, neurons ⁴⁹, and oligodendrocytes ⁵⁰. As it has been shown that Fingolimod crosses the blood-brain barrier ^{48, 51, 52}, it is hypothesized to have additional beneficial effects beyond the reduction in immune activity, in particular related to remyelination ^{53,54}.

1.2 Multiple sclerosis animal models

To investigate disease mechanisms in MScl, several animal model diseases are available ⁵⁵⁻⁵⁷. Animal models enables the investigation of disease aspects on CNS tissue directly, which is seldom possible to the same extent in humans due to obvious ethical reasons. MScl has however not been detected in animals, and none of the animal models fully reflect the disease pathology observed in humans ⁵⁶. Nevertheless, several mouse models exist that portray different pathologies related to MScl, including inflammation and demyelination, and several findings in mouse models have been translated to the human disease. For example, experimental autoimmune encephalomyelitis (EAE) has proven a valuable model to study the effects of different drugs on CNS inflammation ⁵⁸, and famously led to the discovery of the three MScl drugs Glatiramer acetate, Mitoxantrone and Natalizumab ^{55, 58}. As most of the drugs treating MScl is modulating the inflammatory aspects of the disease, developing drugs that promote repair by stimulating remyelination has recently led to an increased interest in demyelination models ^{59, 60}. Several such models are now available (as reviewed in ⁵⁷), but given that toxin-induced demyelination by cuprizone is the approach used in this work, it will be the focus in the following.

1.2.1 Cuprizone

Cuprizone is a dietary-fed copper chelator that facilitates region-specific demyelination in mice ⁶¹. The demyelination is due to the copper dependency of mature oligodendrocytes, the cells that make and maintain the myelin sheets. Even though the exact mechanism behind oligodendrocyte death is not known, recent studies have linked iron-mediated cell death to the oligodendrocyte apoptosis ⁶². Following apoptosis, microglia are recruited and myelin is phagocytosed. If the cuprizone administration is stopped after 5-6 weeks, remyelination is initiated and near complete after a few weeks. Whereas cuprizone administration for 12 weeks can be used to study chronic demyelination ⁶¹. Thus, the cuprizone model enables studies of both de- and remyelination depending on the duration of the cuprizone administration.

1.3 Proteins

1.3.1 Proteins and proteomes

Proteins are essential for the function of every cell in the body, and are built up of covalently bound amino acids that are folded into three-dimensional structures. The sequence of amino acids is determined by genetic information, and the expression of a protein is based on strict regulation of the genome and its transcripts. The genome is defined as the complete set of genetic material present in a cell or organism, and the mapping of the first human genome was completed in 2003⁶³. As a protein complement to the genome there is the proteome, a term coined in 1994⁶⁴, which describes either the complete list of proteins expressed in an organism, or the expression of proteins at a given time in a specific cell or tissue. It is important to note that while the genome is more or less identical in every cell in the body, and more or less constant throughout life, the proteome is highly dynamic⁶⁵. This is famously represented by the larvae and the butterfly; the genome is (predominantly) the same for both the young larvae and the mature butterfly, but the protein expression is different and thus responsible for the massive phenotypic change.

The Human Proteome Project (HPP) was launched in 2010, aiming to detect all of the proteins coded by the human genome⁶⁶. As of late 2020, 90.4% of the 19 773 predicted proteins have been detected⁶⁷. This is however only the start, as most proteins have different activity based on, for example, cellular location, genetic splicing and post-translational processing. The different forms of a protein coded from the same gene are commonly referred to as proteoforms, and the total number of proteoforms is still unknown^{68, 69}.

Proteomics is defined as the large-scale study of proteins and their function⁷⁰ and can be applied to study protein-protein interaction, protein structure, and protein expression and regulation in both health and disease⁶⁹. Proteomics can be focused on the quantitative or qualitative analysis of a few proteins through methods such as Western Blot, enzyme-linked immunosorbent assay (ELISA), immunohistochemistry (IHC) and OLINK, or the simultaneous identification and quantification of thousands of proteins

through mass spectrometry (MS). As IHC and MS are used in the work included in this thesis, these two approaches will be the focus of this thesis.

1.4 Cerebrospinal fluid

1.4.1 Biology

The cerebrospinal fluid (CSF) is a transparent colorless fluid that surrounds the CNS (**Figure 2**), and is produced by the choroid plexus in the brain ventricles. It has a high turnover, as approximately 500mL is produced every day, albeit only 125ml is present in the body at any given time. CSF is of great importance for CNS function. Mechanically, it works as a cushion both reducing the weight of the brain on itself and the spinal cord and as a protective shock absorber. Importantly, CSF also maintains CNS homeostasis by removing waste products from the CNS, can be used to reduce ischemic pressure, and is an important regulator of the sleep-wake cycle. The content of CSF is largely similar to that of plasma, mainly consisting of water and salts. This is due to passive and active transport of molecules across fenestrated capillaries and the blood cerebrospinal fluid barrier in the endothelial cells of the choroid plexus. The majority of its molecules are, in fact, blood-derived (80%) while the remaining constituents are CNS-derived. The concentration of several salts and metabolites are however different between the two body fluids, indicating tight control of CSF constituents ⁷¹.

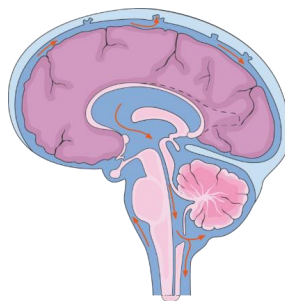


Figure 2: The cerebrospinal fluid (dark blue) in the brain. The red arrows show the direction of flow. CSF also surrounds the spinal cord (not shown). From Creative commons. Servier Medical Art by Servier is licensed under a Creative Commons Attribution 3.0 Unported License.

1.4.2 Cerebrospinal fluid proteins

The protein concentration in CSF is approximately 350 mg/mL, about 200 times lower than in plasma. Similar to plasma, the majority of the total protein amount in the CSF is made up of a few proteins. In fact, 14 proteins comprise close to 80% of the proteins in the CSF, with the most common being serum albumin, which comprises 60% on its own⁷². However, low abundant proteins detected in the CSF show that it has a dynamic range of up to ten orders of magnitude^{72,73}. As CSF is close to the CNS and important for CNS homeostasis, it can be used to detect changes in the abundance of neurological proteins. However, these are commonly of much lower abundance than the high abundant blood proteins. As the dynamic range of CSF exceeds that obtained by some analytical methods⁷⁴, depletion of high abundant proteins prior to analysis and fractionation procedures are commonly performed to quantify proteins of lower abundance. Depletion of the most abundant proteins in CSF prior to proteomic analysis has recently proved a valuable strategy for the detection of over 3300 proteins in CSF⁷⁵. The CSF proteome has been published in several online repositories^{76,77}.

1.5 Biomarkers

A biomarker is defined by the U.S. Food and Drug Administration and the National Institutes of Health as “*A defined characteristic that is measured as an indicator of normal biological processes, pathogenic processes or responses to an exposure or intervention*”⁷⁸. In other words, the definition of a biomarker is quite broad, and spans many types of biological evidence and molecules. Given that the proteome is highly dynamic and changes due to external and internal factors, proteins can thus be biomarkers of both normal and pathological processes.

Protein biomarkers are in current use in diagnosis and treatment of a wide variety of diseases, enabling faster diagnosis and guiding treatment decisions. The most famous clinical protein biomarker is perhaps the routine measurement of C-reactive protein in blood upon a doctor’s visit due to a runny nose. If this protein is over a specific threshold, it implies a bacterial infection, thereby determining whether the patient receives a prescription for antibiotics. In order to be useful in clinical practice, the ideal

biomarker should be easily and reliably measured by tests across multiple locations, exhibit high specificity and sensitivity, be cost effective, and correlate to the disease biology⁷⁹.

Several types of biomarkers are available, and their meaning is explained and reviewed in⁷⁸. Of importance for this work are diagnostic, monitoring, predictive and prognostic biomarkers. Diagnostic biomarkers are largely self-explanatory. Monitoring biomarkers are used to measure the response of a drug or environmental agent, predictive biomarkers are used to separate responders from non-responders prior to therapeutic intervention, and finally, prognostic biomarkers identify the likelihood of certain disease progression in patients with a specific disease.

1.5.1 Biomarker discovery, verification and validation

Commonly, protein biomarker discovery is performed in small sample cohorts, quantifying up to thousands of proteins. Potential biomarkers from the discovery are then verified in a set of 10-50 patient samples, followed by validation of the most successful biomarkers in 100-500 samples, prior to additional clinical validation in 500-1000s of samples^{80, 81}, preferably in multiple independent studies prior to inclusion into clinical practice^{79, 80}. Furthermore, it has long been realized that the “one biomarker - one disease” model may not be appropriate, and that rather a panel of biomarkers will be needed to guide treatment decisions and monitor disease activity^{82, 83}, adding yet another layer of complexity to biomarker validation.

1.5.2 Sample material and biomarker discovery

A wide variety of tissue and fluids can be used in the search for biomarkers. As MScl affects the CNS, brain and spinal cord tissue from model diseases can be investigated to find biomarkers of inflammation, myelination and other processes relevant for the disease. CNS tissue is, for obvious reasons, however rarely obtained from human patients, even though it can yield valuable information about CNS pathology⁸⁴. For the investigation of the human disease, biomarkers are optimally detected in samples that can be obtained by clinical routine analysis, for examples body fluids such as

blood, urine and even tears have all been used as sample material in MScl biomarker discovery⁸⁵⁻⁸⁷.

Due to the CSFs close proximity to the CNS, the CSF proteome is widely studied to identify biomarkers in neurological diseases, and has proven useful for the analysis of neurological pathology⁸⁵. However, as CSF sampling requires a lumbar puncture, it is mainly performed for diagnostic purposes⁸⁸. Thus, biomarkers discovered in CSF should optimally be detected in blood for routine analysis. Of note, several clinically applicable biomarkers for MScl in current use are detectable in serum, detecting specific antibodies against Interferons and Natalizumab for treatment response, or against viruses such as John Cunningham virus in Natalizumab treatment⁷⁹ (**Table 1**).

Table 1: Example of protein biomarkers of MScl in clinical use. Based on⁷⁹.

<i>Protein</i>	<i>Fluid</i>	<i>Biomarker type</i>	<i>Biological function</i>	<i>Interpretation</i>
IgG	Serum/CSF	Diagnostic	Sign of intrathecal IgG synthesis	Evidence of ongoing CNS inflammation
Anti-AQP4	Serum	Diagnostic	Aquaporin 4 antibodies are present in neuromyelitis optica	Discriminates between neuromyelitis optica and MScl
Anti-NZ	Serum	Treatment response	Antibodies developed against Natalizumab treatment	At risk of treatment failure
Anti-IFNB	Serum	Treatment response	Antibodies developed against Interferon beta treatment	At risk of treatment failure
Anti-JC-virus	Serum	Treatment response	JC virus infection can lead to PML in patients receiving Natalizumab	Risk of developing PML during Natalizumab treatment
Anti-VZV	CSF/Serum	Treatment response	Varicella zoster virus infection fatal in fingolimod trial	Vaccination prior to receiving Fingolimod if test is negative

1.5.3 Cerebrospinal fluid biomarkers in multiple sclerosis

Most famously, oligoclonal bands (OCBs) in the CSF is used in the diagnosis of MScl as it implies intrathecal synthesis of immunoglobulin G, that can be used for diagnostic

purposes⁷⁹. Albeit useful, it is not exclusive to MScl as any inflammatory process in the CNS will produce these bands, *e.g.*, meningitis. Furthermore, the relevance of intrathecal synthesis of IgG in MScl was discovered in 1942⁸⁹, and IgG as measured by OCB and IgG index is the only protein biomarker in CSF currently used in the routine diagnosis of MScl⁷⁹. Of note, Anti AQP4 antibodies are used in the diagnostic process to discriminate MScl from neuromyelitis optica.

Extensive research has been performed to find protein biomarkers for MScl that are detectable in CSF^{42, 90-100} (as reviewed in¹⁰¹). However, few, if any, of the proposed biomarkers have yet been sufficiently validated for use in clinical practice. Furthermore, many of the proposed biomarkers in MScl have also been proposed as biomarkers in other neurological diseases. As MScl is a disease characterized by both inflammation and neurodegeneration, it is not a surprise that the proposed biomarkers reflect these two processes. In particular, the chitotriosidase and chitinase-like protein 1 and 2 are expressed by microglia and macrophages, and used as biomarkers of inflammation (as reviewed in¹⁰²). The most famous of these proteins is chitinase 3-like protein 1 (CH3L1), that already in 2010 was discovered as a prognostic marker for the conversion of CIS to CDMS¹⁰³. CH3L1 is expressed in a wide variety of cells, including astrocytes, and has shown biomarker potential in Alzheimer's disease (AD), Amyotrophic lateral sclerosis (ALS), stroke, traumatic brain injury, Creutzfeldt-Jacob disease (CJD) and Parkinson's disease (PD). Similarly, chitotriosidase (CHIT) is increased in MScl, AD, ALS, traumatic brain injury and CJD, and CHI3L2 is increased in MScl and ALS (as reviewed in¹⁰²).

Neurofilaments are the major constituent of neuron cytoskeleton, and occur in three versions: light, heavy and medium. Neurofilament light (NF-L) and heavy (NF-H) have been associated with inflammation-mediated, and acute ongoing axonal damage, respectively (as reviewed in¹⁰⁴ and¹⁰⁵). NF-L is proposed as a monitoring biomarker of drug-mediated effects on axonal damage¹⁰⁶, and a marker for poor prognosis¹⁰⁷⁻¹⁰⁹. Similarly, NF-H has been seen in progressive MScl, and found to be a predictive biomarker for disability progression and brain atrophy^{110, 111}. Neurofilaments have been found increased in AD patients compared to controls¹¹², and are also affected by

several other neurological diseases such as PD¹¹³, ALS¹¹⁴ and CJD¹¹⁵. NF-L has also been found to be increased in the CSF of COVID-19 patients with neurological symptoms¹¹⁶.

Thus, the current status of protein biomarker discovery for MScl is that it generally lacks the proper validation and verification of the suggested candidates. Additionally, the disease-specificity of the most relevant biomarkers seem to be poor. Overall, there is a general lack of studies investigating the specificity and abundance of these proteins across the different neurological diseases.

1.5.4 Proteomic studies of the cuprizone animal model

Relatively few proteomic analyses of the MScl mouse model cuprizone have been performed. In particular, in a study published in 2009, proteomic analysis of cuprizone-fed mice revealed a decrease of myelin proteins such as claudin-11, a marker for oligodendrocytes, and myelin-associated-glycoprotein after six weeks demyelination. Furthermore, the astrocyte and gliosis protein glial fibrillary acidic protein (GFAP) increased during demyelination and decreased during remyelination. After six weeks of cuprizone administration, several mitochondrial proteins were changed. Thus showing that proteomics could detect cuprizone-induced changes¹¹⁷⁻¹¹⁹. A more recent proteomic study detected microglia activation in the cuprizone model after six weeks demyelination, and confirmed little overlap between the animal models cuprizone and the inflammatory model EAE¹²⁰.

1.5.5 Natalizumab monitoring treatment biomarkers from proteomics

Few mass spectrometry-based studies have been published investigating the proteome of patients during treatment^{42, 121}. The effect of the Natalizumab treatment on the CSF proteome have been previously studied, and indicated that Immunoglobulin heavy constant mu (IGHM), haptoglobin and CHI3L1 could be possible treatment biomarkers as they decreased after one year of treatment⁴².

1.6 Mass spectrometry-based proteomics

Mass spectrometry-based proteomics can be split into two main approaches: top-down and bottom-up. In top-down proteomics, intact proteins are investigated by mass spectrometry, while in bottom-up proteomics, proteins are cut into smaller entities called peptides prior to the mass spectrometry analysis. The analysis of proteins through peptide-surrogates in bottom-up proteomics is currently more common than the top-down approaches, as peptides are more easily separated by liquid chromatography, are commonly within the mass range observable by the mass spectrometer, and are more easily identified by mass spectrometry than full length-proteins ¹²².

In addition to these two main approaches, peptides that are already in the sample, *e.g.*, waste products or signal peptides, can also be analyzed by mass spectrometry. These methods, often referred to as peptidomics, have gained popularity over the last years, for example as a means of conserving information about naturally occurring peptides (endopeptidome) in Alzheimer's disease ^{123, 124}.

The peptide-centric approach is however not without its challenges, as peptides are not necessarily unique to one protein (referred to as the protein inference problem), thus significantly increasing the complexity of the downstream data analysis ¹²⁵. Cutting proteins into peptides can also introduce variation in peptide abundances between samples ¹²⁶. Furthermore, only rarely is the full protein sequence detected, making it challenging to investigate the different proteoforms ¹²⁷. Though several advances have been made in the top-down approach in recent years ¹²⁸⁻¹³¹, bottom-up proteomics still dominates the field of mass spectrometry-based proteomics, and will be the focus in the following. A generalized view of the bottom-up mass spectrometric workflow can be seen in **Figure 3**.

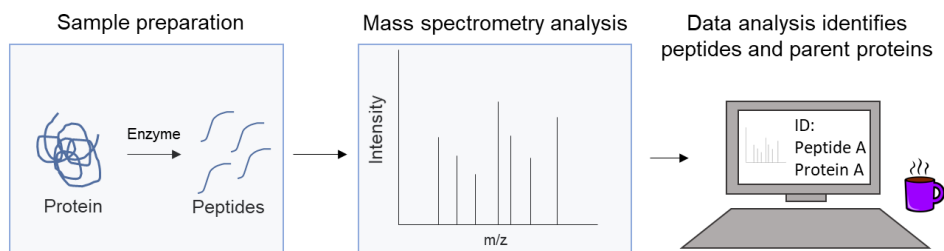


Figure 3: General workflow for the identification of proteins in bottom-up mass spectrometry.

1.6.1 Liquid chromatography

Liquid chromatography (LC) is a technique commonly used in analytical chemistry to separate or isolate molecules. Many different versions are available, depending on the analyte to be isolated and the sample type used. During analysis, the peptides to be analyzed are loaded onto an analytical column containing a hydrophobic stationary phase, where the peptides will interact with varying affinity to the solid phase, mainly based on their hydrophobicity and length. Typically, a gradient of solvent (mobile phase) with increasing hydrophobicity is applied to the analytical column, allowing the migration of peptides through the analytical column based on their solubility in the mobile phase. As the solid solvent is hydrophobic and the mobile phase is polar, it is the opposite of normal phase chromatography, and consequently the method is termed reverse-phase chromatography¹³². Furthermore, as the flow of the mobile phase is controlled by pumps, it is called high performance liquid chromatography (HPLC)¹³³.

The chromatographic gradient can be optimized to reduce the number peptides that co-elute from the column, thereby increasing the number of peptides that can be identified by the mass spectrometer. The resolution of LC columns was further enhanced by nano-LC, nano referencing the flow rates in nanoliter/min as opposed to the commonly used microliter per minute HPLC setups. Nano-LC columns have a small internal diameter allowing optimal peak separation and analysis of low amounts of sample¹³⁴. Importantly, chromatographic separation should be stable across runs so that the time it takes from sample injection to the measurement of the peptide by the mass spectrometer under the given chromatographic conditions (*i.e.*, peptide retention time)

is comparable ^{135, 136}. Reproducible chromatography is important to ensure analytical stability in LC-based mass spectrometry.

1.6.2 Mass spectrometry

A mass spectrometer consists of an ion source, a mass analyzer and a detector. The output from a mass spectrometer is a set of mass spectra, where a molecule's mass to charge ratio (m/z), is plotted against its intensity, commonly used as a measurement of abundance ¹²². The mass spectrum can be used for identification and quantification of a variety of molecules, including metabolites, peptides and proteins. Within the field of proteomics, there are several types of mass spectrometers varying in mass accuracy, speed, sensitivity, and mass range, depending on the components used.

Mass spectrometry analyses of macromolecules such as peptides, proteins and lipids became possible through the invention of soft ionization techniques in the 1980s, allowing the ionization of such molecules without resulting in fragmentation. The two ion sources most commonly used in proteomics are matrix assisted laser desorption ionization (MALDI) and electrospray ionization (ESI) ¹²².

In MALDI, the sample is immersed in a crystalline matrix, and ionized by laser pulsation. Historically, MALDI has been used in the analysis of low complexity samples ¹²², however, it can also be combined with histology, immersing tissue in the crystalline matrix followed by mass spectrometry analysis, as is done in MALDI imaging mass spectrometry (as reviewed in ¹³⁷). Given that the sample is intact following analysis, MALDI imaging enables histological examination of the tissue even after MALDI-MS. Furthermore, three-dimensional maps can be made of the protein expression in the investigated tissue.

Unlike MALDI, ESI ionizes samples in their liquid state, and is commonly coupled to the continuous flow of LC columns. Molecules eluting from the analytical column is subjected to high voltage, the resulting ions are dispersed as a fine spray of charge droplets, followed by solvent evaporation and ion entry into the mass analyzer. Notably, there is a battle for the charges for the eluting peptides in ESI, meaning that

the optimal sensitivity for such systems is obtained when only a low number of analytes elutes from the analytical column at the same time ¹³⁸.

The mass analyzer separates the molecules by their mass to charge ratio (m/z), and the detector registers the number of ions for each m/z value, thereby collecting the data needed to generate the mass spectrum. Commonly the mass analyzer and detector are integrated. There are several types of mass analyzers. Typically, MALDI is coupled to time-of flight mass analyzers (MALDI-TOF). The first TOF analyzers appeared commercially in the 1960s, and their use expanded after the introduction of the soft ionization techniques mentioned above. Here, molecules are dispersed by their speed across an electric field in vacuum, where small molecules travel with the highest velocity and therefore reach the detector first.

In 2005, the first Orbitrap mass spectrometer was released commercially. In the Orbitrap, ions are trapped in an electrostatic field, orbiting an axial electrode. The oscillations of the charged molecules are detected, and transformed into mass spectra using Fourier transformation ^{139, 140}. The Orbitrap has an unparalleled mass accuracy, but is slower than the TOF technology. A third mass analyzer, namely the quadrupole consists of four electrodes that, in addition to measuring the mass of ions, work in concert so that only ions within the selected mass range is stable in the electrostatic field. Mass spectrometers containing different mass analyzers, hybrid mass spectrometers, are commonly equipped with a quadrupole as the first mass analyzer. For example, the TOF has been coupled to a quadrupole, creating a Q-TOF that can be linked to a wide variety of ion sources including ESI. Also, the Thermo Q-Exactive series contain both a quadrupole and an Orbitrap mass analyzer.

Tandem mass spectrometry

In the beginning of mass spectrometry proteomics, the mass and intensity of peptides were collected and used for protein identification, through a method called peptide mass fingerprinting ¹⁴¹. However, as all peptides are built from combinations of the same twenty amino acids, several non-identical peptides can have identical masses, and the method was therefore limited to the analysis of low complexity samples.

In tandem mass spectrometry, referred to as MS/MS, information about the amino acid sequence of a peptide is collected, increasing both the identification confidence and throughput. Specifically, an MS-scan (MS1) is collected for the intact peptide which is then isolated and transported to a collision cell. Here, the peptide is fragmented, commonly by gas bombardment, generating different fragments (**Figure 4**) depending on the method of fragmentation. As the ion types affect the observed mass, they are essential for correct peptide identification in subsequent data analysis. Importantly, the fragment is dependent on retaining a charge during fragmentation to be observable by MS/MS. Common collision cells include collision induced dissociation (CID) and higher-energy CID (HCD), collision methods that both result in mainly b- and y-ions, and Electron-transfer dissociation (ETD) that result in mainly c- and z-ions.

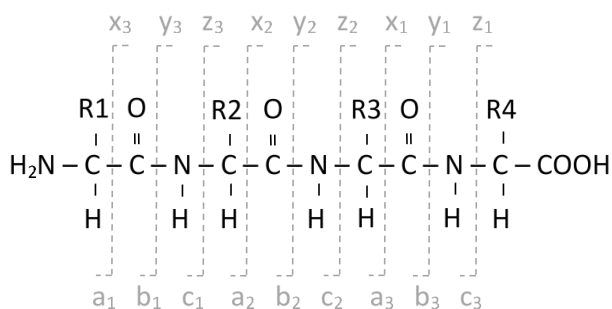


Figure 4: Nomenclature for sequence ions of peptides in mass spectrometry. Here, the peptide bonds connecting a four amino acids long peptide is shown, the variable side chains of the amino acids are designated R1-R4, the possible ions that can be generated are indicated. N-terminal ions a-c are complementary to C-terminal ions x-z. For instance, breaking of the peptide bond between the carbonyl and nitrogen between residue R1 and R2 creates the ions b₁ and y₃.

Following fragmentation, the variably-sized fragments are transported back to the mass analyzer for a second MS scan (MS2). Depending on the sample complexity and analysis strategy, millions of mass spectra can be collected for each sample.

Data-dependent and data-independent mass spectrometry

High-throughput mass spectrometry can have different approaches in selecting peptides for fragmentation, commonly called data-dependent and data-independent acquisition, DDA and DIA, respectively. In DDA, the most intense ions in an MS1 spectrum are selected for isolation and sequential fragmentation by the mass spectrometer. Thus, information from the MS1 spectrum is used to pick precursors for fragmentation on the fly. Precursors not selected for fragmentation thus cannot be identified downstream in one isolated sample. Due to the degree of randomness of the method and chromatographic dependency, the peptides targeted for fragmentation in one sample are not necessarily targeted for fragmentation in all samples in an experiment, or even in multiple injections of the same sample ¹⁴²⁻¹⁴⁴.

Certain mass spectrometry methods aim to fragment everything in each MS1 spectrum. Here, all peptides (precursors) within a pre-determined mass window are collectively fragmented, yielding complex MS2 spectra containing fragments from multiple precursors. As this approach is not dependent on the signal observed in the MS1 spectrum, it is therefore called data-independent acquisition (DIA) (Thermo) or Sequential Window Acquisition of all THEoretical Mass Spectra (SWATH)(SCIEX). These methods quantify peptides based on their MS2 intensities, and have increased quantification accuracy compared to DDA methods ¹⁴⁵. Several techniques exist, all with different names ^{146, 147}, but the principle is the same: aiming to include all of the peptide information in the sample.

Notably, narrow window DIA can achieve quantification of the proteome with superior dynamic range ¹⁴⁸. As mass spectrometers get faster, it is estimated that the isolation window will approximate those used in DDA for all the peptides in a sample. However, this is not yet possible without multiple sample injections. Albeit promising, DIA is currently limited by its ability to identify low abundant peptides, and the development of tools to ensure precise identification, among others ¹⁴⁶. In this thesis, data-dependent mass spectrometry is used.

1.6.3 Quantitative proteomics

Quantitative proteomics aims to quantitatively compare proteins between samples, *e.g.*, comparing the abundance of one or more proteins between healthy and diseased subjects. Quantitative proteomics can further be divided into two different approaches, namely discovery and targeted proteomics. Discovery proteomics utilizes the high-sequencing speed of mass spectrometry, enabling analysis and quantitative comparison of thousands of proteins across samples, while targeted analysis utilizes the selectivity and sensitivity of mass spectrometers, quantifying fewer pre-determined targets with high accuracy even at low concentrations across samples. Notably, methods are also available that combine the two, in particular DIA challenges this separation. Furthermore, peptides can be labelled prior to analysis either by isobaric (TMT, iTRAQ) or metabolic incorporation of stable isotopes (Stable Isotope Labeling by/with Amino acids in Cell culture (SILAC)), or not labeled at all (label-free). As TMT and intensity-based label-free quantification (with and without an internal standard) are used throughout this thesis, they will be the focus in the following.

Tandem mass tag

Tandem mass tags were first introduced by Thomson *et al.* in 2003¹⁴⁹. The method quantified peptides in multiple samples directly in the MS2 spectra, and showed increased signal to noise and fewer missing values compared to traditional MS1 quantification¹⁴⁹. This was achieved through the use of tandem mass tags (TMT) that chemically label individual samples during sample preparation prior to LC-MS/MS analysis. The chemical tag consists of an amine-reactive group, mass normalizer and a mass reporter. During labelling, the amine-reactive group enables covalent linking of the tag to primary amines (the N-terminal and lysine amino acids) of peptides or proteins in the sample. The elemental composition and collective mass of tag is the same for all TMT reagents in a kit, ensuring that peptides with different labels are equally affected by sample preparation¹⁴⁹. Therefore, the samples can be combined after individual labelling which minimizes variation introduced by downstream sample preparation, and enables extensive sample fractionation.

As the placement of heavy nitrogens and carbons vary in the mass reporters (and the balancing mass normalizer), the mass reporters have different isobaric masses that are distinguishable by high-resolution mass spectrometry. During fragmentation in LC-MS/MS analysis, the mass reporters are cleaved off prior to MS2 acquisition. Resultingly, the peptide fragmentation in the high molecular area of an MS2 spectra is used for peptide identification, while the mass reporters in the low molecular area are used for relative quantification of the peptide across the individual samples (**Figure 5**). Furthermore, given an extra fragmentation of the highest intensity MS2 peaks, peptides can be quantified in the MS3 spectrum.

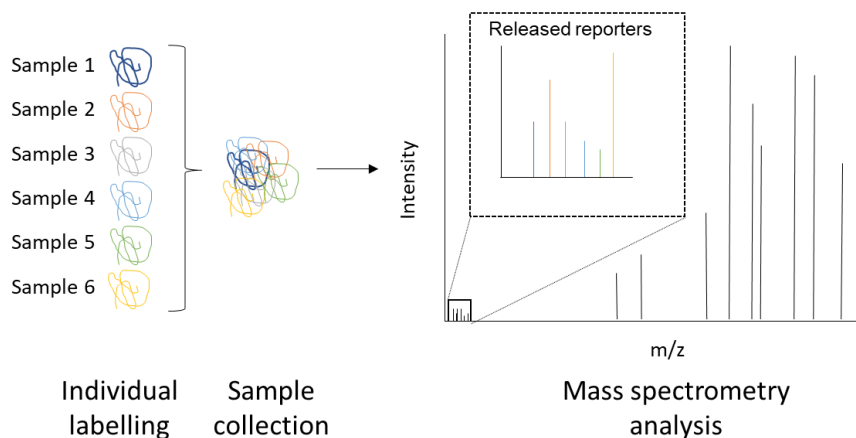


Figure 5: Peptide identification and quantification by tandem mass tags. Samples are individually labelled and simultaneously analyzed by LC-MS/MS. The spectrum is used for peptide identification and the sample-specific mass reporters in the low m/z area enables relative quantification.

The number of samples that can be tagged in one kit has recently expanded to 16¹⁵⁰. Quantification of more than 16 samples by TMT is also made possible by so-called TMT multiplexing – a method where several TMT kits are used, and identical reference samples within each kit is used to enable comparison of samples across TMT experiments.

Intensity-based quantification – extracted ion chromatograms

Commonly, a peptide elutes from the analytical column in a retention time interval, during which the mass spectrometer measures the peptide several times. In intensity-based quantification, a continuous curve is fitted to the discrete measurements of intensity over time, called an extracted ion chromatogram (XIC). Integration of the area under the curve for the ion intensity over time is subsequently used for quantification. An XIC can be estimated for MS1 signals and MS2 fragment spectra, depending on the analytical approach. The high mass accuracy and speed of the mass spectrometer enables accurate quantification, even in complex samples¹⁵¹. A simplified XIC and an example of an experimentally-derived MS2 XIC can be seen in **Figure 6A** and **B**, respectively.

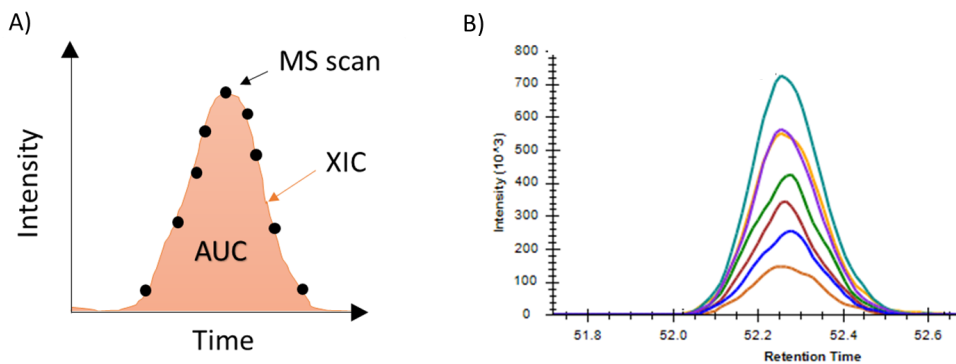


Figure 6: Extracted ion chromatograms. **A)** Simplified view of intensity-based quantification in MS. The intensity for a given mass is collected over time and extracted from MS spectra as discrete datapoints (dots). An ion chromatogram is extracted (an XIC), and the abundance calculated as the area under the curve (AUC). **B)** Example of XICs generated from MS2 spectra of a peptide as seen during targeted data analysis. Here, the eluting peptide is represented by XICs of seven fragment ions (one color each). Picture: A) Homemade, B) Skyline¹⁵².

Label-free discovery proteomics

Discovery proteomics aims to quantify as many proteins as possible in a sample and is commonly used in the exploratory search for disease biomarker candidates¹⁵³. In label-free quantification, peptide abundances are calculated from MS1 signals, using MS2 solely for identification. This quantification method is vulnerable to changes in

chromatography, and off-line fractionation is usually avoided, commonly yielding fewer identified and quantified proteins than experimental workflows that allow extensive fractionation. However, label-free analysis requires few samples preparation steps, and enables the analysis of a large number of samples, and is, perhaps, the most straightforward way to perform discovery-based LC-MS/MS ¹⁵⁴.

Targeted proteomics

In contrast to discovery proteomics, targeted proteomics aims to quantify a limited set of pre-selected targets with great sensitivity, reproducibility and quantitative accuracy ¹⁵⁵. Whereas discovery proteomics is usually applied to scan the proteome to find possible biomarkers for a specific disease, targeted proteomics is commonly used for the validation and verification of biomarker candidates. Here, one or more fragment ions are measured to get an accurate estimate of abundance for the peptide across samples. Commonly, several peptides are measured for each protein.

Targeted experiments can be conducted for relative or absolute quantification of analytes, depending on the addition and purity of internal standards. Filling a niche between antibody-based detection, such as ELISA, and discovery proteomics, targeted proteomics was selected as Method of the Year in the prestigious journal *Nature Methods* in 2013 ¹⁵⁵. Several targeted proteomics techniques are available, namely MS1 targeted methods such as selected ion monitoring (SIM), and MS2 targeted methods such as single reaction monitoring/multiple reaction monitoring (SRM/MRM), and parallel reaction monitoring (PRM) ¹⁵⁶. As MS2 targeted methods are used in this thesis, it will be the focus in the following.

SRM/MRM is performed on triple-quadrupole instruments. In these methods, each peptide fragment is pre-selected and measured individually by mass spectrometry. In PRM on the other hand, all fragments are analyzed together, yielding MS2 spectra similar to that obtained by MS/MS. Resultingly, only peptide masses have to be specified prior to analysis, making the procedure less cumbersome. As the PRM method is commonly conducted using hybrid mass spectrometers such as quadrupole

orbitrap or quadrupole TOF instruments, PRM has a higher mass accuracy and consequently higher selectivity than SRM/MRM methods^{156, 157}.

Targeted quantification using internal standards

Depending on the aim of the targeted experiment, internal standards can be added to normalize differences introduced during LC-MS/MS analysis and improve quantitative accuracy¹²⁶. Such internal standards are usually synthetic peptides labelled with stable isotopes analogous to the peptides of interest. Commonly, stable isotopically labelled peptides (SIL-peptides) are identical to the peptide of interest, except that the C-terminal amino acid (lysine or arginine in tryptic peptides) contain carbons and nitrogens with an extra neutron. This subtle difference adds to the mass of the synthetic peptides, otherwise maintaining their biochemical properties. Therefore, the synthetic standards will be similarly affected by chromatography and mass spectrometric analysis as the endogenous analyte, but the mass difference will be observable by mass spectrometry.

The SIL-peptide(s) can thus be used to normalize differences in abundance introduced by technical variance. During data analysis, the endogenous peptide is compared to that of the SIL-peptide added in known amount to determine the amount of endogenous peptide in the sample (**Figure 7**). Depending on the purity of the internal standard, it can be used to determine the concentration of a peptide in a clinical sample (absolute quantification), or it can be used for accurate relative quantification¹²⁶.

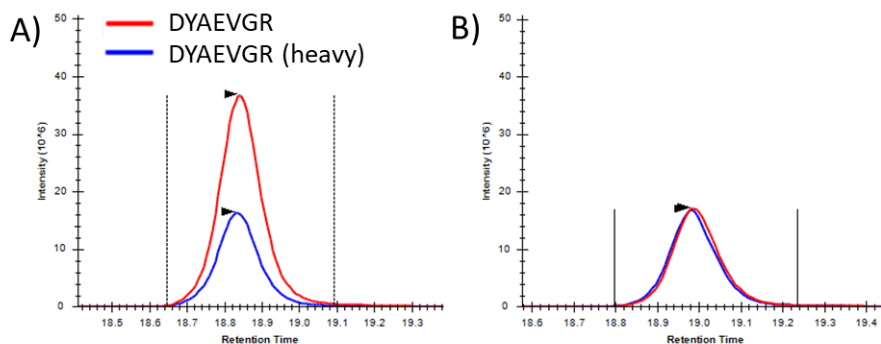


Figure 7: Intensity-based quantification of the peptide DYAEVGR from human haptoglobin during Natalizumab treatment. The endogenous peptide (XIC in red) elutes simultaneously as the stable isotope labelled (SIL) peptide (XIC in blue). **A)** Prior to treatment, the endogenous peptide is more abundant than the SIL-peptide. **B)** during treatment the abundance of the endogenous peptide decreases. Figure: Skyline¹⁵².

Calibration curves

It is important to determine the lowest concentration where a specific peptide can be quantified under the given experimental conditions. Commonly, a calibration curve is generated, varying the concentration of the peptide in question, keeping the levels of the corresponding SIL peptide constant, and measuring the signal response from the mass spectrometer. As the endogenous peptide is often inherent to the matrix one wants to measure, calibration curves are commonly generated in a surrogate matrix. At a certain concentration, the analyte is discernibly higher than the background noise. This concentration value is commonly referred to as the level of detection (LOD). Furthermore, the level of quantification (LOQ) and the upper level of quantification (ULQ) are the lowest and highest concentration where the analyte can be accurately quantified, respectively. The LOQ and ULQ delimits the linear area of the graph, spanning the concentrations of analyte that can be used for quantification. Commonly, calibration curves span at least two orders of magnitude and rarely are both the LOQ and ULQ detected. Several statistical methods exist to estimate the LOD and LOQ^{158, 159}. An example of an experimentally generated calibration curve can be seen in **Figure 8**.

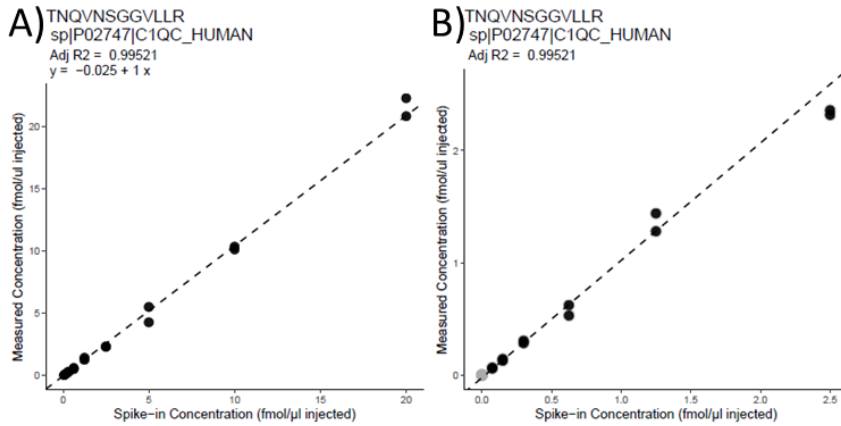


Figure 8: Calibration curve for the peptide TNQVNSGGVLLR of the protein complement component C1q subcomponent C. The calibration curve was based on processed duplicates. The measuring points used in the estimation of the weighted regression line is in black, whereas excluded points are in grey. **A)** Full calibration curve. **B)** The same calibration curve as in A, but zoomed to give a better impression of linearity in the low fmol area.

1.6.4 Sample preparation

Bottom-up mass spectrometry can be used to analyze a multitude of biological samples such as blood, urine, CSF, and cell lines. Common steps in sample preparation are outlined in **Figure 9**, and include protein denaturation, reduction of cysteine bridges followed by alkylation and trypsination. Finally, the sample is desalted prior to LC-MS/MS analysis. If proteins are in a matrix that interfere with trypsination, processing steps might be required prior to sample preparation. Similarly, if labelling strategies are applied, the sample preparation can also include labelling and fractionation steps.

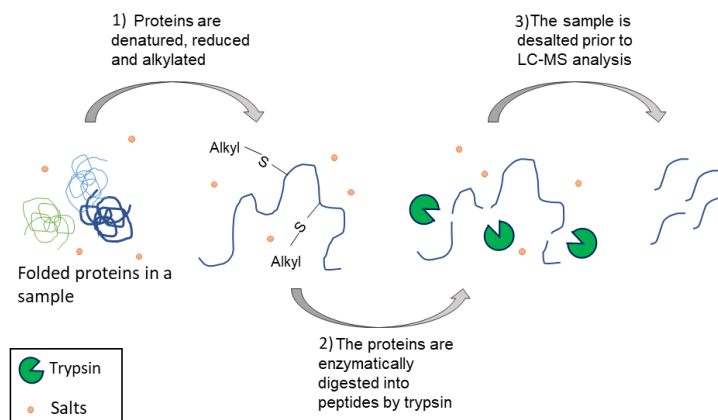


Figure 9: Sample preparation steps in bottom-up proteomics.

Protein digestion

Sample preparation for bottom-up mass spectrometry include sample denaturation and alkylation followed by digestion of proteins into peptides. The transition from protein to peptides is commonly facilitated by the addition of trypsin, an endopeptidase that cut protein sequences C-terminally to the basic amino acids lysine (K) and arginine (R). Trypsin digestion results in an estimated average of 61 peptides per protein with an average of nine amino acids in length, optimal for mass spectrometry analysis ¹⁶⁰. Furthermore, tryptic peptides include at least one basic residue (*i.e.*, R or K) that enhances peptide ionization and peptide fragmentation ¹⁶⁰. However, the extensive use of trypsin commonly restricts the sequence coverage obtainable by mass spectrometry, and the proteins observable ¹⁶¹. Several alternate proteases can be used, depending on the protein or proteoform you wish to study. Alternate proteases commonly yield longer peptides than trypsin ¹⁶², as such, combining these enzymes with trypsination can increase the number of identifications ¹⁶³. In any case, the digestion step is time-consuming commonly extending sample preparation by 16h. The time it takes for peptides of the same protein to be fully cleaved varies, however, and for some peptides, prolonged incubation times leads to peptide degradation or chemical modification which decreases the peptide signal, while other peptides are not fully cleaved even after prolonged incubation times (**Figure 10**).

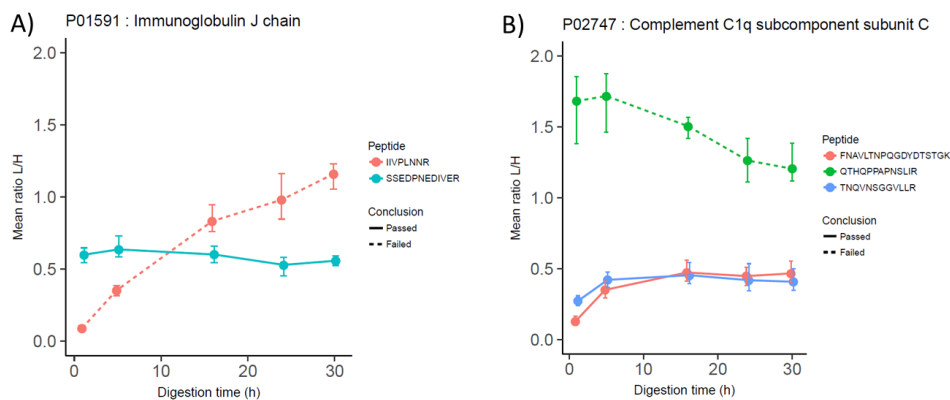


Figure 10: Optimal digestion time vary greatly for peptides of the same protein and affect peptide and protein quantification. Mean of three processed replicates is represented for digestion times 1, 5, 16, 25 and 30 hours. Error bars represent the minimum and maximum values. The signal for each peptide is normalized by an internal standard (L/H). Dotted lines indicate a difference in peptide quantification of more than 20% after 16 h digestion. **A)** Quantification of two peptides representing the protein immunoglobulin J chain show that one peptide (light blue) is readily trypsinated with little increase after only one hour, whereas the other peptide (pink) increases throughout the measured time interval. **B)** Quantification of two peptides of the protein complement C1q subcomponent subunit C behaves similarly (dark blue, red) and is readily trypsinated after 16h, whereas the third peptide (green) decreases after incubation times longer than 5h.

Sample preparation in experiments aiming to determine the absolute concentration of analytes is dependent on controlling this digestion step to get an accurate quantification of the peptides¹²⁶. Similarly, quantification between, for example, disease groups are dependent on insignificant variation in enzyme digestion. To ensure complete tryptic digestion, sample proteins are denatured and cysteine residues alkylated prior to enzymatic digestion during sample preparation (**Figure 9**). A viable way to account for variation introduced by digestion, is to use SIL peptides that have to be digested prior to detection, thereby able to account for differences in protein digestion downstream¹²⁶.

SIL peptides for targeted experiments

Depending on the biochemical properties and chromatography of the peptide, equal analyte concentrations yield different intensity signal. SIL peptides are commonly

added in the same concentration as the endogenous analyte. Estimation of an approximate SIL concentration equal to that of the endogenous peptide in the sample (1:1) should be performed prior to analysis. As peptide concentrations can be sample-specific, these estimates are commonly performed on sample pools. Subsequently, SIL peptide mixes are generated prior to sample preparation. The SIL mix is added to the samples, either prior to enzymatic digestion, sample clean-up or directly prior to MS/MS analysis. The addition step is determined by the type of SIL-peptides and the solution they are in. Some SIL peptides require enzymatic cleavage, either due to a chemical tag (*e.g.*, peptides from jpt), peptides flanking the peptide sequence, or that the entire protein is heavy. Other SIL peptides do not need enzymatic cleavage, but are in a solution that can interfere with chromatography. Adding the standards early in the workflow will allow them to account for more of the variation introduced by the sample preparation ¹²⁶.

As PRM-MS methods mainly measure peptides of interest that are hypothesized to be different between samples, global normalization methods to adjust for technical variance is commonly not performed. Therefore, this targeted analysis is quite vulnerable to biases introduced by sample preparation prior to addition of SIL peptides, and to differences in the addition of SIL peptides themselves. Here, reproducibility can be greatly enhanced by automation and pipetting robots. In any case, including processed replicates, *e.g.*, replicates of the same sample that have been prepared individually, will give an indication of technical variation and reproducibility. Furthermore, including proteins in the targeted study that are hypothesized not to change can serve as an additional verification of discovery results.

Fractionation

In the early days of MS/MS, two-dimensional gel electrophoresis was used to separate proteins prior to trypsination and MALDI-MS analysis ¹²². By adding this fractionation step, the complexity of the sample was reduced and more peptides and proteins could be identified downstream. Due to improvements in technology, liquid chromatography has largely replaced two-dimensional gel electrophoresis as it is generally more sensitive and has better reproducibility ⁹⁴.

Additional methods to reduce sample complexity can also be introduced prior to LC-MS/MS analysis. For example, sample fractionation can be performed at the protein level, either by molecular weight cut-off filters¹²³ or through immunodepletion of high abundant proteins in a sample⁷⁵. Fractionation can also be performed at the peptide level via off-line LC exploiting the chemical abilities of the peptides. In particular, mixed-mode (MM) LC systems can separate peptides based on more than one physical property, *e.g.*, by combining reverse-phase chromatography with cation or anion exchange chromatography (SCX and AX, respectively)^{164, 165}. Furthermore, enrichment strategies are recommended for the analysis of post-translational modifications and can be performed at both the protein and peptide levels, often in combination with off-line fractionation methods¹⁶⁶.

Thus, depending on the analysis, fractionation steps can either enrich the sample for the proteins or peptides of interest, and/or be used to increase the proteome depth by decreasing the sample complexity. However, adding additional sample preparation steps affect the analysis downstream by introducing variation between samples. Thus, fractionation is most often avoided in quantitative label-free analyses, but is commonly performed downstream of sample collection in chemical labelling strategies such as TMT.

1.7 Immunohistochemistry

Histological sections are commonly used to investigate biopsies and guide treatment decisions¹⁶⁷. With this approach, thin tissue sections can be stained by a wide number of histological stains to envision tissue structures or cell populations of interest. For example, the staining Luxol fast blue (LFB) can be used to envision myelin in formalin-fixed material¹⁶⁸. Immunohistochemistry (IHC) uses highly specific antibodies to detect proteins of interest on histological sections and is often combined with histological staining to determine the cellular localization of the proteins of interest¹⁶⁷. Furthermore, quantitative or semi-quantitative scoring systems are used to compare biological events across histological sections^{169, 170}. Thus, IHC can be used to

investigate the effect of drugs on de- and remyelination in the CNS by measuring established markers of demyelination and macrophage activation in mouse models.

1.8 Bioinformatics in quantitative proteomics

1.8.1 Identification and quantification

In label-free discovery proteomics, several thousand MS1 and MS2 spectra can be collected in a single tandem MS run, and thankfully, software tools are available to untangle the information gathered in these spectra. The identification of peptides is performed by bioinformatics tools called search engines¹⁷¹. Commonly, the user provides a database for the spectra to be searched against, expanded with non-existent protein sequences called decoys¹⁷². The search engine then matches the *in silico* digested protein sequences to the experimentally gathered spectra and gives each comparison a score to imply identification confidence. Several search engines have been developed for this purpose (*e.g.*,¹⁷³⁻¹⁷⁶).

Subsequent analysis of the results uses the decoy hits to set an identification score threshold commonly allowing 1% false discoveries. This score on the level of peptide-spectrum matches (PSM) is then combined to the peptide and protein level. Thus, protein identification is a statistical exercise, with false/true positives/negatives that does not require manual input. As this identification procedure may pose somewhat of a black box problem, software tools should allow the inspection of identifications and provide open-source bioinformatic pipelines¹⁷⁷. An example of an identified MS2 spectrum with annotation (annotated mass spectrum) and the peptide identified can be seen in **Figure 11A** and **B**, respectively.

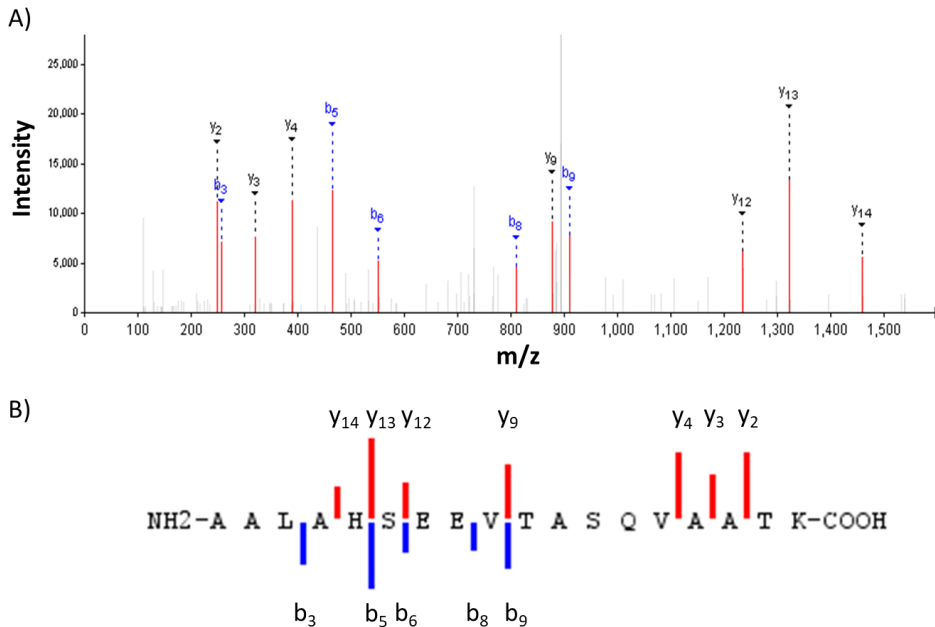


Figure 11: Annotated mass spectra of the peptide AALAHSEEVTASQVAATK from human plectin. **A)** MS2 spectra with m/z values (x-axis) and intensities (y-axis). The b and y ions used to identify the peptide are shown in red, mass values not used for identification are in grey. **B)** The sequence of the peptide identified by the mass spectrum in A. The annotated b and y ions and their spectrum intensity are represented by bars in blue and red, respectively. Picture: PeptideShaker¹⁷⁸, with modifications.

In label-free discovery proteomics, retention time alignment is pivotal for correct identification and quantification of peptides across runs¹⁷⁹. Furthermore, algorithms perform signal normalization, reducing technical variability^{154, 179}. Resultingly, bioinformatics tools are key for both identification and quantification of high-throughput label-free discovery data. Software often covers the entire pipeline of both identification and quantification such as the freely available MaxQuant¹⁸⁰ and the Trans-Proteomic Pipeline¹⁸¹, or commercial software such as Proteome Discoverer (Thermo) and Progenesis LC-MS (Waters).

Though advances have been made in the identification and quantification of PRM data, it is still largely based on manual assessment of peak quality made possible by software such as Skyline^{152, 182}. Here, identification is based on peptide elution, fragment order

and mass accuracy compared to previously stored annotated spectra, stored in a spectral library. Also, if a SIL peptide is added, it provides additional identification confidence. The transparency of the results thus removes black box issues common for high-throughput discovery proteomics and low-throughput immune-assays.

Online storage of data from discovery and targeted proteomic experiments have become increasingly popular, and in some instances demanded, via repositories such as PRIDE¹⁸³ and Panorama¹⁸⁴, allowing data sharing and re-analysis¹⁸⁵, thereby increasing the transparency of mass spectrometry-based proteomics experiments.

1.8.2 Functional analysis and data visualization

The identification and quantification of a large number of analytes can be overwhelming for any researcher. Helped largely by statistical approaches, the dataset is commonly reduced to proteins that are changed between the measured groups. With the growing amount of literature on protein function and interaction, retrieving the information for several hundred proteins can be an immense task. Luckily, databases exist that collect information about protein interactions, functions and/or cellular location taken from literature and structure this knowledge into freely available databases that allow a researcher to investigate whether their protein, or list of proteins of interest have a specific biological interpretation. The databases are overwhelmingly gene-centric, hence information about proteoforms is largely overlooked. Furthermore, the researcher is dependent on these databases being updated¹⁸⁶, correctly annotated and containing the proteins of interest.

Several freely available tools exist for this type of annotation. Perhaps most widely used is the UniProt Knowledgebase¹⁸⁷, an online repository for protein information including function and sequence information. Sequence databases from UniProt is commonly used in the analysis of discovery proteomics data. Furthermore, the Gene Ontology (GO) database^{188, 189}, aims to provide a standardized vocabulary for the annotation of the biological function, cellular process, and molecular function of genes. The release from February 2021 contained close to eight million annotations of 44 000 terms for 1.5 million gene products and close to 5000 species (geneontology.org/stats).

As well-known to most cellular biologists, protein functions are commonly structured into larger reaction chains termed pathways. Here, protein interactions are manually curated from literature and stored into specialized databases. Commonly, these interactions are further curated and included in larger frameworks like Reactome ¹⁹⁰, ¹⁹¹, KEGG ¹⁹² and the commercially available Ingenuity Pathway Analysis (QIAGEN). Recently, the Reactome database has been expanded to include individual reactions for isoforms and post-translational modifications, through a tool called PathwayMatcher, thereby increasing the granularity of the pathway information ¹⁹³.

Determining the significance of the annotation of both GO terms and Reactome pathways is commonly done by overrepresentation analysis (as detailed in ¹⁹⁴). In this approach, proteins in the dataset are first matched to a database, and in a subsequent analysis a biological process or pathway can be enriched in the list of input proteins, compared to what is expected from the background. Hence, providing a background (*e.g.*, all proteins in your sample) is of importance and should be provided if allowed by the tool.

Commonly, the results are provided to the user as a table containing the enriched terms or pathways. Though databases aim to be visual and interactive, it is commonly hard to inspect such data. The Cytoscape software platform ¹⁹⁵ enables the creation and analysis of protein-protein networks, and integration with experimental abundance data that allow visual inspection and user interaction. Furthermore, it provides visualization of the most interesting findings for inclusion in the resulting publication. Protein-protein interactions are commonly illustrated as interaction networks where the protein (gene) is a node, and the interaction is a line between two nodes. Two examples of this type of visualization can be seen in **Figure 12**.

Finally, the STRING ¹⁹⁶ database aims to link information stored in databases such as, but not limited to BIND, DIP, GRID, HPRD, IntAct, MINT, and PID, curated data: Biocarta, BioCyc, GO, KEGG, and Reactome, and even literature abstracts, to enable generation of protein networks based on the combined evidence of physical and functional interactions.

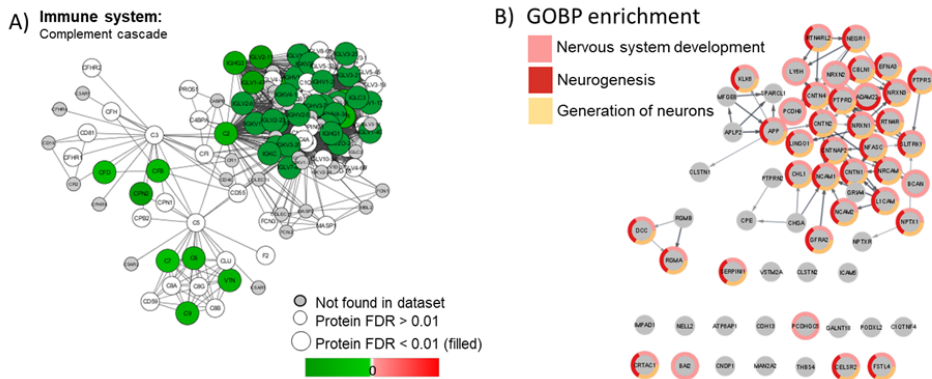


Figure 12: Visualizing the annotation of pathways and biological functions. Each gene is represented by a sphere (node), and the functional interaction between them is a line (edge). The node is labelled by the gene name. **A)** The Reactome pathway “complement cascade” overlain with abundance data from a proteomics experiment. Here, many but not all proteins in this pathway were measured in the dataset, and the proteins that were trusted to change ($FDR < 0.05$) were reduced. **B)** A STRING network show that many of the proteins in the query list are known to interact functionally or physically. GO biological process (GOBP) enrichment reveal that many proteins in this network have neurological function. Picture: ReactomeFIViz, StringApp, Cytoscape.

1.8.3 Databases for protein biomarkers

Knowing how the proteins in your dataset have been changed in previous studies of the same disease can provide valuable information for biomarker discovery studies. Commonly, the results of MS/MS biomarker studies are presented as a short list of the most changed proteins, and the full dataset is either stored in large supplementary tables or in online repositories such as PRIDE. Therefore, a large effort is needed to see whether the proteins have previously been found affected by the disease. Furthermore, it is also highly interesting to know whether the proteins have been found changed in related diseases.

Due to the increase in data accompanying proteomics experiments, this information is not always easily accessible in a journal’s publication format. As an example, the proteins that are found not to change can be highly valuable information for these types of analyses, but rarely makes it into the short protein list in the publication. To address this issue, CSF-PR 2.0⁹⁷ collected the results from MS-based proteomics studies of

neurological diseases. Mainly MScl, but also AD, PD, and ALS. When launched in 2017, the database included 85 datasets with over 2000 proteins, and has since been expanded to include 128 datasets with over 4000 quantified proteins. The datasets have been extracted from published literature and supplementary tables, and made accessible in a user-friendly resource, allowing the user to browse through MS-based proteomics results based on the disease, protein or study of interest. When available, even information down to the peptide level is provided. Furthermore, the results can be exported, and even compared to the user's own dataset ¹⁹⁷.

Other databases are available to help the selection of proteins and peptides for targeted assays by collecting information from online repositories, even streamlining the generation of SRM/MRM assays against FDA approved biomarkers ¹⁹⁸. Thus, collection of proteomics data in such databases provides easy access to complex data and offers information that can be used in future proteomics experiments, in particular for targeted assays and biomarker validation.

2. Aims of the study

The overall aim of the work presented in this thesis was to get a better understanding of the effects of the two MScl treatments Fingolimod and Natalizumab. First, through the investigation of the effects of Fingolimod treatment on de- and remyelination in the MScl mouse model cuprizone. Next, by building robust PRM-assays to investigate a selected set of MScl biomarker candidates known to be affected by the disease. And finally, use the developed assays to investigate the disease-relevance of proteome changes in MScl patients receiving Natalizumab treatment.

The aim for each study was as follows:

Paper I: Investigate if there is an additional benefit of Fingolimod treatment in the CNS, by comparing the proteome of Fingolimod-treated mice to placebo in the de- and remyelinating mouse model cuprizone.

Paper II: Build robust assays against promising MScl biomarker candidates, with the long-term goal of creating a panel of biomarkers to be used for disease-monitoring in clinical practice.

Paper III: Investigate proteome changes of patients undergoing Natalizumab treatment by proteomics discovery, verify the changes, and interpret the findings in an RRMS context by comparison to online datasets in CSF-PR 2.0.

3. Summary of papers

Paper I: To investigate the effect of Fingolimod on the remyelination process, cuprizone was fed to C57Bl/6 mice which were then treated by Fingolimod or placebo to investigate the effect on de- and remyelination via quantitative proteomics and immunohistochemistry (IHC). The mice were fed 0.2% cuprizone chow for six weeks to facilitate demyelination prior to switching to normal chow for the investigation of re-myelination. The effects of Fingolimod to placebo were investigated after six weeks of demyelination, and then one and three weeks after reintroducing normal chow (remyelination). Proteomics analysis revealed a downregulation of sphingosine receptor 1 in the brain of Fingolimod-treated mice at all timepoints, and IHC analysis detected an increased number of oligodendrocytes after three weeks of remyelination. The combined evidence from IHC and proteomics analysis however showed no significant differences of Fingolimod treatment on the degree of remyelination, axonal loss or damage compared to placebo.

Paper II: To utilize the information in the CSF-PR 2.0 database, biomarker candidates from the database were selected for assay generation to enable high quality quantification for future validation of biomarker candidates. Specifically, 25 proteins and 72 peptides were selected for assay-building based on the CSF-PR score, suitable dynamic range of the assay and biological annotation. The peptides were subsequently evaluated based on the inter- and intra-day trypsination reproducibility, optimal trypsination time, and ability to discriminate between MScl and other neurological diseases (OND) in a pilot study. Resultingly, 37 peptides from 21 proteins were included in the assay, including proteins with immunological and neurological activity. The development of calibration curves and the determination of the linear area was performed for 17 of the peptides.

Paper III: To investigate the effect of Natalizumab on the CSF proteome, CSF was sampled from patients undergoing Natalizumab treatment and investigated by discovery and verification proteomics. Proteomics discovery of 56 patients undergoing Natalizumab treatment revealed changes in immunological and neurological proteins

including many known biomarker candidates in MScl and proteins involved in metabolism. The protein changes were compared to RRMS vs OND datasets in the CSF-PR database, and the disease-relevance of the changed proteins were examined. The observed changes in metabolism-related proteins were not reported to be changed between RRMS vs OND and seemed to be treatment-specific. Additionally, proteins that were commonly decreased in RRMS continued to decrease during treatment, perhaps reflecting on-going disease processes not affected by the treatment. Most of the changes seen during the treatment were confirmed by PRM verification. Overall, the study verified the biomarkers suggested from previous studies and further suggested additional processes to monitor in MScl treatment.

4. Methodological considerations

4.1 Brain area selection

For the investigation of the effect of Fingolimod on de- and remyelination in Paper I, brain tissue was lysed. In this experiment, the frontal right hemisphere, including corpus callosum, of the cuprizone-affected mouse brains were analyzed by TMT-mass spectrometry. As the demyelination in cuprizone is specific to certain brain regions, *i.e.*, corpus callosum ⁶¹, other areas of the brain could also have been investigated. Furthermore, a study showed that demyelination is present in the cortex, albeit remyelination is scarce in this area ¹⁹⁹. Direct investigation of the corpus callosum by, for instance, laser capture microdissection could potentially detect more specific changes in the area most affected by cuprizone de- and remyelination. In contrast, the proteomic analysis of the frontal right hemisphere shows global differences to the brain proteome upon de- and remyelination by cuprizone in an area consisting of approximately half glia and half neurons ²⁰⁰. The global proteomics approach has previously been successful in studying de- and remyelination in the cuprizone model ¹¹⁷, indicating that effects would be visible also by using this approach.

4.2 Patient selection

In Paper III, patient CSF samples were received from the Czech-republic for proteomics discovery and verification of protein changes during the MScl treatment Natalizumab. Investigation of patient and sample information revealed differences between a wide range of clinical factors including time of sampling, previous treatment(s), disease aggressiveness and duration. The majority of patients were sampled at the end of the treatment; however some patients were sampled after treatment cessation. As the recommended wash-out period after Natalizumab treatment is 12 weeks prior to switching to other treatments ²⁰¹, patients were included based on whether the second sample was sampled during this time frame.

Furthermore, the patients were under the influence of different MScl treatments when first sampled. As it was unclear from the literature how and if the changes in the CSF proteome would be differently affected by these clinical factors, the experiment was designed such that the group of patients under the effect of interferon beta treatment when first sampled (constituting the largest group) was divided into two groups based on controlled randomization of clinical variables and included in both the discovery and verification studies. The remaining patients were included in the proteomics discovery group.

Efforts were also made during the sample preparation to ensure that differences between patient groups were not introduced by technical variation. Therefore, patients were randomized based on known clinical variables between each step of the sample preparation in the discovery study²⁰².

4.2.1 Removal of outliers

During the investigation of patient samples in Paper III, some of the patients were removed from the study following inspection of the mass spectrometry analysis. The following patients were removed in the discovery study due to interferences. One of the samples was removed as it had a total ion current during mass spectrometry analysis that resembled a cell line more than CSF, increasing the total number of identified proteins by approximately one thousand. A second sample was removed as an update of patient information revealed that he/she was not treated by Natalizumab, and finally, a third sample was removed as it was unclear which sample had been sampled first. The removal of these three patients was based on sample and patient information, and not the quantitative measurements. However, one additional patient was removed in the verification study as the results were consistently irregular across the peptide fold changes, indicating that an error was introduced prior to the addition of SIL peptides. Removing outliers from an experiment should be done with care, as it can give a false impression of the biological variability. Therefore, the statistical results with and without this sample was added to the supplementary information in the final version of the manuscript.

4.2.2 Pooling of samples

Pooled samples were used in the proteomics discovery of the effects of Fingolimod on de- and remyelination in Paper I, and in the testing of peptide stability in Paper II. The pooling of samples is debated, as it arguably makes it impossible to assess individual differences. However, sample pooling is often a trade-off between cost and benefit. A study comparing technical to biological replicates and sample pooling in DIGE experiments concluded that sample pooling of mouse brain samples did not lead to systematic biases of the results, as the mean of individual measurements were equal to the value of the pooled sample²⁰³. This was considered to be due to small biological differences in the mouse brains, and due to the use of internal standards leading to a narrower range of values after the division by a reference. Thus, this study implies that the pooling strategy of mouse brain samples in a TMT experiment accurately reflects the average of the individual samples.

Notably, pooling a larger number of samples reduces the number of replicates needed²⁰³. In the Fingolimod study, each sample pool consisted of two mice, and three pools were measured for each condition across the two TMT experiments. Optimally, more biological samples could have been used in the pooling strategy, but this was not available from the experiment. Furthermore, individual mice could have been measured either by label-free methods or by increasing the number of TMT kits in the experiment, however, identification of low-abundant proteins through extensive sample fractionation was deemed more important. In any case, using this pooling strategy, the findings should be confirmed by individual analysis in future studies as data at the individual sample level is lost when pooling.

In Paper II, sample pools were used for extensive testing of peptides in the generation of assays. Here, CSF from the disease category *other neurological diseases* (OND) was used to test the peptide stability. The pooling strategy ensured that there was enough CSF to test the different assay metrics in a relevant patient category without using valuable MScl patient CSF. Furthermore, the repeated analysis of the OND sample pool provided a well-known reference sample to assess LC-MS/MS stability during patient analysis, a requirement in a Tier two assay¹²⁶. However, some proteins are

commonly lower in neurological controls than in MScl patients, which could explain the poor performance of some of the peptides in the tests prior to assay generation.

4.3 Quantitative proteomics

4.3.1 Reproducibility

Throughout the work presented in this thesis, mass spectrometry-based proteomics is used to identify and evaluate biomarker candidates. Due to great improvements in technology resulting in increasingly more sensitive and faster mass spectrometers, an increasing amount of peptides and proteins can be identified and quantified by LC-MS/MS. The target of many studies has been to quantify as many proteins as possible. However, the quality of the quantification has perhaps not been looked at in enough detail.

Reproducibility can include every step in the pipeline, or it can be used for the mass spectrometry analysis, the sample preparation or the data analysis alone. A study published in 2015 showed that even when different laboratories were given the same dataset, the groups yielded widely different results following statistical testing²⁰⁴, possibly due to the lack of standardization of analysis pipelines. Therefore, selecting biomarkers that were based on more than one study was an important part of the biomarker selection process in Paper II.

4.3.2 Tandem mass tag

As TMT quantification can be considered more accurate than label-free methods^{149, 205} and is compatible with sample fractionation, it was used for the investigation of the brain proteome of Fingolimod-treated cuprizone-fed mice in Paper I. As peptide quantification is based on reporter ion abundance, co-isolation of peptides is a common source of quantification error in TMT experiments. Here, peptides other than the one identified in the MS2 spectrum can affect the reporter ion signal. This phenomenon is called TMT ratio compression²⁰⁶, and can largely be reduced through MS3 quantification that also improves quantification accuracy, however this approach has reduced precision and a lower number of identifications compared to MS2-based

quantification²⁰⁷. TMT MS2 quantification was used in the investigation of de- and remyelination in Paper I.

TMT multiplexing

The TMT strategy is limited by the number of samples that can be analyzed simultaneously by a single kit. In a TMT multiplexing approach, two or more TMT kits are therefore combined for sample analysis. This method was used in Paper I for the analysis of the effect of Fingolimod in CNS during de- and remyelination. In this method, one of the TMT reagents in each kit was used to label a common reference sample, enabling comparison of samples across kits. However, combining kits have been shown to introduce technical variation, showing that the quantification accuracy achieved by TMT is not reproduced when several batches are combined if this effect is not normalized for prior to analysis²⁰⁸.

Such a batch effect was apparent in in Paper I, as principal component analysis of the \log_2 transformed intensities clearly separated the samples into batches on the first component, showing that the greatest source of variability in the data was from technical variation. This could be explained in part by the low biological variation observed in mouse brains²⁰³, and the quantification of over 6000 proteins where the majority were thought not to change between Fingolimod and placebo. Furthermore, the IHC results indicated little or no difference between mice in histological sections of known markers of myelination and inflammation. However, to investigate if this technical variance was masking any potential biological findings, a normalization approach available at the time was tested to remove the batch effect²⁰⁹, but the samples still separated into the batches even after using this scaling. This could be due to the above factors.

To further investigate the removal of the batch effect, available literature was searched. Numerous approaches have been introduced for the removal of batch effects in microarray data, but as the number of samples from each condition was not the same in both TMT experiments (*i.e.*, being an unbalanced experiment), many of the approaches could not be used²¹⁰. Finally, batch removal using linear modelling through

the R package LIMMA was used as recommended²¹⁰. Following the adjustment, the data was analyzed to find the most changed proteins. After the paper was published, several additional methods have since been developed to handle batch effects in proteomics studies^{208,211}.

4.3.3 Sample fractionation

As the brain proteome is estimated to express over 16 000 proteins (Human Protein Atlas²¹²), efforts were made to quantify proteins of low abundance, *e.g.*, surface receptors. In Paper I, samples labelled by TMT were extensively fractionated prior to LC-MS/MS analysis. In short, mixed-mode reverse-phase anion exchange off-line chromatography fractionated each TMT experiment into 58 fractions that were subsequently analyzed by LC-MS/MS. This method was chosen as it has proven superior to peptide separation by MM-SCX methods¹⁶⁵, with the added benefit of avoiding additional sample desalting following fractionation.

4.3.4 Selecting a label-free discovery approach

Label-free proteomics discovery was selected for quantification of the proteome of the 56 patients receiving Natalizumab treatment in Paper III. An isotopic labelling strategy combined with immunodepletion or off-line fractionation as in Paper I would have quantified more of the CSF proteome. Furthermore, as the patients are their own controls, the batch effect will likely be minimal as long as both samples from the same patient were included in the same TMT experiment. However, a label-free approach enables the analysis of a large number of samples, and ensures the possibility to remove samples without affecting the rest of the sample set, should for instance, new clinical data become available. Thus, the strategy to include as many patients as possible while remaining flexible greatly affected the experimental design and choice of quantification strategy.

4.3.5 Technical variation in label-free discovery

As the label-free discovery strategy in Paper III is vulnerable to changes in chromatography and sample preparation, the patient samples were all processed

simultaneously and quality control samples were included to assess inter- and intra-person variability.

The quality controls were analyzed by mass spectrometry prior to running individual patient samples, showing that approximately the same number of proteins were identified and quantified across the twelve processed replicates (84% proteins identified in all samples) with the quantified proteins having an average inter-person CV following normalization of 27%, and an average intra-person variability of 18-22%. This ensured that the sample processing had been successful up to this point. Furthermore, as the quality control samples were randomized also in other sample preparation steps, such as desalting, it gave an estimate of the total technical variation that could be expected from the sample preparation step using the selected workflow.

Following individual analysis, the quality control samples were combined and injected every 8-12 patient sample to assess technical variability during LC-MS/MS. This strategy proved useful for evaluating LC-MS/MS performance. Furthermore, the quality control samples contributed to normalization and retention time alignment during data analysis by MaxQuant. Using the MaxQuant QC program PTXQC ²¹³ showed an alignment success of at least 96% across all samples.

4.3.6 Individual differences in treatment response

In Paper III, the proteome changes in patients receiving Natalizumab treatment were investigated. It would be highly interesting to investigate whether individual changes could be associated with clinical endpoints such as relapses or MRI activity. However, this would require clinical information to an extent that was not available for the patients in the study. Therefore, only a comparison across the entire patient group was performed. In this approach, proteins that are possibly determinant for a low number of patients, or subgroups, will be missed. However, the study shows the general effect of Natalizumab on the CSF proteome, and suggests possible proteins that could be of interest for future individual analysis.

4.4 PRM assay building

4.4.1 PRM versus ELISA

The perhaps most interesting protein biomarkers in CSF are the neurofilaments and chitinase 3-like protein 1 (CHI3L1). However, for various reasons, they are not easily measured by PRM. In the case of neurofilament heavy, it is highly phosphorylated, making peptide selection laborious. In addition, these proteins are of low abundance in CSF. Therefore, an ELISA strategy could perhaps provide more accurate quantification of these proteins. The ELISA strategy is however quite low-throughput, dependent on high quality antibodies^{214,215}, and often requires relatively large volumes of CSF. High quality antibodies are most likely available for these proteins, but not for many of the other proposed biomarkers in MScl, and not in a multiplexed way. In addition, we did not have a large amount of CSF from each patient, hence PRM was selected instead.

4.4.2 PRM method

The biomarker candidates in Paper II had widely different dynamic ranges within CSF, and the selection of a PRM method to measure these proteins was therefore a trade-off between sensitivity, selectivity and throughput. As the PRM assays would be used to measure a large number of peptides accurately between patient groups, a “wide-screen” approach as suggested in¹⁵⁷ was adapted to a 90 min chromatographic gradient.

A smaller test was performed to investigate whether the signal of the peptides with the lowest abundance could be increased by increasing the fill time, as suggested in²¹⁶. In this test, the AUC of peptides with lowest abundance showed a modest signal increase, even when the time spent on ion collection was as suggested for low throughput-high sensitivity experiments (**Figure 9A**). In addition, the XIC of these peptides were in some cases very low even with the longer fill time (**Figure 9B**). Indicating that some peptides cannot be precisely quantified by PRM in the ONDs patient group.

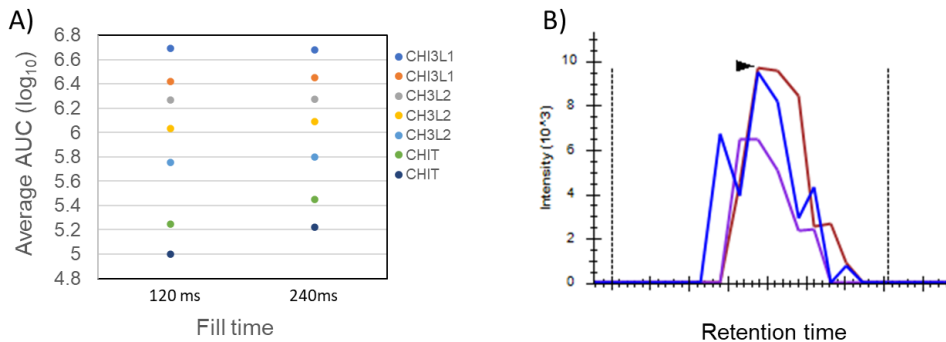


Figure 9: Doubling of ion collection fill time did not lead to a doubling of peptide signal for chitotriosidase or chitinase-like proteins: A) The AUC of the peptides to the displayed proteins. Each point is based on the average of two runs. The increase in AUC is modest for the majority of peptides even after a doubling of fill time. **B)** XIC of a CHIT peptide with 240 ms fill time. The signal is on the border of what can be quantified.

4.4.3 Choice of internal standards

For the generation of assays in Paper II and Paper III, SIL peptides were used as internal standards. Heavy labelled tryptic peptides analogous to the endogenous peptide is commonly used as internal standards. However, several studies have shown that full length synthetic proteins, or peptides with naturally flanking amino acids improves the quantification accuracy^{217, 218}. Optimally, heavy labelled proteins should have been used as internal standards as they would have been subjected to the same trypsination effect as the endogenous peptide. However, the same studies emphasize that true accuracy is elusive in a bottom-up approach, and emphasizes the tight control of trypsination²¹⁸. Note that the SIL peptide standards used in Paper II and III were of different quality and purity.

4.4.4 Peptide tests and cut-offs for PRM-assays

For the development of assays in Paper II, deciding on the level of precision was important prior to designing the assays. Though the long-term aim of the larger project is to develop assays for use in a clinical setting, further verification of biomarker candidates is required prior to clinical assay generation for a smaller subset of proteins. A best practice guide for assay generation was published by the proteomic community

in 2014 ¹²⁶, from where “The Selection of Tier” approach was used to guide the experiment design for our own robust assays. In short, Tier 2 assays require labelled internal standards to consistently measure relative changes of a large number of analytes across samples. The precision required for Tier 2 assays is moderate to high (<20-35% CV required), and the within day and day-to-day stability should be measured. In addition, interferences from different background matrices should be identified, and LC-MS/MS performance monitored.

In order to ensure precision, controlling trypsination is of great importance ^{126, 219-222}. Therefore, peptide surrogates were tested for trypsination stability and optimal trypsination time. In line with the tier requirements, a threshold of <20% CV was set for peptides to pass/fail stability tests, as also proposed in ²²². The testing and inclusion of peptides in the assay is on-going, and the area of linearity was determined for only a subset of the tested proteins. In order to be a full Tier 2 assay, assessment of background interference should be provided, and the linear area defined for all of the peptides.

However, as previously noted, many proteins that are of interest to the disease are less abundant in the control group OND. This includes inflammation markers such as CHI3L1. Therefore, poor performance of these peptides during assay building could be due to too low signal in the reference sample. The linear area of quantification was not determined prior to peptide testing as this is laborious and performed in a substitute matrix, and was thus only performed for the top performing peptides. In the future, technical replicate analysis could provide information about the measurement %CV and be used to indicate whether a peptide is too low-abundant in the chosen sample to be used for peptide testing.

4.4.5 Linear area, LOD and LOQ

Defining the linear area of quantification is important to accurately measure peptides by PRM. In the linear area, an increase in analyte signal is proportionate to an increase in analyte concentration. In many cases, the limit of quantification is estimated and

used as the start of the linear area, *i.e.*, the lowest level of analyte concentration that can be accurately quantified ¹⁵⁸.

During the generation of the calibration curves for Paper II, it became apparent that many peptides had no detectable background/noise in any of the blank samples using the selected PRM-method. Furthermore, if there was noise, it was too low to use as an estimate for the level of detection (LOD) and level of quantification (LOQ) with the methods suggested in the literature. The variation in the lowest quantified analyte concentration was less than <20% CV for most peptides, even in the low amol area at the limit of what is expected to be measurable with the sensitivity of the PRM-method ¹⁵⁷. Resultingly, the lowest point in the linear area with a CV <20% was used as the LOQ, and was expected to be a good estimate of the actual lower limit of quantification. However, the LOD and LLOQ is not determined for these assays, which will be needed to calculate the absolute concentration of analytes ¹²⁶.

4.4.6 CSF-PR in determining disease-relevance

As protein changes during treatment by Natalizumab in Paper III could be due to both treatment effect and disease progression, the observed changes were compared to online datasets in CSF-PR comparing RRMS to OND in order to determine their possible effect on the disease. This enabled the comparison of thousands of proteins in a straightforward manner, otherwise only possible by an extensive literature search. Notably, the datasets in CSF-PR comparing RRMS to OND are mostly based on proteomics analysis of CSF sampled during diagnosis. This could be a possible artefact in this comparison, as the patients receiving Natalizumab are possibly further in the disease development than the RRMS cases in the CSF-PR database.

The patients in the Natalizumab study showed a high heterogeneity in treatment duration and RRMS disease progression. In particular, categories of proteins that were not changed by treatment but that were changed by RRMS could indicate disease processes that are changed early in the disease course but that are not as active in later stage of the disease. Proteins changed only by the treatment could be due to similar reasons. However, it is estimated that the diagnosis of MScl is in any case later in the

disease course than the start of pathophysiological processes, and therefore time of diagnosis could be a poor estimate of disease onset²²³⁻²²⁵. Optimally, MScl patients receiving placebo treatment should have been used as controls in this study to more accurately determine the effects of Natalizumab. This was not possible due to ethical considerations, as previously noted in⁴².

5. Discussion

This thesis is part of a larger MScl project aiming to find biomarkers of clinical use for MScl patients. The work presented in this thesis has focused on using quantitative proteomics to identify protein changes that could shed light on treatment effects for the two drugs Fingolimod (Paper I) and Natalizumab (Paper III) and their influence on disease processes in MScl. Furthermore, information from previous biomarker studies have been used to generate a biomarker assay that can monitor disease processes in patients in a manner that is comparable over time (Paper II).

5.1 Monitoring disease processes in multiple sclerosis

5.1.1 Effects of Fingolimod on remyelination

In Paper I, TMT-based proteomics was used to investigate whether the MScl drug Fingolimod affected the brain proteome in an MScl animal model. The results from both TMT-MS and IHC showed no difference in the established markers of de- and remyelination. Furthermore, few changes were observed in the proteome of the Fingolimod-treated mice compared to placebo. Thus, no beneficial effect on remyelination was observed in this study. However, proteins quantified by proteomics showed concordance with the expected changes during de- and remyelination, including a decrease of GFAP and an increase of myelin proteins such as proteolipid protein (PLP), Myelin-associated glycoprotein (MAG) and Myelin-associated oligodendrocyte basic protein (MOBP) during remyelination, thus indicating the same effects as previously observed by global brain proteomics in the cuprizone model ¹¹⁷.

Quantitative proteomics showed that the S1PR1 receptor and the g-protein subunit GNG5 was less abundant in Fingolimod-treated mice than in placebo both during demyelination and remyelination. Thus, we concluded that the drug enters the brain and affects the brain proteome. As the front part of the brain was examined by proteomics, it is not known which cell type that the downregulation is prominent in, or if the proteins are enriched in areas of de- and remyelination. Furthermore, as cuprizone demyelination is lesion-specific, perhaps investigating these proteins in demyelinated

areas could reveal both the cell type(s) involved, and relevance to lesion formation and repair.

Of note, Siponimod, a next-generation S1PR modulator, has shown to reduce demyelination, axonal damage and microglia activation in the cuprizone model ²²⁶. However, as Siponimod was administered with cuprizone in this study, the observed beneficial effects on neuronal processes might be due to the anti-inflammatory effects of the drug.

5.1.2 Effects of Natalizumab on inflammation, neurological processes and metabolism

In Paper III, the anti-inflammatory drug Natalizumab appeared to affect several processes beyond inflammation. The protein changes representing these processes were compared to previously published studies of RRMS versus controls showing substantial overlap in which proteins were affected, but also some uniqueness. Some processes were affected in the same direction and others in opposite direction between these two comparisons. Particularly interesting were proteins that were decreased in RRMS versus controls and increased after the treatment, including proteins involved in neurological processes. This association has not been this extensively documented before, and could imply previously unknown beneficial effects of the treatment.

Protein markers of de- and remyelination were not explicitly investigated in Paper III, however, several myelin proteins were detected but showed no significant difference in the proteomics discovery study except the oligodendrocyte-myelin glycoprotein that were modestly increased by the treatment. As Natalizumab is not known to affect remyelination, it was not expected to change the myelination processes.

In addition, Paper III also identified changes in metabolism that could be relevant to include as PRM assays in the future in addition to those generated in Paper II. It is not known if the changes in metabolism proteins are due to the Natalizumab treatment, or due to a disease process in RRMS that is not affected by treatment. As such, it is not known if this change in metabolism is beneficial. Including the proteins measured in the verification study in the assay of Paper II, for example, peptides representing

LDHA, LDHB, GC and APOL1, could enable further investigation of these changes and their role in MScl.

5.1.3 Monitoring multiple sclerosis by mass spectrometry-based proteomics

The balance between inflammation, neurological processes, metabolism and de- and remyelination is complex and not fully understood. Investigations in mouse models are valuable to shed light on these mechanisms individually. However, the transferability not only to MScl but to changes in the CSF proteome gives findings in animal models a longer path to clinical validation. Thus, protein changes observable in CSF of MScl patients were the obvious starting point for selecting proteins for assay generation in Paper II.

Proteomics discovery studies have detected protein changes between RRMS and OND patient groups, including several proteins with neurological or immunological activity beyond the most validated biomarkers, *e.g.*, neurofilaments and chitinase-like proteins⁹⁴. Furthermore, proteomics approaches have revealed additional processes to be affected by MScl beyond inflammation and neuronal activity, including extracellular matrix organization and cell adhesion⁹². Albeit less well documented, and further away from clinical verification, investigating the changes of proteins, other than the most validated biomarkers mentioned above, representative for disease processes could reveal more of the disease pathology. Notably, proteomics approaches have previously been successful in determining subgroups of patients with fatigue⁹¹, indicating an added value of including multiple protein markers per process. Furthermore, many of these proteins have not previously been found to change in other neurological diseases as determined by CSF-PR 2.0, and could thus, in contrast to the neurofilaments and chitinase-like proteins, be disease-specific.

Several of the assay peptides were measured in the verification process in Paper III. These included peptides representatives of the proteins neurexin 1-3, neuronal cell adhesion molecule and glutamate receptor 4, all with neurological function, and immunoglobulin J chain and chitinase-3-like protein 2, both with inflammation activity, among others. All of these were changed by the Natalizumab treatment as

proved by the discovery study, and many were also verified by PRM-MS. In Paper III this finding was therefore used as a determination of disease-relevance for the proteins as they have also been found to be affected in RRMS. However, with respect to Paper II, it implies that the assay peptides can reflect processes relevant in MScl beyond the categories they were selected to distinguish (MScl vs OND).

5.1.4 Protein changes across neurological diseases

As mentioned, changes in chitinase-like proteins and neurofilaments are used in the investigation of several neurological diseases, thus are not specific for MScl.

During the analysis of the results in Paper III, the glycolysis proteins LDHA, LDHB and PKM were increased during treatment with Natalizumab according to the discovery study, and largely confirmed by the verification study. Furthermore, CHI3L1 and IGKC that both are increased in RRMS vs controls were found as decreased in our study. Interestingly, these five proteins were included in a biomarker panel for proteins differentiating between AD and non-AD in a recent study ²²⁷.

Of note, the biological meaning of these proteomic changes as part of the Natalizumab treatment is still unknown, and should be investigated further. The patient samples were provided by our collaborators at the Charles University and General University Hospital in Prague in the Czech Republic, and clinical data from the patients at the date of sampling could be available at a later stage and enable correlation analysis between protein changes and clinical endpoints. In any case, the common relevance of these proteins in Natalizumab treatment and AD further confirms that many of the same processes represented by the same proteins are affected by different neurological diseases. Absolute protein abundance values collected across the disease groups and treatment options would enable comparison to see if certain protein levels, or changes in protein levels, are associated with disease development in MScl and/or AD.

5.2 Verification strategy

5.2.1 Database dependencies for biomarker selection

For the analysis of possible biomarker candidates in Paper II and for the analysis of discovery data in Paper III, several tools for biological annotation were used to guide the selection of candidates for further verification. The approach largely verified that the majority of changes in MScl are due to changes in proteins with neurological and immunological activity, and proteins were selected to represent these processes. One of the strengths of proteomics discovery is that the investigation of the proteome is exploratory and thus not dependent on an initial hypothesis. However, comparing proteins and selecting the ones that are the most biologically relevant to include for verification is, in many cases, hypothesis-driven. Furthermore, it is known that the proteome is not equally studied, possibly biasing the selection of biomarker candidates by favoring proteins with more data ²²⁸. This bias is hard to avoid, as proteins with known relevance to the disease are most often picked for downstream verification.

Databases were extensively used in the selection of proteins for the generation of assays in Paper II and for the verification experiment in Paper III. Here, biological function was among the factors emphasized, for the above-mentioned reasons. However, proteins that are consistently different between patient groups are also interesting biomarker candidates, independent of their biological interpretation. As such, collection of data from several studies might increase the likelihood of identify novel biomarker candidates, and strengthen their candidacy for further verification.

5.2.2 A rectangular biomarker verification strategy

A recent study used a discovery approach to identify proteins that were altered in AD by comparing the results from several discovery studies in CSF to find a biomarker panel ²²⁷. This “rectangular” approach was suggested by Geyer *et al.* to substitute the traditional “triangular” biomarker pipeline, as protein changes in the triangular approach commonly could not be subsequently verified ²²⁹, possibly due to the proteomic discovery identifying changes that are exclusive to the discovery population as they are commonly based on few samples. The creation of a biomarker panel based

on several discovery studies, they argue, increases the chance of removing study-specific confounders and detect more robust protein changes. Thus, accumulation of discovery studies over time will build up a database of proteomic patterns in response to health and disease that can be associated to different health states.

This rectangular approach is unconventional, but when applied to AD, it identified a panel of proteins that changed similarly in three different discovery studies comparing AD to non-AD ²²⁷. These proteins showed good correlation to the available literature, as proteins within the neuronal system, inflammation and metabolism were affected by AD.

In essence, this approach is similar to the approach in Paper II, where proteomics analyses of several cohorts are combined in the CSF-PR resource. We believe this strategy is the best way to ensure that the most promising candidates are chosen for verification. However, the number of possible biomarkers from CSF-PR was high. With more studies being added to the CSF-PR database, further refinement of the biomarker panel is possible.

Interestingly, the suggested rectangular approach could result in plasma proteome profiling by proteomics entering a clinical setting ²²⁷. This is opposed to the triangular approach where the endpoint is to measure a biomarker or a biomarker panel by more targeted methods. This thought is intriguing; however, it is dependent on extensive standardization of mass spectrometry-based methods and experiment design not currently available.

5.2.3 Quantification of low-abundant biomarkers

It has been argued that a distinction should be made between detectable and quantifiable peptides in mass spectrometry-based experiments. The linear area of quantification is not commonly determined in a discovery approach, as such, the magnitude of change cannot be accurately estimated at the level required for a quantitative approach ²³⁰. Pino *et al.* emphasize that the assessment of linearity is not necessarily needed for discovering differences between samples, but it is a requirement when estimating the magnitude of the difference ²³⁰.

Typically, low-abundant proteins such as CHI3L1 and CHIT are often quantified in proteomics discovery studies, however, quite paradoxically, the protein is seldomly quantified by the more sensitive PRM method. This was observed during the peptide stability tests performed in paper II, and was emphasized by the quantification of these proteins in Paper III. In the discovery study of Paper III, CHI3L1 and CHIT were significantly reduced by the Natalizumab treatment, but during verification, it became clear that the most changed protein, CHIT, could not be quantified by PRM as it was lower than the estimated LOQ in most samples.

This has led us to wonder if these proteins are too low-abundant to get a quantifiable measurement of peptide fragments, as needed in a PRM approach. During peptide testing, the signal for these low-abundant peptides increased with decreasing collision energy. In this case, more accurately quantifying the unfragmented peptide, perhaps by selected-ion monitoring, would be more appropriate for the quantification of these low abundant peptides. In this case, the linearity of the peptide signal should be assessed in order to determine if the difference in abundance is quantifiable, as mentioned above. Alternately, these proteins are commonly measured by ELISA assays, and can supplement the PRM-MS analysis.

5.3 Signal or noise

5.3.1 Technical vs biological variation

During the analysis of Paper I, the apparent batch effect between TMT experiments was a greater source of variation than that of the biological variation. This was also noted in the paper of Karp *et al.* ²⁰³, indicating that monitoring of the technical variability should be used to inform the selection of the number of biological replicates to include in the study, and thus ensure that technical variability does not overshadow the biological changes.

Upon discovering the batch effect introduced by combining TMT-experiments in Paper I, the data was heavily investigated based on the available literature at the time to properly manage this technical variability. This resulted in three different datasets, one

with the traditional *t*-test, one with internal reference scaling (as proposed in ²⁰⁹), and one after the batch effect was removed by linear modelling (final dataset). These approaches confirmed many of the same proteins as changed between Fingolimod and placebo. In particular, the downregulation of the S1PR1 receptor and the g-protein GNG5 in Fingolimod-treated mice was observed across the datasets, indicating a robustness of the observed changes.

However, since publication of Paper I, additional improved methods have been proposed for dealing with batch effects. In particular, one approach has been incorporated into the MaxQuant pipeline ²¹¹. Thus, in future studies, the batch effect can hopefully be more effectively managed.

Evaluating the biological signal compared to an estimate of both biological and technical noise is commonly done by power calculations. Thus, aiming to find the number of patients required to be able to identify a given change in the data with a given confidence. Notably, the CSF proteome has been found to be variable both between and within patients ²³¹, and could greatly benefit from such an analysis ⁹¹. However, this effect is not necessarily the same across proteins in a dataset, as some proteins are markedly more variable than others ²³¹. Thus, individual assessment of variability based on technical replicates can identify proteins that are more precisely quantified with the selected approach and help guide biomarker selection.

The technical variation was monitored by the addition of quality control (QC) samples during the analysis of CSF from Natalizumab patients in Paper III. The QC samples were mainly used as a control of sample preparation, however, the estimates of technical variation could also be included in the analysis and selection of proteins for downstream verification.

Technical variation was also monitored for each peptide in Paper II. From the various investigation of peptide stability used in the paper, there are many measurements of variation that were used to include or exclude peptides from the final assay including inter- and intra-day variation. Thus, we have good estimates of how these peptides are affected by the technical variation introduced by the analytical pipeline. Including these

estimates in the evaluation of protein changes in patient samples to determine the effect size needed to discern noise from real biological differences is an intriguing thought, and could aid further refinement of proteins in the developed biomarker assays.

5.3.2 Absolute relative quantification

Creating absolute assays that can measure the absolute abundance of proteins and peptides could make proteomic results more comparable over time. In principle, adding an internal peptide with known concentration should provide an absolute measurement of the peptide in the sample that can be used to calculate protein abundance.

However, a study by Shuford *et al.* compared the quantification of three different peptide standards (tryptic SIL peptides and peptides with flanking amino acid residues) to that of full-length recombinant protein SIL²¹⁸. The results were discouraging – the quantification of the protein varied not only between different denaturing conditions, but also greatly between the internal standards used, confirming that both sample preparation and the choice of internal standard have a great impact on the peptide quantification. Even the full length SIL protein did not accurately quantify the protein, arguably due to dissimilarities in tryptic digestion between the endogenous and heavy labelled standard. The results were however comparable within each denaturing condition and calibrator, implying that all standards can be used for relative quantification.

For the development of absolute assays in Paper II, controlling the tryptic digestion was considered essential. The best performing peptides showed great digestion stability after 16 hours, and low inter-day variation, enabling precise measurement of the peptide in the pipeline. However, it could be argued that the assay only precisely measures the peptide product under the given condition.

Notably, these limitations are also evident from ELISA measurements, with different kits/antibodies quantifying the same protein yielding very different results^{114, 232}, and thus the quantification accuracy as observed by antibody-based assays may only be directly comparable within the same experiment^{114, 214, 232}.

Interestingly, Shuford *et al.* also utilized a well-prepared external calibrator with known concentration of the analyte, which greatly improved quantification accuracy²¹⁸. The use of an external calibrator has also been suggested by the MacCoss lab, for standardization of proteomics results over time and across labs²³³. As this has been shown to greatly improve the quantification accuracy, this approach could have been combined with internal standards to ensure comparable quantification over time for the assays developed in Paper II. However, true quantification accuracy in absolute terms is most likely an elusive goal, also for targeted assays of the highest quality¹²⁶.

6. Conclusion

In this work, several neurological and immunological proteins were included in a high precision assay with proteins reflecting MScl disease processes. The protein assay can be used in wide-screen protein verification studies with precision that enables comparison over time. The inclusion of additional biomarkers in the assay is dynamic and on-going, with the long-term goal of monitoring multiple neurological diseases in a clinical setting. However, the assay is already capable of monitoring disease relevant processes, as indicated by the verified protein changes in the Natalizumab study.

Furthermore, quantitative proteomics was used to investigate treatment effect/mechanisms of two different drugs treating MScl. First, by investigating the effect of Fingolimod on the CNS proteome in an MScl animal model, and second by investigating proteome changes in the CSF of MScl patients undergoing Natalizumab treatment. The former indicated no direct effect of demyelination in the mouse model, while the latter confirmed that MScl is a disease driven by neurological and immunological processes partly affected by treatment, and implicated that metabolic changes, in particular steroid metabolism and glycolysis, should be investigated and monitored in future research.

7. Future perspectives

The downregulation of S1PR1 and GNG5 as an effect of Fingolimod treatment confirms that the drug crosses the blood-brain barrier, and thus functions inside the brain. Albeit studies have shown that de- and remyelination processes can be observed in a global proteomic approach, perhaps investigating the localization of S1PR1 and GNG5 in mouse brains could give a further indication of whether these proteins are functionally linked, and which cell population that are most affected, thus indicating possible downstream effects that were not obtainable by the global approach. In addition, investigating Siponimod in a similar fashion could be interesting, to further study the effect of this drug on the myelination processes.

The proteomic changes observed during Natalizumab treatment highlighted the previously known processes affected by the drug, in addition to new processes not previously linked to the treatment. Associating these verified protein changes to individual patient information of clinical relevance (such as MRI activity, relapses or disability progression) could help identify clinically relevant biomarkers to monitor during Natalizumab treatment, and in particular to potentially facilitate early drug switching. Furthermore, the study of paired CSF samples has proven valuable for the detection of disease mechanisms other than the well-documented neurological and inflammation processes. As such, it would be of great interest to investigate paired CSF samples also in future studies to learn more about MS disease mechanisms.

In order to widen the processes monitored by the assays, markers for both demyelination and metabolic changes could be added to the assays generated in Paper II. Use of an external standard would also be of interest, to ensure even better comparability over time. Furthermore, work to standardize and collect information from the PRM studies, allowing for easy access to the underlying data, should be developed to keep track of, for example, which peptides that have been tested and the variation for each peptide. This could be done in parallel to running patient samples, thus helping to optimize and standardize both the laboratory methods and the data collection, to further facilitate comparison over time.

References

1. Thompson, A.J., et al., *Multiple sclerosis*. Lancet, 2018. **391**(10130): p. 1622-1636.
2. Compston, A., *The 150th anniversary of the first depiction of the lesions of multiple sclerosis*. J Neurol Neurosurg Psychiatry, 1988. **51**(10): p. 1249-52.
3. JM, C., *Histologie de la sclérose en plaques*. Gazette des Hopitaux, Paris, 1868(41): p. 554-55.
4. Browne, P., et al., *Atlas of Multiple Sclerosis 2013: A growing global problem with widespread inequity*. Neurology, 2014. **83**(11): p. 1022-4.
5. Grytten, N., Ø. Torkildsen, and K.M. Myhr, *Time trends in the incidence and prevalence of multiple sclerosis in Norway during eight decades*. Acta Neurol Scand, 2015. **132**(199): p. 29-36.
6. Magyari, M. and P.S. Sorensen, *Comorbidity in Multiple Sclerosis*. Front Neurol, 2020. **11**: p. 851.
7. Lunde, H.M.B., et al., *Survival and cause of death in multiple sclerosis: a 60-year longitudinal population study*. J Neurol Neurosurg Psychiatry, 2017. **88**(8): p. 621-625.
8. Fagnani, C., et al., *Twin studies in multiple sclerosis: A meta-estimation of heritability and environmentality*. Mult Scler, 2015. **21**(11): p. 1404-13.
9. Jersild, C., et al., *Histocompatibility determinants in multiple sclerosis, with special reference to clinical course*. Lancet, 1973. **2**(7840): p. 1221-5.
10. Gregory, S.G., et al., *Interleukin 7 receptor alpha chain (IL7R) shows allelic and functional association with multiple sclerosis*. Nat Genet, 2007. **39**(9): p. 1083-91.
11. Consortium, I.M.S.G., *Multiple sclerosis genomic map implicates peripheral immune cells and microglia in susceptibility*. Science, 2019. **365**(6460).
12. Berg-Hansen, P., et al., *Prevalence of multiple sclerosis among immigrants in Norway*. Mult Scler, 2015. **21**(6): p. 695-702.
13. Dean, G. and J.F. Kurtzke, *On the risk of multiple sclerosis according to age at immigration to South Africa*. Br Med J, 1971. **3**(5777): p. 725-9.
14. Munger, K.L., et al., *Vitamin D intake and incidence of multiple sclerosis*. Neurology, 2004. **62**(1): p. 60-5.
15. Smolders, J., et al., *An Update on Vitamin D and Disease Activity in Multiple Sclerosis*. CNS Drugs, 2019. **33**(12): p. 1187-1199.
16. Bach, J.F., *The effect of infections on susceptibility to autoimmune and allergic diseases*. N Engl J Med, 2002. **347**(12): p. 911-20.
17. Bach, J.F., *Revisiting the Hygiene Hypothesis in the Context of Autoimmunity*. Front Immunol, 2020. **11**: p. 615192.
18. Guan, Y., et al., *The role of Epstein-Barr virus in multiple sclerosis: from molecular pathophysiology to in vivo imaging*. Neural Regen Res, 2019. **14**(3): p. 373-386.
19. Stys, P.K., et al., *Will the real multiple sclerosis please stand up?* Nat Rev Neurosci, 2012. **13**(7): p. 507-14.
20. Sen, M.K., et al., *Revisiting the Pathoetiology of Multiple Sclerosis: Has the Tail Been Wagging the Mouse?* Front Immunol, 2020. **11**: p. 572186.

21. Banerjee, T.K., et al., *Conversion of clinically isolated syndrome to multiple sclerosis: a prospective multi-center study in Eastern India*. *Mult Scler J Exp Transl Clin*, 2019. **5**(2): p. 2055217319849721.
22. Çınar, B.P. and S. Özakbaş, *Prediction of Conversion from Clinically Isolated Syndrome to Multiple Sclerosis According to Baseline Characteristics: A Prospective Study*. *Noro Psikiyatrs Ars*, 2018. **55**(1): p. 15-21.
23. Gaetani, L., et al., *High risk of early conversion to multiple sclerosis in clinically isolated syndromes with dissemination in space at baseline*. *J Neurol Sci*, 2017. **379**: p. 236-240.
24. McDonald, W.I., et al., *Recommended diagnostic criteria for multiple sclerosis: guidelines from the International Panel on the diagnosis of multiple sclerosis*. *Ann Neurol*, 2001. **50**(1): p. 121-7.
25. Polman, C.H., et al., *Diagnostic criteria for multiple sclerosis: 2010 revisions to the McDonald criteria*. *Ann Neurol*, 2011. **69**(2): p. 292-302.
26. Thompson, A.J., et al., *Diagnosis of multiple sclerosis: 2017 revisions of the McDonald criteria*. *Lancet Neurol*, 2018. **17**(2): p. 162-173.
27. Lublin, F.D., et al., *Defining the clinical course of multiple sclerosis: the 2013 revisions*. *Neurology*, 2014. **83**(3): p. 278-86.
28. Muraro, P.A., et al., *Long-term Outcomes After Autologous Hematopoietic Stem Cell Transplantation for Multiple Sclerosis*. *JAMA Neurol*, 2017. **74**(4): p. 459-469.
29. Kvistad, S.A.S., et al., *Safety and efficacy of autologous hematopoietic stem cell transplantation for multiple sclerosis in Norway*. *Mult Scler*, 2020. **26**(14): p. 1889-1897.
30. Hauser, S.L. and B.A.C. Cree, *Treatment of Multiple Sclerosis: A Review*. *Am J Med*, 2020. **133**(12): p. 1380-1390.e2.
31. Paty, D.W. and D.K. Li, *Interferon beta-1b is effective in relapsing-remitting multiple sclerosis. II. MRI analysis results of a multicenter, randomized, double-blind, placebo-controlled trial. UBC MS/MRI Study Group and the IFNB Multiple Sclerosis Study Group*. *Neurology*, 1993. **43**(4): p. 662-7.
32. Kinkel, R.P., et al., *IM interferon beta-1a delays definite multiple sclerosis 5 years after a first demyelinating event*. *Neurology*, 2006. **66**(5): p. 678-84.
33. Torkildsen, Ø., K.M. Myhr, and L. Bø, *Disease-modifying treatments for multiple sclerosis - a review of approved medications*. *Eur J Neurol*, 2016. **23 Suppl 1**(Suppl 1): p. 18-27.
34. Brown, J.W.L., et al., *Association of Initial Disease-Modifying Therapy With Later Conversion to Secondary Progressive Multiple Sclerosis*. *Jama*, 2019. **321**(2): p. 175-187.
35. Hutchinson, M., *Natalizumab: A new treatment for relapsing remitting multiple sclerosis*. *Ther Clin Risk Manag*, 2007. **3**(2): p. 259-68.
36. Tubridy, N., et al., *The effect of anti-alpha4 integrin antibody on brain lesion activity in MS. The UK Antegren Study Group*. *Neurology*, 1999. **53**(3): p. 466-72.
37. Lobb, R.R. and M.E. Hemler, *The pathophysiologic role of alpha 4 integrins in vivo*. *J Clin Invest*, 1994. **94**(5): p. 1722-8.

38. Guagnozzi, D. and R. Caprilli, *Natalizumab in the treatment of Crohn's disease*. *Biologics*, 2008. **2**(2): p. 275-84.
39. Polman, C.H., et al., *A randomized, placebo-controlled trial of natalizumab for relapsing multiple sclerosis*. *N Engl J Med*, 2006. **354**(9): p. 899-910.
40. Rudick, R.A., et al., *Natalizumab plus interferon beta-1a for relapsing multiple sclerosis*. *N Engl J Med*, 2006. **354**(9): p. 911-23.
41. Huggett, B., *How Tysabri survived*. *Nat Biotechnol*, 2009. **27**(11): p. 986.
42. Stoop, M.P., et al., *Effects of natalizumab treatment on the cerebrospinal fluid proteome of multiple sclerosis patients*. *J Proteome Res*, 2013. **12**(3): p. 1101-7.
43. Gunnarsson, M., et al., *Axonal damage in relapsing multiple sclerosis is markedly reduced by natalizumab*. *Ann Neurol*, 2011. **69**(1): p. 83-9.
44. Ottervald, J., et al., *Multiple sclerosis: Identification and clinical evaluation of novel CSF biomarkers*. *J Proteomics*, 2010. **73**(6): p. 1117-32.
45. Chiba, K., et al., *FTY720, a novel immunosuppressant, induces sequestration of circulating mature lymphocytes by acceleration of lymphocyte homing in rats. I. FTY720 selectively decreases the number of circulating mature lymphocytes by acceleration of lymphocyte homing*. *J Immunol*, 1998. **160**(10): p. 5037-44.
46. Kappos, L., et al., *A placebo-controlled trial of oral fingolimod in relapsing multiple sclerosis*. *N Engl J Med*, 2010. **362**(5): p. 387-401.
47. Calabresi, P.A., et al., *Safety and efficacy of fingolimod in patients with relapsing-remitting multiple sclerosis (FREEDOMS II): a double-blind, randomised, placebo-controlled, phase 3 trial*. *Lancet Neurol*, 2014. **13**(6): p. 545-56.
48. Chun, J. and H.P. Hartung, *Mechanism of action of oral fingolimod (FTY720) in multiple sclerosis*. *Clin Neuropharmacol*, 2010. **33**(2): p. 91-101.
49. Pébay, A., et al., *Sphingosine-1-phosphate induces proliferation of astrocytes: regulation by intracellular signalling cascades*. *Eur J Neurosci*, 2001. **13**(12): p. 2067-76.
50. Jaillard, C., et al., *Edg8/SIP5: an oligodendroglial receptor with dual function on process retraction and cell survival*. *J Neurosci*, 2005. **25**(6): p. 1459-69.
51. Brinkmann, V., *Sphingosine 1-phosphate receptors in health and disease: mechanistic insights from gene deletion studies and reverse pharmacology*. *Pharmacol Ther*, 2007. **115**(1): p. 84-105.
52. Groves, A., Y. Kihara, and J. Chun, *Fingolimod: direct CNS effects of sphingosine 1-phosphate (SIP) receptor modulation and implications in multiple sclerosis therapy*. *J Neurol Sci*, 2013. **328**(1-2): p. 9-18.
53. Miron, V.E., et al., *Fingolimod (FTY720) enhances remyelination following demyelination of organotypic cerebellar slices*. *Am J Pathol*, 2010. **176**(6): p. 2682-94.
54. Yazdi, A., M. Ghasemi-Kasman, and M. Javan, *Possible regenerative effects of fingolimod (FTY720) in multiple sclerosis disease: An overview on remyelination process*. *J Neurosci Res*, 2020. **98**(3): p. 524-536.
55. Denic, A., et al., *The relevance of animal models in multiple sclerosis research*. *Pathophysiology*, 2011. **18**(1): p. 21-9.

-
56. Lassmann, H. and M. Bradl, *Multiple sclerosis: experimental models and reality*. Acta Neuropathol, 2017. **133**(2): p. 223-244.
 57. Torre-Fuentes, L., et al., *Experimental models of demyelination and remyelination*. Neurologia, 2020. **35**(1): p. 32-39.
 58. Al-Ani, M.R., et al., *Rituximab Prevents the Development of Experimental Autoimmune Encephalomyelitis (EAE): Comparison with Prophylactic, Therapeutic or Combinational Regimens*. J Inflamm Res, 2020. **13**: p. 151-164.
 59. Plemel, J.R., W.Q. Liu, and V.W. Yong, *Remyelination therapies: a new direction and challenge in multiple sclerosis*. Nat Rev Drug Discov, 2017. **16**(9): p. 617-634.
 60. Cunniffe, N. and A. Coles, *Promoting remyelination in multiple sclerosis*. J Neurol, 2021. **268**(1): p. 30-44.
 61. Matsushima, G.K. and P. Morell, *The neurotoxicant, cuprizone, as a model to study demyelination and remyelination in the central nervous system*. Brain Pathol, 2001. **11**(1): p. 107-16.
 62. Jhelum, P., et al., *Ferroptosis Mediates Cuprizone-Induced Loss of Oligodendrocytes and Demyelination*. J Neurosci, 2020. **40**(48): p. 9327-9341.
 63. *Finishing the euchromatic sequence of the human genome*. Nature, 2004. **431**(7011): p. 931-45.
 64. Anderson, N.L. and N.G. Anderson, *Proteome and proteomics: new technologies, new concepts, and new words*. Electrophoresis, 1998. **19**(11): p. 1853-61.
 65. Robles, M.S., J. Cox, and M. Mann, *In-vivo quantitative proteomics reveals a key contribution of post-transcriptional mechanisms to the circadian regulation of liver metabolism*. PLoS Genet, 2014. **10**(1): p. e1004047.
 66. *A gene-centric human proteome project: HUPO--the Human Proteome organization*. Mol Cell Proteomics, 2010. **9**(2): p. 427-9.
 67. Adhikari, S., et al., *A high-stringency blueprint of the human proteome*. Nat Commun, 2020. **11**(1): p. 5301.
 68. Smith, L.M. and N.L. Kelleher, *Proteoform: a single term describing protein complexity*. Nat Methods, 2013. **10**(3): p. 186-7.
 69. Aebersold, R. and M. Mann, *Mass-spectrometric exploration of proteome structure and function*. Nature, 2016. **537**(7620): p. 347-55.
 70. Pandey, A. and M. Mann, *Proteomics to study genes and genomes*. Nature, 2000. **405**(6788): p. 837-46.
 71. Tumani, H., *Physiology and Constituents of CSF*, in *Cerebrospinal Fluid in Clinical Neurology*, F. Deisenhammer, et al., Editors. 2015, Springer International Publishing: Cham. p. 25-34.
 72. Roche, S., A. Gabelle, and S. Lehmann, *Clinical proteomics of the cerebrospinal fluid: Towards the discovery of new biomarkers*. Proteomics Clin Appl, 2008. **2**(3): p. 428-36.
 73. Hühmer, A.F., et al., *Protein analysis in human cerebrospinal fluid: Physiological aspects, current progress and future challenges*. Dis Markers, 2006. **22**(1-2): p. 3-26.

-
74. Kaufmann, A. and S. Walker, *Comparison of linear intrascan and interscan dynamic ranges of Orbitrap and ion-mobility time-of-flight mass spectrometers*. Rapid Commun Mass Spectrom, 2017. **31**(22): p. 1915-1926.
 75. Macron, C., et al., *Deep Dive on the Proteome of Human Cerebrospinal Fluid: A Valuable Data Resource for Biomarker Discovery and Missing Protein Identification*. J Proteome Res, 2018. **17**(12): p. 4113-4126.
 76. Gulbrandsen, A., et al., *In-depth characterization of the cerebrospinal fluid (CSF) proteome displayed through the CSF proteome resource (CSF-PR)*. Mol Cell Proteomics, 2014. **13**(11): p. 3152-63.
 77. Zhang, Y., et al., *A comprehensive map and functional annotation of the normal human cerebrospinal fluid proteome*. J Proteomics, 2015. **119**: p. 90-9.
 78. Califf, R.M., *Biomarker definitions and their applications*. Exp Biol Med (Maywood), 2018. **243**(3): p. 213-221.
 79. Paul, A., M. Comabella, and R. Gandhi, *Biomarkers in Multiple Sclerosis*. Cold Spring Harb Perspect Med, 2019. **9**(3).
 80. Parker, C.E. and C.H. Borchers, *Mass spectrometry based biomarker discovery, verification, and validation--quality assurance and control of protein biomarker assays*. Mol Oncol, 2014. **8**(4): p. 840-58.
 81. Rifai, N., M.A. Gillette, and S.A. Carr, *Protein biomarker discovery and validation: the long and uncertain path to clinical utility*. Nat Biotechnol, 2006. **24**(8): p. 971-83.
 82. Paulovich, A.G., et al., *The interface between biomarker discovery and clinical validation: The tar pit of the protein biomarker pipeline*. Proteomics Clin Appl, 2008. **2**(10-11): p. 1386-1402.
 83. Anderson, N.L. and N.G. Anderson, *The human plasma proteome: history, character, and diagnostic prospects*. Mol Cell Proteomics, 2002. **1**(11): p. 845-67.
 84. Haider, L., et al., *The topography of demyelination and neurodegeneration in the multiple sclerosis brain*. Brain, 2016. **139**(Pt 3): p. 807-15.
 85. Farias, A.S., et al., *Ten years of proteomics in multiple sclerosis*. Proteomics, 2014. **14**(4-5): p. 467-80.
 86. Salvisberg, C., et al., *Exploring the human tear fluid: discovery of new biomarkers in multiple sclerosis*. Proteomics Clin Appl, 2014. **8**(3-4): p. 185-94.
 87. Singh, V., et al., *Proteomics urine analysis of pregnant women suffering from multiple sclerosis*. J Proteome Res, 2015. **14**(5): p. 2065-73.
 88. Engelborghs, S., et al., *Consensus guidelines for lumbar puncture in patients with neurological diseases*. Alzheimers Dement (Amst), 2017. **8**: p. 111-126.
 89. Kabat, E.A., D.H. Moore, and H. Landow, *AN ELECTROPHORETIC STUDY OF THE PROTEIN COMPONENTS IN CEREBROSPINAL FLUID AND THEIR RELATIONSHIP TO THE SERUM PROTEINS*. J Clin Invest, 1942. **21**(5): p. 571-7.
 90. Kroksveen, A.C., et al., *Quantitative proteomics suggests decrease in the secretogranin-1 cerebrospinal fluid levels during the disease course of multiple sclerosis*. Proteomics, 2015. **15**(19): p. 3361-9.

-
91. Opsahl, J.A., et al., *Label-free analysis of human cerebrospinal fluid addressing various normalization strategies and revealing protein groups affected by multiple sclerosis*. *Proteomics*, 2016. **16**(7): p. 1154-65.
 92. Kroksveen, A.C., et al., *In-Depth Cerebrospinal Fluid Quantitative Proteome and Deglycoproteome Analysis: Presenting a Comprehensive Picture of Pathways and Processes Affected by Multiple Sclerosis*. *J Proteome Res*, 2017. **16**(1): p. 179-194.
 93. Mosleth, E.F., et al., *Cerebrospinal fluid proteome shows disrupted neuronal development in multiple sclerosis*. *Sci Rep*, 2021. **11**(1): p. 4087.
 94. Kroksveen, A.C., et al., *Cerebrospinal fluid proteomics in multiple sclerosis*. *Biochim Biophys Acta*, 2015. **1854**(7): p. 746-56.
 95. Kroksveen, A.C., et al., *Cerebrospinal fluid proteome comparison between multiple sclerosis patients and controls*. *Acta Neurol Scand Suppl*, 2012(195): p. 90-6.
 96. Rajalahti, T., et al., *A multivariate approach to reveal biomarker signatures for disease classification: application to mass spectral profiles of cerebrospinal fluid from patients with multiple sclerosis*. *J Proteome Res*, 2010. **9**(7): p. 3608-20.
 97. Guldbrandsen, A., et al., *CSF-PR 2.0: An Interactive Literature Guide to Quantitative Cerebrospinal Fluid Mass Spectrometry Data from Neurodegenerative Disorders*. *Mol Cell Proteomics*, 2017. **16**(2): p. 300-309.
 98. Hinsinger, G., et al., *Chitinase 3-like proteins as diagnostic and prognostic biomarkers of multiple sclerosis*. *Mult Scler*, 2015. **21**(10): p. 1251-61.
 99. Schutzer, S.E., et al., *Gray matter is targeted in first-attack multiple sclerosis*. *PLoS One*, 2013. **8**(9): p. e66117.
 100. Stoop, M.P., et al., *Decreased Neuro-Axonal Proteins in CSF at First Attack of Suspected Multiple Sclerosis*. *Proteomics Clin Appl*, 2017. **11**(11-12).
 101. Singh, V., A. Tripathi, and R. Dutta, *Proteomic Approaches to Decipher Mechanisms Underlying Pathogenesis in Multiple Sclerosis Patients*. *Proteomics*, 2019. **19**(16): p. e1800335.
 102. Pintea, R., X. Montalban, and M. Comabella, *Chitinases and chitinase-like proteins as biomarkers in neurologic disorders*. *Neurol Neuroimmunol Neuroinflamm*, 2021. **8**(1).
 103. Comabella, M., et al., *Cerebrospinal fluid chitinase 3-like 1 levels are associated with conversion to multiple sclerosis*. *Brain*, 2010. **133**(Pt 4): p. 1082-93.
 104. Harris, V.K., J.F. Tuddenham, and S.A. Sadiq, *Biomarkers of multiple sclerosis: current findings*. *Degener Neurol Neuromuscul Dis*, 2017. **7**: p. 19-29.
 105. Khalil, M., et al., *Neurofilaments as biomarkers in neurological disorders*. *Nat Rev Neurol*, 2018. **14**(10): p. 577-589.
 106. Kuhle, J., et al., *Fingolimod and CSF neurofilament light chain levels in relapsing-remitting multiple sclerosis*. *Neurology*, 2015. **84**(16): p. 1639-43.
 107. Sandberg, L., et al., *Vitamin D and axonal injury in multiple sclerosis*. *Mult Scler*, 2016. **22**(8): p. 1027-31.

108. Martínez, M.A., et al., *Glial and neuronal markers in cerebrospinal fluid predict progression in multiple sclerosis*. *Mult Scler*, 2015. **21**(5): p. 550-61.
109. Varhaug, K.N., et al., *Neurofilament light chain predicts disease activity in relapsing-remitting MS*. *Neurol Neuroimmunol Neuroinflamm*, 2018. **5**(1): p. e422.
110. Petzold, A., *The prognostic value of CSF neurofilaments in multiple sclerosis at 15-year follow-up*. *J Neurol Neurosurg Psychiatry*, 2015. **86**(12): p. 1388-90.
111. Petzold, A., et al., *Elevated CSF neurofilament proteins predict brain atrophy: A 15-year follow-up study*. *Mult Scler*, 2016. **22**(9): p. 1154-62.
112. Dhiman, K., et al., *Cerebrospinal fluid neurofilament light concentration predicts brain atrophy and cognition in Alzheimer's disease*. *Alzheimers Dement (Amst)*, 2020. **12**(1): p. e12005.
113. Lin, Y.S., et al., *Levels of plasma neurofilament light chain and cognitive function in patients with Alzheimer or Parkinson disease*. *Sci Rep*, 2018. **8**(1): p. 17368.
114. Poesen, K. and P. Van Damme, *Diagnostic and Prognostic Performance of Neurofilaments in ALS*. *Front Neurol*, 2018. **9**: p. 1167.
115. Kanata, E., et al., *Cerebrospinal fluid neurofilament light in suspected sporadic Creutzfeldt-Jakob disease*. *J Clin Neurosci*, 2019. **60**: p. 124-127.
116. Virhammar, J., et al., *Biomarkers for central nervous system injury in cerebrospinal fluid are elevated in COVID-19 and associated with neurological symptoms and disease severity*. *Eur J Neurol*, 2020.
117. Werner, S.R., et al., *Proteomic analysis of demyelinated and remyelinating brain tissue following dietary cuprizone administration*. *J Mol Neurosci*, 2010. **42**(2): p. 210-25.
118. Gudi, V., et al., *Regional differences between grey and white matter in cuprizone induced demyelination*. *Brain Res*, 2009. **1283**: p. 127-38.
119. Hibbits, N., et al., *Astrogliosis during acute and chronic cuprizone demyelination and implications for remyelination*. *ASN Neuro*, 2012. **4**(6): p. 393-408.
120. Oveland, E., et al., *Cuprizone and EAE mouse frontal cortex proteomics revealed proteins altered in multiple sclerosis*. *Sci Rep*, 2021. **11**(1): p. 7174.
121. Jia, Y., et al., *Development of protein biomarkers in cerebrospinal fluid for secondary progressive multiple sclerosis using selected reaction monitoring mass spectrometry (SRM-MS)*. *Clin Proteomics*, 2012. **9**(1): p. 9.
122. Aebersold, R. and M. Mann, *Mass spectrometry-based proteomics*. *Nature*, 2003. **422**(6928): p. 198-207.
123. Hansson, K.T., et al., *Expanding the cerebrospinal fluid endopeptidome*. *Proteomics*, 2017. **17**(5).
124. Skillbäck, T., et al., *A novel quantification-driven proteomic strategy identifies an endogenous peptide of pleiotrophin as a new biomarker of Alzheimer's disease*. *Sci Rep*, 2017. **7**(1): p. 13333.
125. Nesvizhskii, A.I. and R. Aebersold, *Interpretation of shotgun proteomic data: the protein inference problem*. *Mol Cell Proteomics*, 2005. **4**(10): p. 1419-40.

-
126. Carr, S.A., et al., *Targeted peptide measurements in biology and medicine: best practices for mass spectrometry-based assay development using a fit-for-purpose approach*. Mol Cell Proteomics, 2014. **13**(3): p. 907-17.
 127. Duncan, M.W., R. Aebersold, and R.M. Caprioli, *The pros and cons of peptide-centric proteomics*. Nat Biotechnol, 2010. **28**(7): p. 659-64.
 128. Fornelli, L., et al., *Advancing Top-down Analysis of the Human Proteome Using a Benchtop Quadrupole-Orbitrap Mass Spectrometer*. J Proteome Res, 2017. **16**(2): p. 609-618.
 129. Park, J., et al., *Informed-Proteomics: open-source software package for top-down proteomics*. Nat Methods, 2017. **14**(9): p. 909-914.
 130. Toby, T.K., L. Fornelli, and N.L. Kelleher, *Progress in Top-Down Proteomics and the Analysis of Proteoforms*. Annu Rev Anal Chem (Palo Alto Calif), 2016. **9**(1): p. 499-519.
 131. Brown, K.A., et al., *Top-down proteomics: challenges, innovations, and applications in basic and clinical research*. Expert Rev Proteomics, 2020. **17**(10): p. 719-733.
 132. Shaw, C., *Peptide purification by reverse-phase HPLC*. Methods Mol Biol, 1994. **32**: p. 275-87.
 133. Regnier, F.E., *High-performance liquid chromatography of biopolymers*. Science, 1983. **222**(4621): p. 245-52.
 134. Wilson, S.R., et al., *Nano-LC in proteomics: recent advances and approaches*. Bioanalysis, 2015. **7**(14): p. 1799-815.
 135. Fitch, W.L., et al., *Using LC Retention Times in Organic Structure Determination: Drug Metabolite Identification*. Drug Metab Lett, 2018. **12**(2): p. 93-100.
 136. Henneman, A. and M. Palmblad, *Retention Time Prediction and Protein Identification*. Methods Mol Biol, 2020. **2051**: p. 115-132.
 137. Norris, J.L. and R.M. Caprioli, *Analysis of tissue specimens by matrix-assisted laser desorption/ionization imaging mass spectrometry in biological and clinical research*. Chem Rev, 2013. **113**(4): p. 2309-42.
 138. Steen, H. and M. Mann, *The ABC's (and XYZ's) of peptide sequencing*. Nat Rev Mol Cell Biol, 2004. **5**(9): p. 699-711.
 139. Makarov, A., *Electrostatic axially harmonic orbital trapping: a high-performance technique of mass analysis*. Anal Chem, 2000. **72**(6): p. 1156-62.
 140. Hu, Q., et al., *The Orbitrap: a new mass spectrometer*. J Mass Spectrom, 2005. **40**(4): p. 430-43.
 141. Pappin, D.J., P. Hojrup, and A.J. Bleasby, *Rapid identification of proteins by peptide-mass fingerprinting*. Curr Biol, 1993. **3**(6): p. 327-32.
 142. Michalski, A., J. Cox, and M. Mann, *More than 100,000 detectable peptide species elute in single shotgun proteomics runs but the majority is inaccessible to data-dependent LC-MS/MS*. J Proteome Res, 2011. **10**(4): p. 1785-93.
 143. Bruderer, R., et al., *Extending the limits of quantitative proteome profiling with data-independent acquisition and application to acetaminophen-treated three-dimensional liver microtissues*. Mol Cell Proteomics, 2015. **14**(5): p. 1400-10.

-
144. Tabb, D.L., et al., *Repeatability and reproducibility in proteomic identifications by liquid chromatography-tandem mass spectrometry*. J Proteome Res, 2010. **9**(2): p. 761-76.
 145. Barkovits, K., et al., *Reproducibility, Specificity and Accuracy of Relative Quantification Using Spectral Library-based Data-independent Acquisition*. Mol Cell Proteomics, 2020. **19**(1): p. 181-197.
 146. Zhang, F., et al., *Data-Independent Acquisition Mass Spectrometry-Based Proteomics and Software Tools: A Glimpse in 2020*. Proteomics, 2020. **20**(17-18): p. e1900276.
 147. Messner, C.B., et al., *Ultra-fast proteomics with Scanning SWATH*. Nat Biotechnol, 2021.
 148. Panchaud, A., et al., *Precursor acquisition independent from ion count: how to dive deeper into the proteomics ocean*. Anal Chem, 2009. **81**(15): p. 6481-8.
 149. Thompson, A., et al., *Tandem mass tags: a novel quantification strategy for comparative analysis of complex protein mixtures by MS/MS*. Anal Chem, 2003. **75**(8): p. 1895-904.
 150. Thompson, A., et al., *TMTpro: Design, Synthesis, and Initial Evaluation of a Proline-Based Isobaric 16-Plex Tandem Mass Tag Reagent Set*. Anal Chem, 2019. **91**(24): p. 15941-15950.
 151. Lesur, A. and B. Domon, *Advances in high-resolution accurate mass spectrometry application to targeted proteomics*. Proteomics, 2015. **15**(5-6): p. 880-90.
 152. Pino, L.K., et al., *The Skyline ecosystem: Informatics for quantitative mass spectrometry proteomics*. Mass Spectrom Rev, 2020. **39**(3): p. 229-244.
 153. Zhou, W., E.F. Petricoin, 3rd, and C. Longo, *Mass Spectrometry-Based Biomarker Discovery*. Methods Mol Biol, 2017. **1606**: p. 297-311.
 154. Cox, J., et al., *Accurate proteome-wide label-free quantification by delayed normalization and maximal peptide ratio extraction, termed MaxLFQ*. Mol Cell Proteomics, 2014. **13**(9): p. 2513-26.
 155. Marx, V., *Targeted proteomics*. Nat Methods, 2013. **10**(1): p. 19-22.
 156. Borràs, E. and E. Sabidó, *What is targeted proteomics? A concise revision of targeted acquisition and targeted data analysis in mass spectrometry*. Proteomics, 2017. **17**(17-18).
 157. Bourmaud, A., S. Gallien, and B. Domon, *Parallel reaction monitoring using quadrupole-Orbitrap mass spectrometer: Principle and applications*. Proteomics, 2016. **16**(15-16): p. 2146-59.
 158. Mani, D.R., S.E. Abbatiello, and S.A. Carr, *Statistical characterization of multiple-reaction monitoring mass spectrometry (MRM-MS) assays for quantitative proteomics*. BMC Bioinformatics, 2012. **13 Suppl 16**(Suppl 16): p. S9.
 159. Galitzine, C., et al., *Nonlinear Regression Improves Accuracy of Characterization of Multiplexed Mass Spectrometric Assays*. Mol Cell Proteomics, 2018. **17**(5): p. 913-924.
 160. Vandermarliere, E., M. Mueller, and L. Martens, *Getting intimate with trypsin, the leading protease in proteomics*. Mass Spectrom Rev, 2013. **32**(6): p. 453-65.

-
161. Tsiatsiani, L. and A.J. Heck, *Proteomics beyond trypsin*. *Febs j*, 2015. **282**(14): p. 2612-26.
 162. Giansanti, P., et al., *Six alternative proteases for mass spectrometry-based proteomics beyond trypsin*. *Nat Protoc*, 2016. **11**(5): p. 993-1006.
 163. Dau, T., G. Bartolomucci, and J. Rappsilber, *Proteomics Using Protease Alternatives to Trypsin Benefits from Sequential Digestion with Trypsin*. *Anal Chem*, 2020. **92**(14): p. 9523-9527.
 164. Shen, Y., et al., *Ultra-high-efficiency strong cation exchange LC/RPLC/MS/MS for high dynamic range characterization of the human plasma proteome*. *Anal Chem*, 2004. **76**(4): p. 1134-44.
 165. Phillips, H.L., et al., *Shotgun proteome analysis utilising mixed mode (reversed phase-anion exchange chromatography) in conjunction with reversed phase liquid chromatography mass spectrometry analysis*. *Proteomics*, 2010. **10**(16): p. 2950-60.
 166. Batth, T.S., C. Francavilla, and J.V. Olsen, *Off-line high-pH reversed-phase fractionation for in-depth phosphoproteomics*. *J Proteome Res*, 2014. **13**(12): p. 6176-86.
 167. Magaki, S., et al., *An Introduction to the Performance of Immunohistochemistry*. *Methods Mol Biol*, 2019. **1897**: p. 289-298.
 168. Kluver, H. and E. Barrera, *A method for the combined staining of cells and fibers in the nervous system*. *J Neuropathol Exp Neurol*, 1953. **12**(4): p. 400-3.
 169. Lindner, M., et al., *Sequential myelin protein expression during remyelination reveals fast and efficient repair after central nervous system demyelination*. *Neuropathol Appl Neurobiol*, 2008. **34**(1): p. 105-14.
 170. Hiremath, M.M., et al., *Microglial/macrophage accumulation during cuprizone-induced demyelination in C57BL/6 mice*. *J Neuroimmunol*, 1998. **92**(1-2): p. 38-49.
 171. Verheggen, K., et al., *Anatomy and evolution of database search engines-a central component of mass spectrometry based proteomic workflows*. *Mass Spectrom Rev*, 2020. **39**(3): p. 292-306.
 172. Elias, J.E. and S.P. Gygi, *Target-decoy search strategy for mass spectrometry-based proteomics*. *Methods Mol Biol*, 2010. **604**: p. 55-71.
 173. Cox, J., et al., *Andromeda: a peptide search engine integrated into the MaxQuant environment*. *J Proteome Res*, 2011. **10**(4): p. 1794-805.
 174. Dorfer, V., et al., *MS Amanda, a universal identification algorithm optimized for high accuracy tandem mass spectra*. *J Proteome Res*, 2014. **13**(8): p. 3679-84.
 175. Geer, L.Y., et al., *Open mass spectrometry search algorithm*. *J Proteome Res*, 2004. **3**(5): p. 958-64.
 176. Perkins, D.N., et al., *Probability-based protein identification by searching sequence databases using mass spectrometry data*. *Electrophoresis*, 1999. **20**(18): p. 3551-67.
 177. Vaudel, M., et al., *Shedding light on black boxes in protein identification*. *Proteomics*, 2014. **14**(9): p. 1001-5.
 178. Vaudel, M., et al., *PeptideShaker enables reanalysis of MS-derived proteomics data sets*. *Nat Biotechnol*, 2015. **33**(1): p. 22-4.

-
179. Matthiesen, R. and A.S. Carvalho, *Methods and algorithms for relative quantitative proteomics by mass spectrometry*. *Methods Mol Biol*, 2010. **593**: p. 187-204.
 180. Tyanova, S., T. Temu, and J. Cox, *The MaxQuant computational platform for mass spectrometry-based shotgun proteomics*. *Nat Protoc*, 2016. **11**(12): p. 2301-2319.
 181. Deutsch, E.W., et al., *Trans-Proteomic Pipeline, a standardized data processing pipeline for large-scale reproducible proteomics informatics*. *Proteomics Clin Appl*, 2015. **9**(7-8): p. 745-54.
 182. Bereman, M.S., et al., *The development of selected reaction monitoring methods for targeted proteomics via empirical refinement*. *Proteomics*, 2012. **12**(8): p. 1134-41.
 183. Perez-Riverol, Y., et al., *The PRIDE database and related tools and resources in 2019: improving support for quantification data*. *Nucleic Acids Res*, 2019. **47**(D1): p. D442-d450.
 184. Sharma, V., et al., *Panorama Public: A Public Repository for Quantitative Data Sets Processed in Skyline*. *Mol Cell Proteomics*, 2018. **17**(6): p. 1239-1244.
 185. Vaudel, M., et al., *Exploring the potential of public proteomics data*. *Proteomics*, 2016. **16**(2): p. 214-25.
 186. Wadi, L., et al., *Impact of outdated gene annotations on pathway enrichment analysis*. *Nat Methods*, 2016. **13**(9): p. 705-6.
 187. *UniProt: the universal protein knowledgebase in 2021*. *Nucleic Acids Res*, 2021. **49**(D1): p. D480-d489.
 188. Ashburner, M., et al., *Gene ontology: tool for the unification of biology. The Gene Ontology Consortium*. *Nat Genet*, 2000. **25**(1): p. 25-9.
 189. *The Gene Ontology resource: enriching a Gold mine*. *Nucleic Acids Res*, 2021. **49**(D1): p. D325-d334.
 190. Jassal, B., et al., *The reactome pathway knowledgebase*. *Nucleic Acids Res*, 2020. **48**(D1): p. D498-d503.
 191. Fabregat, A., et al., *Reactome pathway analysis: a high-performance in-memory approach*. *BMC Bioinformatics*, 2017. **18**(1): p. 142.
 192. Kanehisa, M., et al., *KEGG as a reference resource for gene and protein annotation*. *Nucleic Acids Res*, 2016. **44**(D1): p. D457-62.
 193. Sánchez, L.F.H., et al., *PathwayMatcher: proteoform-centric network construction enables fine-granularity multiomics pathway mapping*. *Gigascience*, 2019. **8**(8).
 194. Mi, H., et al., *Large-scale gene function analysis with the PANTHER classification system*. *Nat Protoc*, 2013. **8**(8): p. 1551-66.
 195. Shannon, P., et al., *Cytoscape: a software environment for integrated models of biomolecular interaction networks*. *Genome Res*, 2003. **13**(11): p. 2498-504.
 196. Szklarczyk, D., et al., *STRING v11: protein-protein association networks with increased coverage, supporting functional discovery in genome-wide experimental datasets*. *Nucleic Acids Res*, 2019. **47**(D1): p. D607-d613.

-
197. Guldbrandsen, A., et al., *Essential Features and Use Cases of the Cerebrospinal Fluid Proteome Resource (CSF-PR)*. *Methods Mol Biol*, 2019. **2044**: p. 377-391.
 198. Bhowmick, P., et al., *An Update on MRMAssayDB: A Comprehensive Resource for Targeted Proteomics Assays in the Community*. *J Proteome Res*, 2021.
 199. Wergeland, S., et al., *The cuprizone model: regional heterogeneity of pathology*. *Apmis*, 2012. **120**(8): p. 648-57.
 200. Herculano-Houzel, S., B. Mota, and R. Lent, *Cellular scaling rules for rodent brains*. *Proc Natl Acad Sci U S A*, 2006. **103**(32): p. 12138-43.
 201. Sellner, J. and P.S. Rommer, *A review of the evidence for a natalizumab exit strategy for patients with multiple sclerosis*. *Autoimmun Rev*, 2019. **18**(3): p. 255-261.
 202. Burger, B., M. Vaudel, and H. Barsnes, *Importance of Block Randomization When Designing Proteomics Experiments*. *J Proteome Res*, 2021. **20**(1): p. 122-128.
 203. Karp, N.A. and K.S. Lilley, *Investigating sample pooling strategies for DIGE experiments to address biological variability*. *Proteomics*, 2009. **9**(2): p. 388-97.
 204. Choi, M., et al., *ABRF Proteome Informatics Research Group (iPRG) 2015 Study: Detection of Differentially Abundant Proteins in Label-Free Quantitative LC-MS/MS Experiments*. *J Proteome Res*, 2017. **16**(2): p. 945-957.
 205. Megger, D.A., et al., *Comparison of label-free and label-based strategies for proteome analysis of hepatoma cell lines*. *Biochim Biophys Acta*, 2014. **1844**(5): p. 967-76.
 206. Savitski, M.M., et al., *Measuring and managing ratio compression for accurate iTRAQ/TMT quantification*. *J Proteome Res*, 2013. **12**(8): p. 3586-98.
 207. Hogrebe, A., et al., *Benchmarking common quantification strategies for large-scale phosphoproteomics*. *Nat Commun*, 2018. **9**(1): p. 1045.
 208. Brenes, A., et al., *Multibatch TMT Reveals False Positives, Batch Effects and Missing Values*. *Mol Cell Proteomics*, 2019. **18**(10): p. 1967-1980.
 209. Plubell, D.L., et al., *Extended Multiplexing of Tandem Mass Tags (TMT) Labeling Reveals Age and High Fat Diet Specific Proteome Changes in Mouse Epididymal Adipose Tissue*. *Mol Cell Proteomics*, 2017. **16**(5): p. 873-890.
 210. Nygaard, V., E.A. Rødland, and E. Hovig, *Methods that remove batch effects while retaining group differences may lead to exaggerated confidence in downstream analyses*. *Biostatistics*, 2016. **17**(1): p. 29-39.
 211. Yu, S.H., P. Kyriakidou, and J. Cox, *Isobaric Matching between Runs and Novel PSM-Level Normalization in MaxQuant Strongly Improve Reporter Ion-Based Quantification*. *J Proteome Res*, 2020. **19**(10): p. 3945-3954.
 212. Uhlén, M., et al., *Proteomics. Tissue-based map of the human proteome*. *Science*, 2015. **347**(6220): p. 1260419.
 213. Bielow, C., G. Mastrobuoni, and S. Kempa, *Proteomics Quality Control: Quality Control Software for MaxQuant Results*. *J Proteome Res*, 2016. **15**(3): p. 777-87.

214. Baker, M., *Reproducibility crisis: Blame it on the antibodies*. *Nature*, 2015. **521**(7552): p. 274-6.
215. Aebersold, R., A.L. Burlingame, and R.A. Bradshaw, *Western blots versus selected reaction monitoring assays: time to turn the tables?* *Mol Cell Proteomics*, 2013. **12**(9): p. 2381-2.
216. Gallien, S., et al., *Technical considerations for large-scale parallel reaction monitoring analysis*. *J Proteomics*, 2014. **100**: p. 147-59.
217. Scott, K.B., I.V. Turko, and K.W. Phinney, *Quantitative performance of internal standard platforms for absolute protein quantification using multiple reaction monitoring-mass spectrometry*. *Anal Chem*, 2015. **87**(8): p. 4429-35.
218. Shuford, C.M., et al., *Absolute Protein Quantification by Mass Spectrometry: Not as Simple as Advertised*. *Anal Chem*, 2017. **89**(14): p. 7406-7415.
219. Addona, T.A., et al., *Multi-site assessment of the precision and reproducibility of multiple reaction monitoring-based measurements of proteins in plasma*. *Nat Biotechnol*, 2009. **27**(7): p. 633-41.
220. Kuzyk, M.A., et al., *Multiple reaction monitoring-based, multiplexed, absolute quantitation of 45 proteins in human plasma*. *Mol Cell Proteomics*, 2009. **8**(8): p. 1860-77.
221. Shuford, C.M., et al., *Peptide production and decay rates affect the quantitative accuracy of protein cleavage isotope dilution mass spectrometry (PC-IDMS)*. *Mol Cell Proteomics*, 2012. **11**(9): p. 814-23.
222. Grant, R.P. and A.N. Hoofnagle, *From lost in translation to paradise found: enabling protein biomarker method transfer by mass spectrometry*. *Clin Chem*, 2014. **60**(7): p. 941-4.
223. Wijnands, J.M.A., et al., *Health-care use before a first demyelinating event suggestive of a multiple sclerosis prodrome: a matched cohort study*. *Lancet Neurol*, 2017. **16**(6): p. 445-451.
224. Habek, M. and M. Krbot Skorić, *Autonomic nervous system: a key player in prodromal multiple sclerosis?* *Clin Auton Res*, 2020. **30**(2): p. 97-99.
225. Yamout, B. and M. Al Khawajah, *Radiologically isolated syndrome and multiple sclerosis*. *Mult Scler Relat Disord*, 2017. **17**: p. 234-237.
226. Behrangi, N., F. Fischbach, and M. Kipp, *Mechanism of Siponimod: Anti-Inflammatory and Neuroprotective Mode of Action*. *Cells*, 2019. **8**(1).
227. Bader, J.M., et al., *Proteome profiling in cerebrospinal fluid reveals novel biomarkers of Alzheimer's disease*. *Mol Syst Biol*, 2020. **16**(6): p. e9356.
228. Burger, B., et al., *Analyzing the Structure of Pathways and Its Influence on the Interpretation of Biomedical Proteomics Data Sets*. *J Proteome Res*, 2018. **17**(11): p. 3801-3809.
229. Geyer, P.E., et al., *Revisiting biomarker discovery by plasma proteomics*. *Mol Syst Biol*, 2017. **13**(9): p. 942.
230. Pino, L.K., et al., *Matrix-Matched Calibration Curves for Assessing Analytical Figures of Merit in Quantitative Proteomics*. *J Proteome Res*, 2020. **19**(3): p. 1147-1153.
231. Schilde, L.M., et al., *Protein variability in cerebrospinal fluid and its possible implications for neurological protein biomarker research*. *PLoS One*, 2018. **13**(11): p. e0206478.

-
232. Kinn Rød, A.M., et al., *Comparison of commercial ELISA assays for quantification of corticosterone in serum*. *Sci Rep*, 2017. **7**(1): p. 6748.
 233. Pino, L.K., et al., *Calibration Using a Single-Point External Reference Material Harmonizes Quantitative Mass Spectrometry Proteomics Data between Platforms and Laboratories*. *Anal Chem*, 2018. **90**(21): p. 13112-13117.

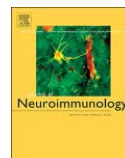
Paper I



ELSEVIER

Contents lists available at ScienceDirect

Journal of Neuroimmunology

journal homepage: www.elsevier.com/locate/jneuroim

Fingolimod downregulates brain sphingosine-1-phosphate receptor 1 levels but does not promote remyelination or neuroprotection in the cuprizone model

Agnes E. Nystad^{a,b,*}, Ragnhild Reehorst Lereim^{c,d}, Stig Wergeland^{1a,b}, Eystein Oveland^c, Kjell-Morten Myhr^{b,e}, Lars Bø^a, Øivind Torkildsen^{a,b}

^a Norwegian Multiple Sclerosis Competence Centre, Department of Neurology, Haukeland University Hospital, Bergen, Norway

^b Department of Clinical Medicine, University of Bergen, Bergen, Norway

^c Proteomics Unit at University of Bergen (PROBE), Department of Biomedicine, University of Bergen, Norway

^d Computational Biology Unit (CBU), Department of Informatics, University of Bergen, Bergen, Norway

^e Neuro-SysMed, Department of Neurology, Haukeland University Hospital, Bergen, Norway

ARTICLE INFO

Keywords:

Fingolimod

Cuprizone

Remyelination

Multiple sclerosis

Quantitative proteomics

Sphingosine-1-phosphate receptors

ABSTRACT

Fingolimod is used to treat patients with relapsing-remitting multiple sclerosis; it crosses the blood-brain barrier and modulates sphingosine-1-phosphate receptors (S1PRs). Oligodendrocytes, astrocytes, microglia, and neuronal cells express S1PRs, and fingolimod could potentially improve remyelination and be neuroprotective. We used the cuprizone animal model, histo-, immunohistochemistry, and quantitative proteomics to study the effect of fingolimod on remyelination and axonal damage. Fingolimod was functionally active during remyelination by downregulating S1PR1 brain levels, and fingolimod-treated mice had more oligodendrocytes in the secondary motor cortex after three weeks of remyelination. However, there were no differences in remyelination or axonal damage compared to placebo. Thus, fingolimod does not seem to directly promote remyelination or protect against axonal injury or loss when given after cuprizone-induced demyelination.

1. Introduction

Multiple sclerosis (MS) is a chronic immune-mediated disease, characterized by inflammation, demyelination, and axonal degeneration of the central nervous system (CNS) (Lassmann, 2018). Current treatments target the inflammatory aspects of MS but do not directly promote CNS remyelination (Plemler et al., 2017). Pro-remyelinating substances may be an important supplement to immunomodulating therapies to optimize MS therapy. Fingolimod (2-amino-2-[2-(4-octylphenyl)ethyl]propane-1,3-diol) (Kiuchi et al., 1998) is used in the treatment of relapsing-remitting multiple sclerosis (RRMS) (Kappos et al., 2010; Calabresi et al., 2014; Thompson et al., 2018). The medication binds to and modulates sphingosine-1-phosphate receptors (S1PRs), causing sequestration of lymphocytes within lymph nodes by S1P₁ downregulation, which reduces lymphocyte infiltration into the CNS parenchyma (Chiba et al., 1998; Brinkmann et al., 2000). A wide range of cell types within the CNS expresses S1PRs, including oligodendrocytes (Jaillard et al., 2005), neurons, astrocytes (Pebay et al.,

2001) and microglia (Chun and Hartung, 2010). Fingolimod crosses the blood-brain barrier (Brinkmann, 2007; Chun and Hartung, 2010; Groves et al., 2013) and may have a direct impact on CNS remyelination. However, results from experimental studies on the effects of fingolimod on remyelination are inconsistent. In vitro studies have indicated that fingolimod enhances remyelination in cerebellar slices (Miron et al., 2010) and promotes remyelination in a rat CNS spheroid culture (Jackson et al., 2011). In vivo, fingolimod improved remyelination following lysolecithin-induced demyelination in mice (Yazdi et al., 2015) and promoted the proliferation and differentiation of oligodendrocyte progenitors facilitating remyelination in experimental autoimmune encephalomyelitis (EAE) (Zhang, Zhang et al., 2015). However, other studies have not found that fingolimod improves remyelination (Hu et al., 2011; Kim et al., 2011; Alme et al., 2015; Slowik et al., 2015; Kim et al., 2018). A recent review indicates that fingolimod might have a direct and regulatory role in remyelination and that the dose of fingolimod and the time of administration are crucial to the remyelination process (Yazdi et al., 2019). In the present

Abbreviations: S1P, Sphingosine-1-phosphate; S1PRs, sphingosine-1-phosphate receptors

* Corresponding author at: Department of Neurology, Haukeland University Hospital, Jonas Lies road 65, 5021 Bergen, Norway.

E-mail address: agnes.elisabeth.nystad@helse-bergen.no (A.E. Nystad).

<https://doi.org/10.1016/j.jneuroim.2019.577091>

Received 20 September 2019; Received in revised form 22 October 2019; Accepted 22 October 2019

0165-5728/© 2019 Published by Elsevier B.V.

study, we aimed to clarify if fingolimod could promote remyelination and possibly diminish axonal damage in the cerebrum of mice in the cuprizone model for de- and remyelination.

2. Materials and methods

Additional information is available in the Supplementary methods.

2.1. Mice

Forty-eight, female, five-week-old c57Bl/6 mice were obtained from Taconic (Tornbjerg, Denmark), mean weight was $18,54 \text{ g} \pm 1,14$ (SD). The mice were housed six together in GreenLine type II cages (Scanbur, Karlslunde, Denmark), in standard laboratory conditions. Food and tap water were available ad libitum. Cage maintenance was performed once a week, and the same individuals handled the mice throughout the experimental period. The experiment followed the recommendations of the Federation of European Laboratory Animal Science Associations, and the protocol was approved by the Norwegian Animal Research Authority (permit # 2013-5682).

2.2. Study design, cuprizone, and fingolimod/placebo administration

After 12 days of acclimatization, the mice ($n = 48$) were randomized into four groups: healthy controls ($n = 6$), cuprizone controls ($n = 6$), cuprizone + fingolimod ($n = 18$) and cuprizone + placebo ($n = 18$). We added 0.2% cuprizone (bis-cyclohexanone-oxalidihydrazone, Sigma-Aldrich, St. Louis, MO, USA) to milled mouse chow for six weeks, to induce demyelination. Subsequently, mice were fed normal chow. Fingolimod, 1 mg/kg (Hu et al., 2011; Kim et al., 2011; Deshmukh et al., 2013) reconstituted in distilled water or placebo (equivalent volume of water), was administered by oral gavage once daily from week 5. There was a one week overlap in cuprizone exposure and fingolimod treatment to make sure that fingolimod was taken up and phosphorylated to its active compound during the cuprizone exposure (Fig. S1A). For unknown reasons, one mouse died during the experiment resulting in 47 mice for analysis.

2.3. Histopathology and immunohistochemistry

In anesthesia by midazolam (Dormicum "Roche") and fentanyl/fuanisone (Hypnorm "VetaPharma"), the animals were euthanized by cardiac puncture after five weeks (cuprizone controls), six weeks (DM, maximal demyelination), one week of remyelination (1RM) and after three weeks of remyelination (3RM) (Fig. S1A). Brains were dissected and post-fixed in 4% formaldehyde for at least seven days before paraffin embedding. For analyses, we used 3–7 μm coronal sections from the bregma $\pm 1 \text{ mm}$ (Paxinos, 2008). Sections were histochemically stained with Luxol Fast Blue (LFB) to evaluate myelination. Before immunostaining, paraffin-embedded sections were dewaxed and rehydrated, and antigens were retrieved by microwaving sections in either TRIS-EDTA (pH 9.0) or citrate buffer (pH 6.1) (Nystad et al., 2014). Sections were stained for myelin (anti-Proteolipid Protein, PLP), mature oligodendrocytes (Neurite Outgrowth Inhibitor Protein A, NOGO-A), astrocytes (Glial Fibrillary Acidic Protein, GFAP), macrophages and microglia (MAC-3), T-cells (CD3), axonal transection and loss (respectively, amyloid precursor protein A4, APP, and phosphorylated neurofilament light, NFL). The use of buffers, dilutions, incubation times, and temperatures for the antibodies are specified in Table S1. Sections were blocked with peroxidase blocking solution and visualized with EnVision 3.3. – diaminobenzidine (1:50, 3 min at RT) (DAKO, Glostrup, Denmark). Furthermore, counterstained with hematoxylin, dehydrated, and fixed. Brain tissue from healthy or demyelinated mice controls served as controls for all stainings.

2.4. Analyses of brain sections

We used light microscopy to analyze the sections (Zeiss Axio Imager.A2, Oberkochen, Germany). Myelin loss (LFB staining) was quantified by two blinded observers, using a semi-quantitative scoring system from no (0) to complete demyelination (3) as described before (Nystad et al., 2014). Reactive astrocytosis (GFAP immunoreactivity) was evaluated by a semi-quantitative scale as no (0), minimal (1), moderate (2) or extensive (3) (Wergeland et al., 2012). To evaluate the density of mature oligodendrocytes (NOGO-A immunopositive cells), activated microglia and macrophages (MAC-3 immunopositive cells), T-cells (CD3 immunopositive cells) and acute axonal damage (APP immunopositive cells), one blinded observer counted immunopositive cells within an area of 0.0625 mm^2 at $40\times$, using an ocular morphometric grid. Immunopositivity for pan-phosphorylated NFL and PLP was quantified using digital densitometry. The area of interest was photographed with identical exposure settings at $40\times$ magnifications (Zeiss Axio Imager.A2 with AxioCam ERc5 digital camera). Greyscale images were thresholded using ImageJ, v1.41 (Research Services Branch, National Institute of Mental Health, Bethesda, Maryland, USA) to diminish background staining. Immunopositivity was expressed as the area of immunopositivity relative to (%) the total image area. Sections were assessed in the midline of the corpus callosum (CC), the lateral corpus callosum area, the supplemental somatosensory area, the secondary motor cortex (M2) and deep grey matter – striatum (Fig. S1B).

2.5. Statistical methods

We did a priori sample size calculations based on the differences in the myelin content between calcitriol- and placebo-treated mice from (Nystad et al., 2014), a sample size of six animals per experimental group would give a power of 0.7 (mean LFB.score of $2.0 \pm \text{SD } 0.6$ and $1.0 \pm \text{SD } 0.6$ after three weeks of remyelination). Kolmogorov-Smirnov and Shapiro-Wilk tests of normality were used to test the assumption of normally distributed data. We used independent sample *t*-tests to compare parametric data and the Mann-Whitney test for non-parametric data. Differences were considered significant at $p < 0.05$. The calculations were carried out unblinded, using Statistical Package for the Social Sciences (IBM Corp. Released 2017. IBM SPSS Statistics for Windows, Version 25.0. Armonk, NY: IBM Corp).

2.6. Quantitative proteomics

We prepared the samples of mouse brain lysates as previously described (Lereim et al., 2016). Briefly, the individual frontal right hemisphere of mice receiving fingolimod or placebo were lysed in 4% SDS, 100 mM Tris/HCl pH 7.6, 0.1 M DTT, and the protein concentration estimated. Before digestion, the samples were pooled (Table S2), and 50 μg of each pool was digested by the Filter-aided sample preparation (FASP) protocol (Wiśniewski et al., 2009). The samples were tagged by a tandem mass tag (TMT) 10-plex set (Thermo Scientific) that was split in two, enabling simultaneous tagging of 20 samples; 18 sample pools and two identical reference samples enabling combining and comparing the two 10 plexes (Table S2). Each TMT 10 plex experiment was fractionated by mixed-mode reverse phase chromatography as previously described (Lereim et al., 2016). This resulted in 58 fractions each 10 plex that was lyophilized and dissolved in 1% formic acid (FA)/2% acetonitrile (ACN) prior to LC-MS/MS analysis (supplementary methods). Following LC-MS/MS, peptides were identified, quantified, and normalized in Proteome discoverer 2.0 (Thermo Scientific). The samples were analyzed by the statistical software limma (Ritchie et al., 2015) in R. The script used to analyze the samples and create the graphics is available on GitHub (<https://github.com/RagnhildRLereim/Fingolimod>). We analyzed Gene Ontology Biological process enrichment for the proteins considered to be significantly different in Panther

(Thomas et al., 2006; Mi et al., 2019). The proteomics data is available in the PRIDE database (Vizcaino et al., 2016) under accession PXD012676 (Username: reviewer53224@ebi.ac.uk, Password: VJxAVcS). For additional information about the quantitative proteomics experiment, see Supplementary methods.

3. Results

3.1. Effects of fingolimod treatment on the brain proteome during remyelination

Using TMT labeling and proteomics, we identified 7949 proteins, of which 7183 were quantified. In total, the same 6386 proteins were identified and quantified in both TMT 10-plexes and formed the basis of our statistical analysis with three mini pools for each condition, where each pool contained equal amounts of two biological replicates (Table S2). Significant proteomic changes were seen in the dataset ($p < 0.01$, \log_2 fold change (FC) Fingolimod – Placebo < -0.2 , > 0.2) between the fingolimod and the placebo-treated animals, albeit the distribution of mean expression values were narrow (Fig. S2) and comparison analysis showed moderate fold changes (min \log_2 FC -1.17, max = 1.7, normal values = 0.4–3.2). A detailed table of the significant proteins from each comparison can be found in Supplementary tables S3–S5. Gene Ontology enrichment analysis of these proteins did not show any significantly overrepresented biological processes at any time point.

3.2. Fingolimod was functionally active during remyelination by downregulating S1PR1 levels

The two proteins, S1PR1, and guanine nucleotide-binding protein gamma 5 (GNG5) were significantly regulated in the samples from the fingolimod-treated mice compared to placebo at all measured time points (Fig. 1). Both S1PR1 and GNG5 were less abundant in samples from fingolimod-treated mice; however, only S1PR1 was significant after false discovery rate (FDR) correction ($q < 0.01$). At one week of remyelination, the protein Lysosomal thioesterase (PPT2) was significantly downregulated in the samples from fingolimod-treated mice after FDR correction.

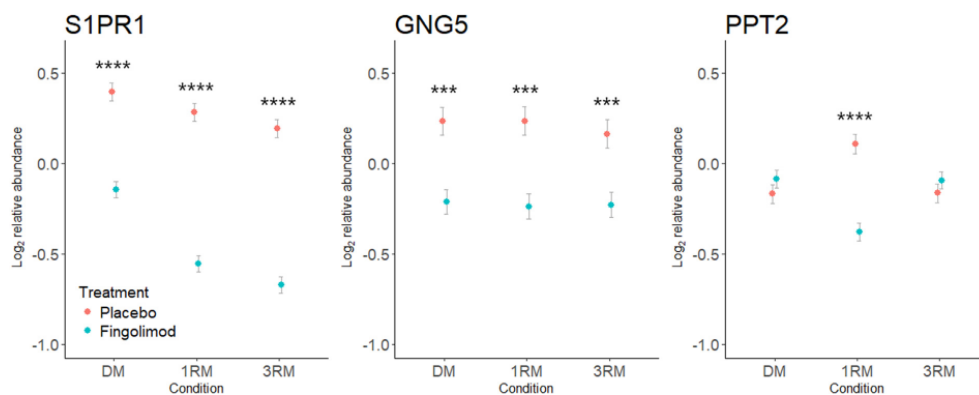


Fig. 1. Protein levels of S1PR1, GNG5 and PPT2 measured by quantitative proteomics.

Sphingosine-1-phosphate receptor-1 (S1PR1) and guanine nucleotide binding protein gamma 5 (GNG5) were significantly less abundant (p -value < 0.01 , \log_2 FC Fingolimod – Placebo > 0.2 , < -0.2) in fingolimod animals after six weeks of demyelination (DM), one week of remyelination (1RM) and 3 weeks of remyelination (3RM). S1PR1 was significantly different in all comparisons after FDR correction (q -value < 0.05). Lysosomal thioesterase (PPT2) was significantly downregulated at 1RM in fingolimod-treated mice after FDR correction. The average \log_2 abundance is plotted; the error bars represent the standard deviation based on three sample pools containing two biological replicates each.

*** = p -value < 0.001 , **** = p -value ≤ 0.0001 .

3.3. Fingolimod did not affect remyelination

3.3.1. Remyelination in the corpus callosum and the cortex

There was a detectable loss of myelin in the midline of the corpus callosum (CC), as measured by LFB score after five weeks in the cuprizone-treated mice ($1.5 \pm \text{SD } 0.5$) compared to healthy controls ($0.33 \pm \text{SD } 0.52$, $p = 0.036$) (Fig. 2, Table S6A). There was no difference in myelin loss in the CC between the fingolimod group and placebo group after six weeks of demyelination (DM: 1.83 vs. 2.0, $p = 0.38$), one week of remyelination (1RM: 2.2 vs. 2.1, $p = 1.0$) or three weeks of remyelination (3RM: 1.7 vs. 1.25, $p = 0.40$) (Fig. 2, Table S6B–D). Similarly, there were no differences in PLP staining, at any time point (DM: $p = 0.64$, 1RM: $p = 0.96$, 3RM: $p = 0.28$, Fig. 3, Table S6B–D). Fingolimod did not affect the density of mature oligodendrocytes (NOGO-A, DM: $p = 0.58$, 1RM: $p = 0.31$, 3RM: $p = 0.90$, Fig. 4, Table S6B–D). In the secondary motor cortex, there was no difference in the LFB score (DM: $p = 1.0$, 1RM: $p = 0.77$, 3RM: $p = 1.0$) or PLP immunopositivity (DM: $p = 0.128$, 1RM: $p = 0.481$, 3RM: $p = 0.662$) between the intervention groups. The density of mature oligodendrocytes was increased in fingolimod-treated mice compared to mice in the placebo group after three weeks of remyelination ($5.17 \pm \text{SD } 4.26$ vs. $1.6 \pm \text{SD } 0.55$, $p = 0.032$). However, the number of mature oligodendrocytes were not increased in fingolimod mice after six weeks of demyelination ($p = 0.23$) or at one week of remyelination ($p = 0.66$) compared to placebo mice (Table S7B–D).

3.3.2. Proteomic markers of remyelination

During the remyelination phase, there was a time-dependent increase in proteins involved in myelination (Fig. 5). There were, however, no differences in levels of myelin basic protein (MBP), myelin-associated glycoprotein (MAG), myelin-oligodendrocyte glycoprotein (MOG), oligodendrocyte-myelin glycoprotein (OMG), myelin expression factor 2 (MYEF2), myelin-associated oligodendrocyte basic protein (MOBP), myelin transcription factor 1-like protein (MYT1L) or PLP between the intervention groups at any time points (Fig. 5). Correspondingly, no difference was detected in the protein abundance of NOGO between fingolimod- and placebo-treated mice at any time point (Fig. S3).

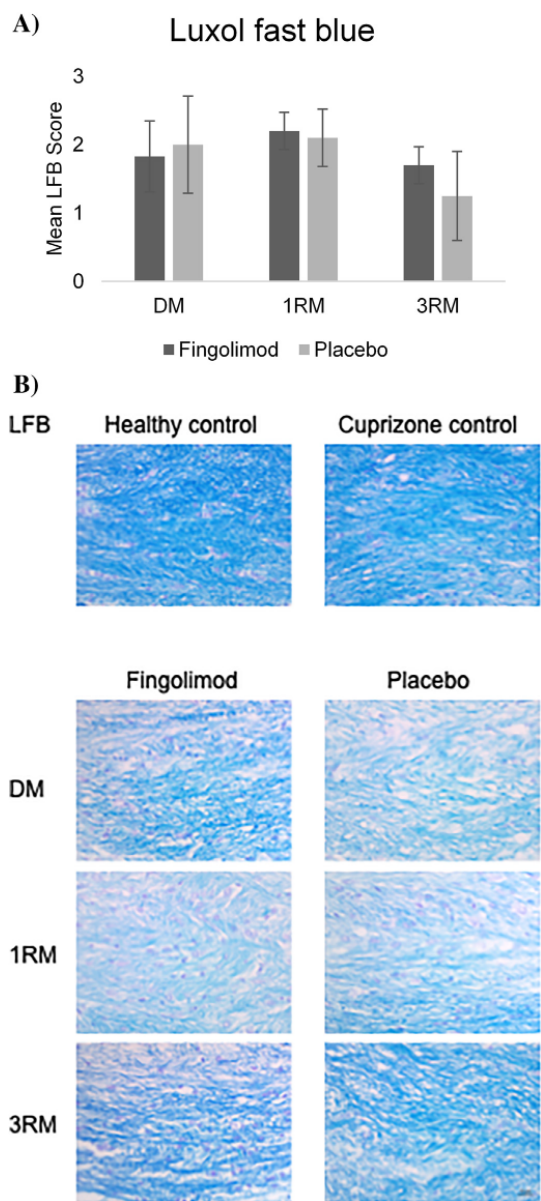


Fig. 2. Myelin loss measured by Luxol fast blue.

A) Myelin loss in the midline of corpus callosum in the placebo and fingolimod group after six weeks of demyelination (DM), one week of remyelination (1RM) and three weeks of remyelination (3RM), as measured by Luxol fast blue. Scale: no (0), minimal (0.5), < 33% (1), 33–66% (2) and > 66% (3) demyelination. Data presented as mean, error bars: \pm 1 SD. Number (n) of animals included: DM placebo (n: 6), DM fingolimod (n: 6), 1RM placebo (n: 6), 1RM fingolimod (n: 5), 3RM placebo (n: 5), 3RM fingolimod (n: 5).

B) Luxol Fast Blue (LFB) stained sections. DM = six weeks of demyelination, 1RM = one week of remyelination, 3RM = three weeks of remyelination. All images at 40 \times . (For interpretation of the references to colour in this figure legend, the reader is referred to the web version of this article.)

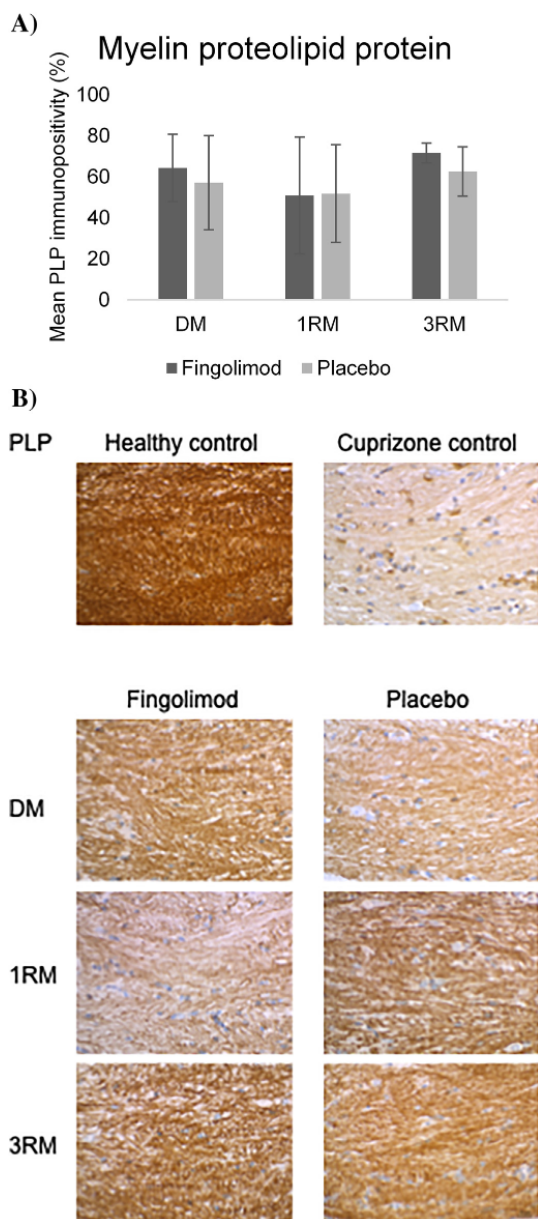


Fig. 3. Myelin loss measured by proteolipid protein immunoreactivity.

A) Immunoreactivity in % for PLP in the fingolimod and placebo group after six weeks of demyelination, one week of remyelination and three weeks of remyelination. There were no differences between the groups at any time point. Sections were scored in the midline of corpus callosum. Data presented as mean, error bars: \pm 1 SD. Number (n) of animals included: DM placebo (n: 5), DM fingolimod (n: 5), 1RM placebo (n: 4), 1RM fingolimod (n: 4), 3RM placebo (n: 4), 3RM fingolimod (n: 5).

B) PLP and hematoxylin stained sections. DM = six weeks of demyelination, 1RM = one week of remyelination, 3RM = three weeks of remyelination. All images at 40 \times .

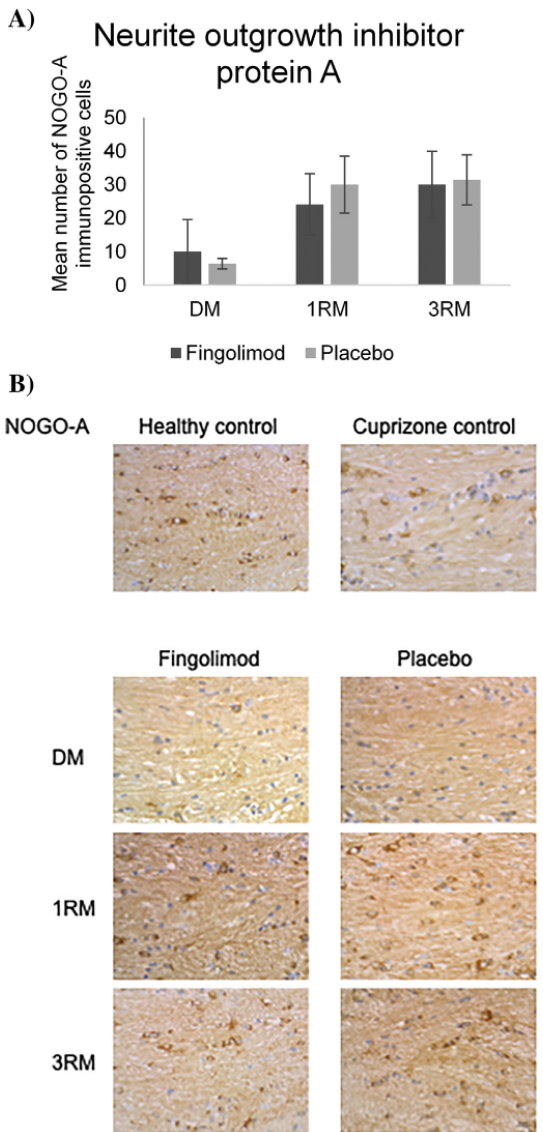


Fig. 4. Mature oligodendrocytes measured by Neurite outgrowth inhibitor protein A immunoreactivity.

A) Number of mature oligodendrocytes in the fingolimod and placebo group after six weeks of demyelination, one week of remyelination and three weeks of remyelination. There were no differences between the fingolimod and the placebo group at any time point. Cell counts are provided as mean number of cells per 0.0625 mm², in the midline of the corpus callosum. Error bars: \pm 1 SD. Number (n) of animals included: DM placebo (n: 5), DM fingolimod (n: 3), 1RM placebo (n: 6), 1RM fingolimod (n: 5), 3RM placebo (n: 5), 3RM fingolimod (n: 6).

B) NOGO-A and hematoxylin stained sections. DM = six weeks of demyelination, 1RM = one week of remyelination, 3RM = three weeks of remyelination. All images at 40 \times .

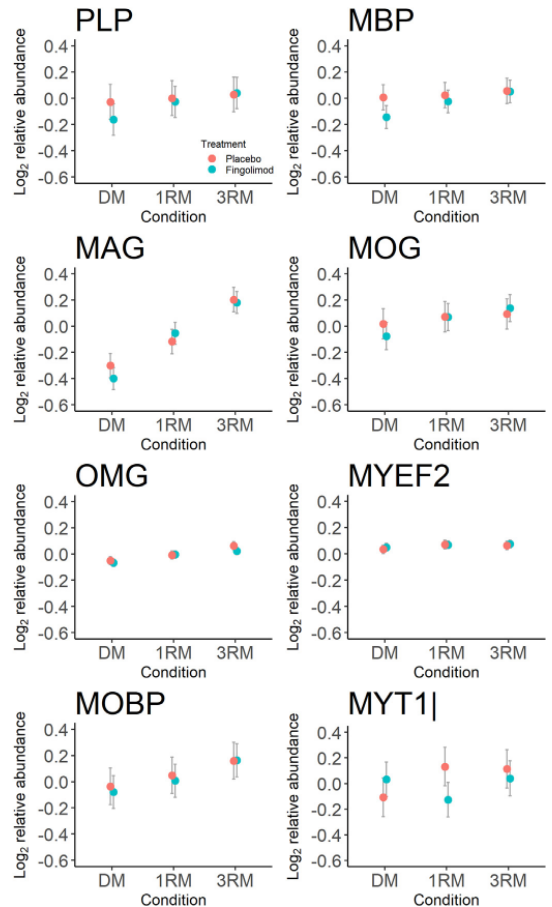


Fig. 5. Myelin protein levels measured by quantitative proteomics. The average log₂ abundances based on three pools, each containing two biological replicates and their standard deviation. PLP: Myelin Proteolipid Protein, MBP: myelin basic protein, MAG: myelin-associated glycoprotein, MOG: myelin-oligodendrocyte glycoprotein, OMG: oligodendrocyte-myelin glycoprotein, MYEF2: myelin expression factor 2, MOBP: myelin-associated oligodendrocyte basic protein, MYT1|: myelin transcription factor 1-like protein. DM = six weeks of demyelination, 1RM = one week of remyelination, 3RM = three weeks of remyelination.

3.4. Fingolimod did not affect astrocytosis or microglia activation

3.4.1. Astrocytosis and microglia activation in the corpus callosum and the cortex

There was increased GFAP immunopositivity in the CC of cuprizone controls compared to healthy controls ($0.7 \pm$ SD 0.27 vs. $1.83 \pm$ SD 0.58, $p = 0.024$, Table S6A). Astrocytosis remained moderate to minimal during remyelination in the fingolimod and placebo groups. No differences in astrocytosis were detected at any time points (DM: $p = 0.93$, 1RM: $p = 0.36$, 3RM: $p = 0.81$, Fig. 6, Table S6B–D). Increased microglia and macrophage activation, as measured by the density of MAC-3 immunopositive cells, was observed in the cuprizone controls compared to healthy controls ($0.0 \pm$ SD 0.0 vs. $14 \pm$ SD 6.56, $p = 0.018$, Table S6A). We found no difference in MAC-3 immunopositivity between the fingolimod or placebo exposed mice at any time points (DM: $p = 0.058$, 1RM: $p = 0.42$, 3RM: $p = 0.10$, Fig. 7,

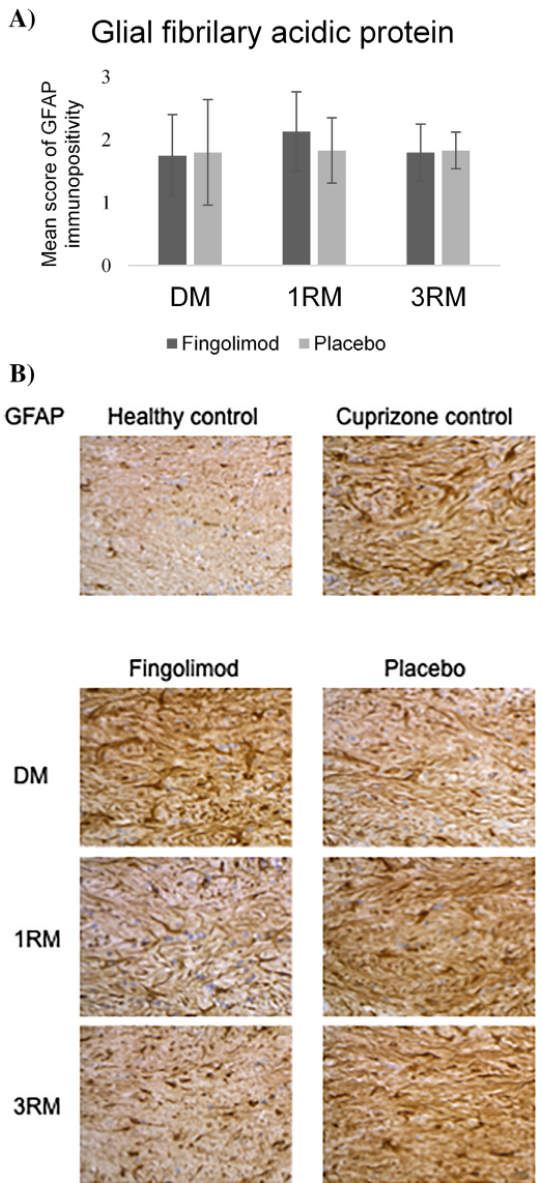


Fig. 6. Astrocytosis measured by Glial fibrillary acidic protein immunoreactivity.

A) Degree of GFAP immunopositivity in the fingolimod and placebo group after six weeks of demyelination, one week of remyelination and three weeks of remyelination. We could not find any difference between the fingolimod and the placebo group at any time point. Scale: no (0), minimal (1), moderate (2), severe (3) astrocytosis. Sections were scored in the midline of corpus callosum. Data presented as mean, error bars: \pm 1 SD. Number (n) of animals included: DM placebo (n: 5), DM fingolimod (n: 4), 1RM placebo (n: 6), 1RM fingolimod (n: 6), 3RM placebo (n: 4), 3RM fingolimod (n: 5).

B) GFAP and hematoxylin stained sections. DM = six weeks of demyelination, 1RM = one week of remyelination, 3RM = three weeks of remyelination. All images at 40 \times .

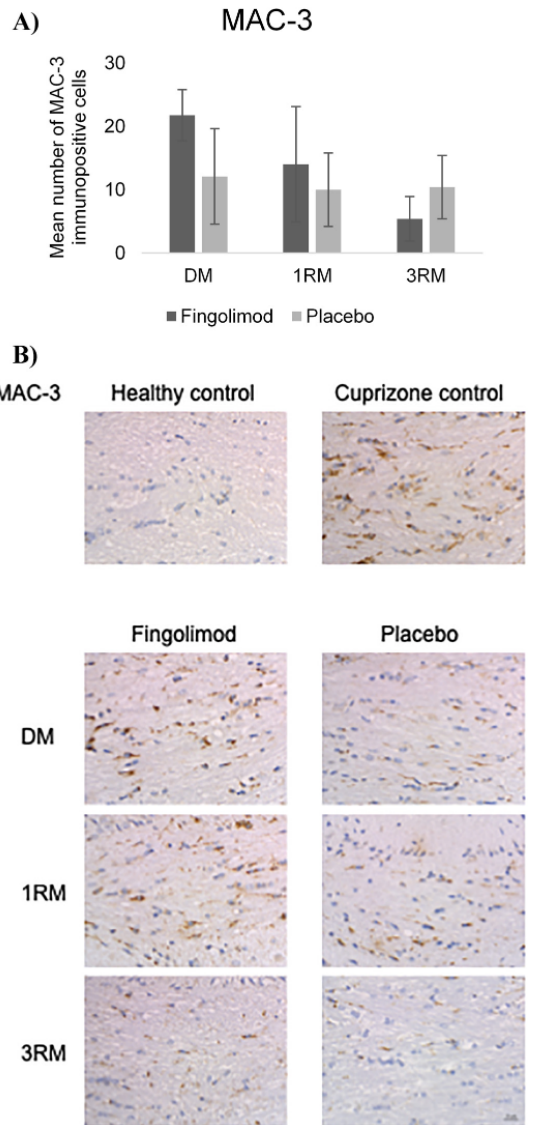


Fig. 7. Microglia/macrophages measured by MAC-3 immunoreactivity.

A) Number of microglia/macrophages (MAC-3 immunopositivity) in the fingolimod and placebo group after six weeks of demyelination, one week of remyelination and three weeks of remyelination. There were no significant differences between the fingolimod and the placebo group at any time point. Cell counts are provided as mean number of cells per 0.0625 mm², in the midline of the corpus callosum. Error bars: \pm 1 SD. Number (n) of animals included: DM placebo (n: 5), DM fingolimod (n: 4), 1RM placebo (n: 6), 1RM fingolimod (n: 6), 3RM placebo (n: 5), 3RM fingolimod (n: 5).

B) MAC-3 and hematoxylin stained sections. DM = six weeks of demyelination, 1RM = one week of remyelination, 3RM = three weeks of remyelination. All images at 40 \times .

Table S6B–D). As expected, (Matsushima and Morell, 2001; Wergeland et al., 2012) we only observed 0–3 CD3 immunopositive lymphocytes per counted area and no differences between the groups (Fig. S4, Table S6A–D). In the secondary motor cortex, there was no difference in astrocytosis (DM: $p = 0.16$, 1RM: $p = 0.17$, 3RM: $p = 0.64$) or MAC-3 immunopositivity (DM: $p = 0.95$, 1RM: $p = 0.65$, 3RM: $p = 0.78$, Table S7B–D) between the fingolimod and placebo exposed mice at any time points.

3.4.2. Proteomic markers of astrocytosis and microglia activation

There was a reduction in the average \log_2 abundances of GFAP in both intervention groups from six weeks of demyelination throughout the remyelination phase (Fig. S3). After one week of remyelination, the fingolimod-treated mice had increased proteomic expression of MAC-3 ($p < 0.01$). The difference was not considered significant under our criteria as the fold change was $< 20\%$ compared to placebo. Thus, there were no differences ($p < 0.01$, \log_2 FC $> \pm 0.2$) between the fingolimod-treated and placebo-treated animals (Fig. S3).

3.5. Fingolimod did not lead to less axonal loss

3.5.1. Axonal damage in corpus callosum and the cortex

Cuprizone exposure led to an increased density of APP-positive bulbs in the CC (0.0 cells/ $0.0625\text{mm}^2 \pm \text{SD } 0.0$ vs. $29.0 \pm \text{SD } 28.5$, $p = 0.002$, Table S6A). Treatment with fingolimod caused no difference in acute axonal damage compared to placebo at the different time points (DM: $p = 0.80$, 1RM: $p = 0.25$, 3RM: $p = 0.35$, Fig. 8, Table S6B–D). In the lateral CC, the fingolimod-treated mice had significantly more APP-positive bulbs after 3RM compared to placebo ($11.0 \pm \text{SD } 4.2$ vs. $3.4 \pm \text{SD } 2.51$, $p = 0.006$).

The cuprizone exposed mice had less NFL immunopositivity than the healthy controls ($90.87 \pm \text{SD } 2.55$ vs. $63.2 \pm \text{SD } 24.89$, $p = 0.041$, Table S6A). There were, however, no differences in NFL loss between the fingolimod-treated and placebo-treated mice (DM: $p = 0.81$, 1RM: $p = 0.30$, 3RM: $p = 0.26$, Fig. 9, Table S6B–D). In the secondary motor cortex, we found no APP-positive bulbs in the fingolimod or placebo group. The fingolimod group had less NFL immunopositivity after six weeks of demyelination ($9.37 \pm \text{SD } 4.25$ vs. $19.9 \pm \text{SD } 5.19$, $p = 0.005$, Table S7B). However, there were no differences between the groups at later time points (Table S7C–D).

3.5.2. Proteomic markers of axonal damage

There were no differences ($p < 0.01$, \log_2 FC $> \pm 0.2$) between the fingolimod- and placebo-treated mice in the proteomic expression of APP or NFL (Fig. S3).

4. Discussion

Fingolimod downregulated S1PR1 in the cerebrum of cuprizone-treated mice at all time points investigated. When examining the corpus callosum and the secondary motor cortex in cuprizone mice, at three different time points, we found that fingolimod given after cuprizone-induced demyelination did not enhance remyelination, as supported by our earlier experiments in the cerebellum (Alme et al., 2015) and by other groups (Hu et al., 2011; Kim et al., 2011; Slowik et al., 2015; Kim et al., 2018). In our study, fingolimod increased the number of mature oligodendrocytes in the secondary motor cortex after three weeks of remyelination but did not improve remyelination. There could be several explanations for this discrepancy. Gudi et al. found that the density of oligodendrocytes is lower in the cortex compared to the corpus callosum. Moreover, oligodendrocytes may not be capable of driving the remyelination process in the cortex as in the corpus callosum. They hypothesized that the demyelination process in the cortex may be delayed compared to corpus callosum or that signals that drive the remyelination process in corpus callosum are deficient in the cortex. Further, they speculated that few mature oligodendrocytes might not

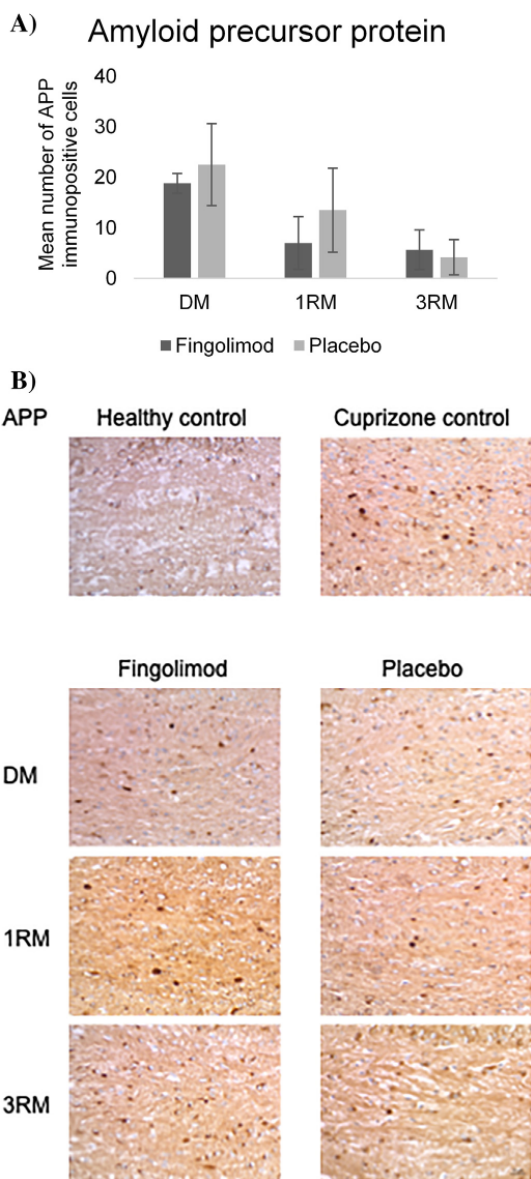


Fig. 8. Acute axonal damage measured by Amyloid precursor protein immunoreactivity.

A) Number of APP immunopositive bulbs in the fingolimod and placebo group after six weeks of demyelination, one week of remyelination and three weeks of remyelination. There was no difference between the fingolimod and the placebo group at any time point. Cell counts are provided as mean number of cells per 0.0625mm^2 , in the midline of the corpus callosum. Error bars: ± 1 SD. Number (n) of animals included: DM placebo (n: 6), DM fingolimod (n: 6), 1RM placebo (n: 6), 1RM fingolimod (n: 5), 3RM placebo (n: 5), 3RM fingolimod (n: 6).

B) APP and hematoxylin stained sections. DM = six weeks of demyelination, 1RM = one week of remyelination, 3RM = three weeks of remyelination. All images at $40\times$.

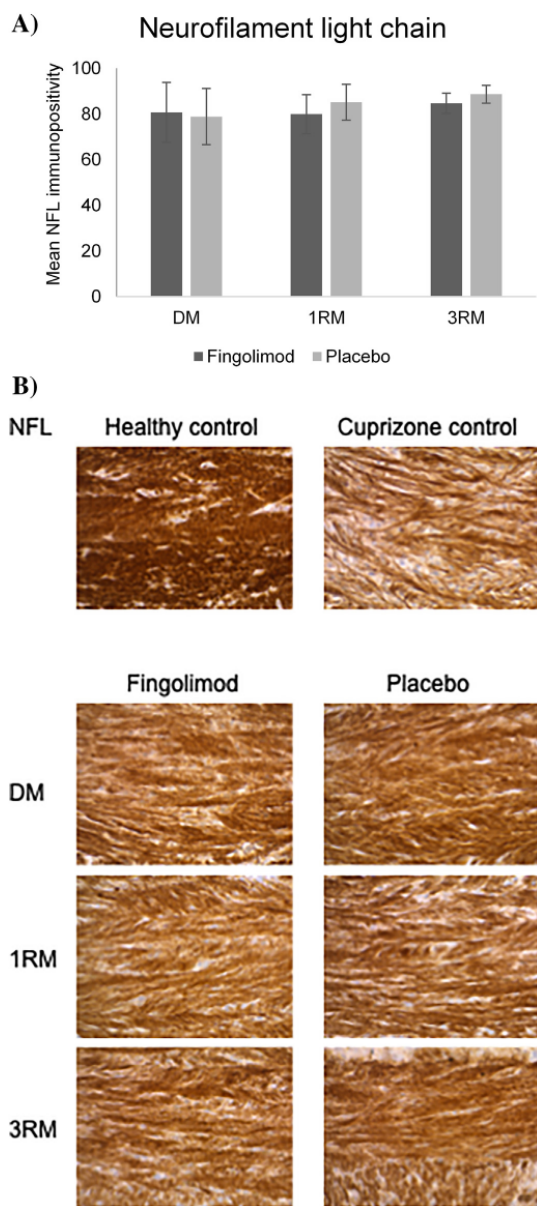


Fig. 9. Axonal loss measured by Neurofilament light chain immunoreactivity. A) Immunoreactivity in % for NFL in the fingolimod and placebo group after six weeks of demyelination, one week of remyelination and three weeks of remyelination. There were no differences between the groups at any time point. Sections were scored in the midline of corpus callosum. Data presented as mean, error bars: \pm 1 SD. Number (n) of animals included: DM placebo (n: 6), DM fingolimod (n: 6), 1RM placebo (n: 6), 1RM fingolimod (n: 6), 3RM placebo (n: 3), 3RM fingolimod (n: 6).

B) NFL and hematoxylin stained sections. DM = six weeks of demyelination, 1RM = one week of remyelination, 3RM = three weeks of remyelination. All images at 40 \times .

have the capacity to drive detectable remyelination (Gudi et al., 2009). Another possibility is that fingolimod stimulates the recruitment and differentiation of oligodendrocytes in the cortex yet fails to increase remyelination of the axons. Electron microscopy (EM) is considered the gold standard for assessing remyelination but was not used to assess remyelination in this experiment. However, Lindner et al. have demonstrated that EM correlates well with LFB myelin staining (Lindner et al., 2008) and Wergeland et al. have found that PLP staining detect myelin-regeneration after one week of cuprizone withdrawal (Wergeland et al., 2012).

The cuprizone model is a well-described and reliable animal model (Matsushima and Morell, 2001; Torkildsen et al., 2008; Kipp et al., 2009; Wergeland et al., 2012). Through our IHC and proteomic analyses, we demonstrate the well-established time-dependent changes in remyelination (Matsushima and Morell, 2001; Lindner et al., 2008; Kipp et al., 2009; Werner et al., 2010) in both fingolimod- and placebo-treated cuprizone mice. After six weeks of cuprizone-induced demyelination, myelin proteins are reduced with a subsequent increase during recovery in cuprizone mice compared to controls. Furthermore, the protein abundance of GFAP is increased after six weeks, and gradually returns to control levels during remyelination (Werner et al., 2010). Correspondingly, we show downregulation of myelin and upregulation of GFAP protein levels after six weeks of demyelination. As expected, the myelin protein levels increased, and GFAP levels decreased throughout the remyelination phase. Proteomics appeared to have a higher sensitivity than IHC for monitoring the time-dependent changes in GFAP. This difference may be due to variations in the areas that were analyzed. Although the cuprizone model does not directly mimic MS pathology, robust de- and remyelination in the absence of adaptive immune responses makes this model well suited to study remyelination (Kipp and Amor, 2012). It is not possible to generalize results directly from the model to humans, yet findings can indicate effects on remyelination and the mechanisms involved.

To our knowledge, the present study is the first to apply proteomics to elucidate the mechanisms of action of fingolimod on remyelination and axonal damage after cuprizone exposure. Fingolimod treatment caused downregulation of the total level of S1PR1 in the mouse brain. Healthy control mice treated with fingolimod would have strengthened our study. Nevertheless, the difference in the S1PR1 abundance between the fingolimod and placebo group is reliable, as S1PR1 was significantly downregulated after FDR correction ($q < 0.01$).

S1P levels decrease during cuprizone exposure but recover during remyelination after cuprizone withdrawal (Kim et al., 2012). The level of S1P also decreases in cuprizone exposed mice cotreated with fingolimod (Kim et al., 2018). In healthy CBA/CAHarc mice, S1PR1 is up-regulated after two months of intraperitoneal treatment with fingolimod (7.5 mg/kg/week) compared to vehicle control (Gupta et al., 2017). Fingolimod regulates S1PRs in cuprizone mice but does not prevent a cuprizone-induced S1P drop (Kim et al., 2018). In cuprizone exposed mice, the expression of S1PR1 was moderately increased, and S1PR3 and -5 significantly increased compared to controls. However, only the protein level of S1PR1 was downregulated by fingolimod cotreatment (Kim et al., 2018). Unlike us, Kim et al. did not investigate S1PRs protein levels during remyelination after fingolimod rescue treatment.

In the proteomics experiment, we analyzed the right frontal brain section; thus, the quantified proteins represent the bulk of proteins originating from different cell types in this particular section. Therefore, we cannot rule out that S1PR1 and other proteins could be more down- or upregulated in some cell types than others or be differently regulated in other parts of the CNS. Both S1PR1 and GNG5 were less abundant in samples from fingolimod-treated mice than placebo-treated mice. After one week of remyelination, the protein PPT2 was downregulated in fingolimod-treated mice. The aforementioned proteins are, to our knowledge, not known to be involved in the remyelination process. The GNG5 is a G-protein and an interactor with

S1PR1 (Huttlin et al., 2017). Therefore, both S1PR1 and GNG5 could be downregulated because of a refractory phase of signaling occurring after prolonged activation of the S1PR1 pathway. Such a non-responsive phase of signaling might occur as a negative feedback mechanism set to follow by internalization of receptor complexes by endocytosis followed by degradation by the lysosomal pathway (Reeves et al., 2016). PPT2 is a lysosomal enzyme involved in removing thioester-linked fatty acyl groups from various substrates, including G-proteins, during lysosomal degradation processes (Soyombo and Hofmann, 1997). However, its role in S1PR1 signaling is not clear (Reeves et al., 2016). Myelin proteins (MOG, MAG, MBP, MOBP, PLP) (Han et al., 2013) and proteins reflecting axonal damage and loss (APP, NFL) (Teunissen et al., 2005) were not regulated between the fingolimod-treated and placebo-treated groups. Thus, the results support that fingolimod does not promote the remyelination process or mitigate axonal loss.

In our experiment, principal component analysis of the log₂ relative protein abundances showed an apparent batch effect between the two TMT experiments, likely introduced by technical variance. In unbalanced experiments, especially when the sample sizes are small, a technical variance can overshadow biological variance and induce differences between groups. Attempts were made to reduce the technical variance observed by applying a normalization strategy for combining TMT experiments (Plubell et al., 2017), though without improvement (data not shown). Several methods to tackle batch effects exist (Leek et al., 2010; Nygaard et al., 2016), limma (Ritchie et al., 2015) was selected due to the unbalanced nature of the study and the small number of biological replicates in each group. A linear model was created, taking the batch effect into account, prior to empirical Bayes statistics for differential Expression and Benjamini Hochberg FDR correction. After FDR correction, the downregulation of the S1PR1 receptor was identified.

In the lysolcithin model, force-feeding fingolimod (0.3 mg/kg and 1 mg/kg) before lysophosphatidylcholine (LPC) exposure decreased inflammation and the extent of demyelination; and the low dose of fingolimod increased oligodendrocyte precursor cells recruitment, oligodendrogenesis, and remyelination (Yazdi et al., 2015). However, inflammatory cytokines may cause cell death and prevent oligodendrocyte precursor cell differentiation (Feldhaus et al., 2004); the enhanced myelination may thus have been caused by a reduced inflammation with subsequent less demyelination (Yazdi et al., 2015). Oral fingolimod did not promote remyelination after LPC injection or after cuprizone exposure (Hu et al., 2011). At a late disease stage, where the axonal loss is prominent, there is less capacity to compensate for nerve damage and further nerve loss; this will consequently increase functional impairment. In line with our results, Hu et al. concluded that patients treated with fingolimod might benefit from add-on therapy to promote remyelination.

Prophylactic treatment with fingolimod (0.4 mg/kg) in EAE Dark Agouti (DA) rats prevents the onset and development of EAE symptoms. Rescue therapy with fingolimod reversed EAE symptoms and restored the nerve conductance in rats with fully established EAE. The fingolimod and the control group had comparable levels of remyelination. The authors speculated that fingolimod could exert a centralized effect in the CNS through interaction with S1PRs on glial cells, yet, they did not exclude that the effect of fingolimod is due to its known anti-inflammatory effect (Balatoni et al., 2007). During relapsing EAE early intervention with fingolimod inhibited subsequent relapses and neurodegeneration, yet late initiated, long-term treatment could not impede the disease deterioration in progressive EAE (Al-Izki et al., 2011). Fingolimod (0.3 mg/kg) initiated at EAE symptom onset, promoted proliferation and differentiation of oligodendrocyte precursor cell in mice, and increased the MBP levels (Zhang et al., 2015). The findings could be a consequence of attenuated inflammation and myelin protection, rather than remyelination through direct CNS effects, as the same group found that fingolimod (0.3 mg/kg) alone failed to enhance

remyelination in the secondary progressive (SP) stage of EAE (Zhang et al., 2017). Due to the interference of and indirect effects by the systemic immune cell responses, it is challenging to monitor remyelination separately in the EAE model.

Fingolimod may enhance the MBP expression and remyelination at low doses (< 5 nM in vitro and 0.3 mg/kg/day in vivo). However, fingolimod seems to cause oligodendrocyte death at higher concentrations (Zhang et al., 2017). In humans, oligodendrocyte precursor cells and mature oligodendrocytes may show dose-dependent, cell-type-specific, and differing cytoskeletal responses to fingolimod. Miron et al. indicated that disparities in human- and rat oligodendrocyte-responses make it challenging to transfer interpretations from rodent in vitro studies to human cells (Miron et al., 2008a). In another study, fingolimod had dose- and time-dependent effects on process extension, differentiation, and survival in oligodendrocyte precursor cells (Miron et al., 2008b). Moreover, a low dose (100 pmol/L) fingolimod could enhance remyelination and affect oligodendrocyte precursor cells in organotypic cerebellar slices after LPC-induced demyelination (Miron et al., 2010). In the rat telencephalon reaggregate spheroid cell culture system, 1 and 10 nM fingolimod did not affect remyelination when given before LPC-induced demyelination (Jackson et al., 2011). Slowik et al. gave mice a low dose (0.3 mg/kg) of fingolimod after cuprizone-induced demyelination, yet there was no difference in remyelination between the fingolimod and placebo after acute or chronic demyelination. However, fingolimod seemed to decrease axonal damage (Slowik et al., 2015).

In the present study, we used 1 mg/kg/day fingolimod, as used in several other studies (Kataoka et al., 2005; Al-Izki et al., 2011; Hu et al., 2011; Kim et al., 2011; Kim et al., 2018). We found that fingolimod does not decrease acute axonal injury or axonal loss after acute cuprizone demyelination, as fingolimod-treated mice compared to placebo had increased acute axonal injury (APP immunoreactivity) after three weeks of remyelination. However, this was not confirmed by proteomic analyses, as we found no difference in axonal damage or loss between the intervention groups. We cannot exclude that a lower dose of fingolimod could have a beneficial effect. Kim et al. found that fingolimod given during cuprizone exposure led to diminished injury to oligodendrocytes, myelin, and axons (Kim et al., 2011) and suppressed astrogliosis and microgliosis (Kim et al., 2018). Nonetheless, fingolimod (1 mg or 5 mg/kg) did not reduce inflammation, oligodendrocytes loss, or enhance remyelination if given after the occurrence of oligodendrocyte apoptosis and myelin damage (Kim et al., 2018). Thus, whether fingolimod is administered before or during cuprizone exposure would affect the degree of de- and remyelination. The discrepant findings between our results and other studies could be due to the chosen animal model, degree and capacity of de- and remyelination, experimental settings, the time point for fingolimod initiation, doses, duration of treatment, and different brain regions analyzed.

Our data give a new insight into the mechanisms of action behind fingolimod during remyelination. Based on the current research, the hypothetical direct effect of fingolimod on S1PRs in the brain does not appear to have any significant influence on remyelination. The INFORMS study, a phase three, randomized controlled trial (RCT), did not find any advantages of fingolimod in primary progressive MS patients, as they found no effect on brain volume loss and disability progression (Lublin et al., 2016). This supports that fingolimod has to be given at an early disease stage, before damage has occurred, to exert neuroprotective effects. Another RCT (EXPAND), investigated the impact of the selective S1P₁ and S1P₅ modulator, siponimod, on patients with secondary progressive MS. The results showed that siponimod, to some extent, reduced the risk of disability progression and could be used to treat patients with secondary progressive MS (Kappos et al., 2018). In the future, well-designed clinical trials are necessary to determine to what extent fingolimod and other substances may affect myelin repair and axonal loss in MS patients.

5. Conclusion

Fingolimod was functionally active during remyelination by downregulating S1PR1 brain levels in fingolimod-treated cuprizone mice. We detected more oligodendrocytes in the secondary motor cortex after three weeks of remyelination in the fingolimod compared to placebo-exposed mice. However, HC, IHC, and proteomic analyses detected no differences in the degree of remyelination, axonal damage or loss in fingolimod-treated mice compared to placebo. In conclusion, fingolimod does not seem to directly promote remyelination or protect against axonal injury or loss when given after cuprizone-induced demyelination.

Acknowledgments

We thank Edith Fick for excellent technical assistance and Håvard Nyhagen Henriksen for proofreading of the manuscript. Neuro-SysMed is jointly hosted by Haukeland University Hospital and University of Bergen, and supported as a Centre for Clinical Treatment Research (FKB) by grants from The Research Council of Norway, project number 288164.

Funding

This work was funded by the University of Bergen K1, Kristian Gerhard Jebsen Foundation, and grants from Novartis, Norway AS. Fingolimod was provided by Material Transfer Management, NIBR Operational Alliances, Fabrikstrasse 28-Z1.28.1, Novartis Campus, CH-4056 Basel, Switzerland.

Author contributions

Conceptualization, Ø.T., S.W. and L.B.; *Methodology*, Ø.T., S.W., E.O., and L.B.; *Investigation*, A.E.N., R.R.L., E.O. and S.W.; *Formal Analysis*, A.E.N., R.R.L., E.O. and S.W.; *Writing – Original Draft*, A.E.N.; *Writing – Review & Editing*, All authors; *Visualization*, A.E.N., S.W.; *Supervision*, Ø.T., E.O. and S.W.; *Funding Acquisition*, Ø.T., S.W., K.M. and L.B.

Declaration of competing interest

Agnes E. Nystad has received an unrestricted research grant from Novartis.

Ragnhild Reehorst Lereim: none.

Stig Wergeland has received speaker honoraria from Biogen and Novartis.

Eystein Oveland: none.

Kjell-Morten Myhr has received unrestricted research grants to his institution and/or scientific advisory board or speakers honoraria from Almirall, Biogen,

Genzyme, Merck, Novartis, Roche and Teva; and has participated in clinical trials organized by Biogen, Merck, Novartis, and Roche.

Lars Bø has received unrestricted research grants to his institution and/or scientific advisory board or speakers honoraria from Almirall, Biogen, Genzyme, Merck, Novartis, Roche and Teva; and has participated in clinical trials organized by Biogen, Merck, Novartis, Roche, and Genzyme.

Øivind Torkildsen has received speaker honoraria from and served on scientific advisory boards for Biogen, Sanofi-Aventis, Merck, and Novartis.

Appendix A. Supplementary data

Supplementary data to this article can be found online at <https://doi.org/10.1016/j.jneuroim.2019.577091>.

References

- Al-Izki, S., Pryce, G., Jackson, S.J., Giovannoni, G., Baker, D., 2011. Immunosuppression with FTY720 is insufficient to prevent secondary progressive neurodegeneration in experimental autoimmune encephalomyelitis. *Mult. Scler. J.* 17 (8), 939–948.
- Alme, M.N., Nystad, A.E., Bo, L., Myhr, K.M., Vedeler, C.A., Wergeland, S., Torkildsen, O., 2015. Fingolimod does not enhance cerebellar remyelination in the cuprizone model. *J. Neuroimmunol.* 285, 180–186.
- Balaton, B., Storch, M.K., Swoboda, E.M., Schonborn, V., Koziel, A., Lambrou, G.N., Hiestand, P.C., Weissert, R., Foster, C.A., 2007. FTY720 sustains and restores neuronal function in the DA rat model of MOG-induced experimental autoimmune encephalomyelitis. *Brain Res. Bull.* 74 (5), 307–316.
- Brinkmann, V., 2007. Sphingosine 1-phosphate receptors in health and disease: mechanistic insights from gene deletion studies and reverse pharmacology. *Pharmacol. Ther.* 115 (1), 84–105.
- Brinkmann, V., Pinschewer, D., Chiba, K., Feng, L., 2000. FTY720: a novel transplantation drug that modulates lymphocyte traffic rather than activation. *Trends Pharmacol. Sci.* 21 (2), 49–52.
- Calabresi, P.A., Radue, E.W., Goodin, D., Jeffery, D., Rammohan, K.W., Reder, A.T., Vollmer, T., Agus, M.A., Kappos, L., Stites, T., Li, B., Cappiello, L., von Rosenstiel, P., Lublin, F.D., 2014. Safety and efficacy of fingolimod in patients with relapsing-remitting multiple sclerosis (FREEDOMS II): a double-blind, randomised, placebo-controlled, phase 3 trial. *Lancet Neurol.* 13 (6), 545–556.
- Chiba, K., Yanagawa, Y., Masubuchi, Y., Kataoka, H., Kawaguchi, T., Ohtsuki, M., Hoshino, Y., 1998. FTY720, a novel immunosuppressant, induces sequestration of circulating mature lymphocytes by acceleration of lymphocyte homing in rats. 1. FTY720 selectively decreases the number of circulating mature lymphocytes by acceleration of lymphocyte homing. *J. Immunol.* 160 (10), 5037–5044.
- Chun, J., Hartung, H.P., 2010. Mechanism of action of oral fingolimod (FTY720) in multiple sclerosis. *Clin. Neuropharmacol.* 33 (2), 91–101.
- Deshmukh, V.A., Tardif, V., Lyssiotis, C.A., Green, C.C., Kerman, B., Kim, H.J., Padmanabhan, K., Swoboda, J.G., Ahmad, I., Kondo, T., Gage, F.H., Theofilopoulos, A.N., Lawson, B.R., Schultz, P.G., Lairson, L.L., 2013. A regenerative approach to the treatment of multiple sclerosis. *Nature* 502 (7471), 327–332.
- Feldhaus, B., Dietzel, I.D., Heumann, R., Berger, R., 2004. Effects of interferon-gamma and tumor necrosis factor-alpha on survival and differentiation of oligodendrocyte progenitors. *J. Soc. Gynecol. Investig.* 11 (2), 89–96.
- Groves, A., Kihara, Y., Chun, J., 2013. Fingolimod: direct CNS effects of sphingosine 1-phosphate (S1P) receptor modulation and implications in multiple sclerosis therapy. *J. Neurol. Sci.* 328 (0), 9–18.
- Gudi, V., Moharrehg-Khiabani, D., Skripuletz, T., Koutsoudaki, P.N., Kotsiari, A., Skuljec, J., Trebst, C., Stangel, M., 2009. Regional differences between grey and white matter in cuprizone induced demyelination. *Brain Res.* 1283, 127–138.
- Gupta, V.K., M, M., Klistorner, A., Graham, S., 2017. Mapping proteomics changes induced by fingolimod in different regions of the brain and retina. *Mult. Scler. J.* 23 (3, suppl), 680–975.
- Han, H., Myllykoski, M., Ruskamo, S., Wang, C., Kursula, P., 2013. Myelin-specific proteins: a structurally diverse group of membrane-interacting molecules. *BioFactors* 39 (3), 233–241.
- Hu, Y.H., Lee, X.H., Ji, B.X., Guckian, K., Apicco, D., Pepinsky, R.B., Miller, R.H., Mi, S., 2011. Sphingosine 1-phosphate receptor modulator fingolimod (FTY720) does not promote remyelination in vivo. *Mol. Cell. Neurosci.* 48 (1), 72–81.
- Huttlin, E.L., Bruckner, R.J., Paulo, J.A., Cannon, J.R., Ting, L., Baltier, K., Colby, G., Gewareb, F., Gygi, M.P., Parzen, H., Szypt, J., Tam, S., Zarraga, G., Pontano-Vaites, L., Swarup, S., White, A.E., Schwegge, D.K., Rad, R., Erickson, B.K., Obar, R.A., Gurusarsha, K.G., Li, K., Artavanis-Tsakonas, S., Gygi, S.P., Harper, J.W., 2017. Architecture of the human interactome defines protein communities and disease networks. *Nature* 545 (7655), 505–509.
- Jackson, S.J., Giovannoni, G., Baker, D., 2011. Fingolimod modulates microglial activation to augment markers of remyelination. *J. Neuroinflammation* 8 (76), 1742–2094.
- Jaillard, C., Harrison, S., Stankoff, B., Aigrot, M.S., Calver, A.R., Duddy, G., Walsh, F.S., Pangalos, M.N., Arimura, N., Kaibuchi, K., Zalc, B., Lubetzki, C., 2005. Edg8/S1P5: an oligodendroglial receptor with dual function on process retraction and cell survival. *J. Neurosci.* 25 (6), 1459–1469.
- Kappos, L., E. W. Radue, P. O'Connor, C. Polman, R. Hohlfeld, P. Calabresi, K. Selmaj, C. Agoropoulou, M. Leyk, L. Zhang-Auberson, P. Burtin and F. S. Group, 2010. A placebo-controlled trial of oral fingolimod in relapsing multiple sclerosis. *N. Engl. J. Med.* 362 (5), 387–401.
- Kappos, L., Bar-Or, A., Cree, B.A.C., Fox, R.J., Giovannoni, G., Gold, R., Vermersch, P., Arnold, D.L., Arnold, S., Scherz, T., Wolf, C., Wallstrom, E., Dahlke, F., Investigators, E.C., 2018. Siponimod versus placebo in secondary progressive multiple sclerosis (EXPAND): a double-blind, randomised, phase 3 study. *Lancet* 391 (10127), 1263–1273.
- Kataoka, H., Sugahara, K., Shimano, K., Teshima, K., Koyama, M., Fukumari, A., Chiba, K., 2005. FTY720, sphingosine 1-phosphate receptor modulator, ameliorates experimental autoimmune encephalomyelitis by inhibition of T cell infiltration. *Cell. Mol. Immunol.* 2 (6), 439–448.
- Kim, H.J., Miron, V.E., Dukala, D., Proia, R.L., Ludwin, S.K., Traka, M., Antel, J.P., Soliven, B., 2011. Neurobiological effects of sphingosine 1-phosphate receptor modulation in the cuprizone model. *FASEB J.* 25 (5), 1509–1518.
- Kim, S., Steelman, A.J., Zhang, Y., Kinney, H.C., Li, J., 2012. Aberrant upregulation of astroglial ceramide potentiates oligodendrocyte injury. *Brain Pathol.* 22 (1), 41–57.
- Kim, S., Bielawski, J., Yang, H., Kong, Y., Zhou, B., Li, J., 2018. Functional antagonism of sphingosine-1-phosphate receptor 1 prevents cuprizone-induced demyelination. *Glia* 66 (3), 654–669.

- Kipp, M., Amor, S., 2012. FTY720 on the way from the base camp to the summit of the mountain: relevance for remyelination. *Mult. Scler.* 18 (3), 258–263.
- Kipp, M., Clarner, T., Dang, J., Copray, S., Beyer, C., 2009. The cuprizone animal model: new insights into an old story. *Acta Neuropathol.* 118 (6), 723–736.
- Kiuchi, M., Adachi, K., Kohara, T., Teshima, K., Masubuchi, Y., Mishina, T., Fujita, T., 1998. Synthesis and biological evaluation of 2,2-disubstituted 2-aminoethanols: analogues of FTY720. *Bioorg. Med. Chem. Lett.* 8 (1), 101–106.
- Lassmann, H., 2018. Multiple sclerosis pathology. *Cold Spring Harb. Perspect. Med.* 8 (3).
- Leek, J.T., Scharpf, R.B., Bravo, H.C., Simcha, D., Langmead, B., Johnson, W.E., Geman, D., Baggerly, K., Izarary, R.A., 2010. Tackling the widespread and critical impact of batch effects in high-throughput data. *Nat. Rev. Genet.* 11 (10), 733–739.
- Lereim, R.R., Oveland, E., Xiao, Y., Torkildsen, O., Wergeland, S., Myhr, K.M., Sun, S.C., Berven, F.S., 2016. The brain proteome of the ubiquitin ligase Peli1 knock-out mouse during experimental autoimmune encephalomyelitis. *J. Proteomics Bioinform.* 9 (9), 209–219.
- Lindner, M., Heine, S., Haastert, K., Garde, N., Fokuhl, J., Linsmeier, F., Grothe, C., Baumgartner, W., Stangel, M., 2008. Sequential myelin protein expression during remyelination reveals fast and efficient repair after central nervous system demyelination. *Neuropathol. Appl. Neurobiol.* 34 (1), 105–114.
- Lublin, F., Miller, D.H., Freedman, M.S., Cree, B.A., Wolinsky, J.S., Weiner, H., Lubetzki, C., Hartung, H.P., Montalban, X., Uitendaele, B.M., Merschhemke, M., Li, B., Putzki, N., Liu, F.C., Haring, D.A., Kappos, L., 2016. Oral fingolimod in primary progressive multiple sclerosis (INFORMS): a phase 3, randomised, double-blind, placebo-controlled trial. *Lancet* 387 (10023), 1075–1084.
- Matsushima, G.K., Morell, P., 2001. The neurotoxicant, cuprizone, as a model to study demyelination and remyelination in the central nervous system. *Brain Pathol.* 11 (1), 107–116.
- Mi, H., Muruganujan, A., Ebert, D., Huang, X., Thomas, P.D., 2019. PANTHER version 14: more genomes, a new PANTHER GO-slim and improvements in enrichment analysis tools. *Nucleic Acids Res.* 47 (D1), D419–D426.
- Miron, V.E., Hall, J.A., Kennedy, T.E., Soliven, B., Antel, J.P., 2008a. Cyclical and dose-dependent responses of adult human mature oligodendrocytes to fingolimod. *Am. J. Pathol.* 173 (4), 1143–1152.
- Miron, V.E., Jung, C.G., Kim, H.J., Kennedy, T.E., Soliven, B., Antel, J.P., 2008b. FTY720 modulates human oligodendrocyte progenitor process extension and survival. *Ann. Neurol.* 63 (1), 61–71.
- Miron, V.E., Ludwin, S.K., Darlington, P.J., Jarjour, A.A., Soliven, B., Kennedy, T.E., Antel, J.P., 2010. Fingolimod (FTY720) enhances remyelination following demyelination of organotypic cerebellar slices. *Am. J. Pathol.* 176 (6), 2682–2694.
- Nygaard, V., Rodland, E.A., Hovig, E., 2016. Methods that remove batch effects while retaining group differences may lead to exaggerated confidence in downstream analyses. *Biostatistics* 17 (1), 29–39.
- Nystad, A.E., Wergeland, S., Aksnes, L., Myhr, K.M., Bø, L., Torkildsen, Ø., 2014. Effect of high-dose 1,25 dihydroxyvitamin D3 on remyelination in the cuprizone model. *APMIS* 122 (12), 1178–1186.
- Paxinos, G., 2008. In: Franklin, Keith B.J., Paxinos, George (Eds.), *The Mouse Brain in Stereotaxic Coordinates*. Elsevier Academic Press, 2008, Amsterdam; London.
- Pebay, A., Toutant, M., Premont, J., Calvo, C.F., Venance, L., Cordier, J., Glowinski, J., Tence, M., 2001. Sphingosine-1-phosphate induces proliferation of astrocytes: regulation by intracellular signalling cascades. *Eur. J. Neurosci.* 13 (12), 2067–2076.
- Plemel, J.R., Liu, W.Q., Yong, V.W., 2017. Remyelination therapies: a new direction and challenge in multiple sclerosis. *Nat. Rev. Drug Discov.* 16 (9), 617–634.
- Plubell, D.L., Wilmarth, P.A., Zhao, Y., Fenton, A.M., Minnier, J., Reddy, A.P., Klimek, J., Yang, X., David, L.L., Pampir, N., 2017. Extended multiplexing of tandem mass tags (TMT) labeling reveals age and high fat diet specific proteome changes in mouse epididymal adipose tissue. *Mol. Cell. Proteomics* 16 (5), 873–890.
- Reeves, P.M., Kang, Y.L., Kirchhausen, T., 2016. Endocytosis of ligand-activated sphingosine 1-phosphate receptor 1 mediated by the clathrin-pathway. *Traffic* 17 (1), 40–52.
- Ritchie, M.E., Phipson, B., Wu, D., Hu, Y., Law, C.W., Shi, W., Smyth, G.K., 2015. limma powers differential expression analyses for RNA-sequencing and microarray studies. *Nucleic Acids Res.* 43 (7), e47.
- Slowik, A., Schmidt, T., Beyer, C., Amor, S., Clarner, T., Kipp, M., 2015. The sphingosine 1-phosphate receptor agonist FTY720 is neuroprotective after cuprizone-induced CNS demyelination. *Br. J. Pharmacol.* 172 (1), 80–92.
- Soyombo, A.A., Hofmann, S.L., 1997. Molecular cloning and expression of palmitoyl-protein thioesterase 2 (PPT2), a homolog of lysosomal palmitoyl-protein thioesterase with a distinct substrate specificity. *J. Biol. Chem.* 272 (43), 27456–27463.
- Teunissen, C.E., Dijkstra, C., Polman, C., 2005. Biological markers in CSF and blood for axonal degeneration in multiple sclerosis. *Lancet Neurol.* 4 (1), 32–41.
- Thomas, P.D., Kejariwal, A., Guo, N., Mi, H., Campbell, M.J., Muruganujan, A., Lazareva-Ulitsky, B., 2006. Applications for protein sequence-function evolution data: mRNA/protein expression analysis and coding SNP scoring tools. *Nucleic Acids Res.* 34 (Web Server issue), W645–W650.
- Thompson, A.J., Baranzini, S.E., Geurts, J., Hemmer, B., Ciccarelli, O., 2018. Multiple sclerosis. *Lancet* 391 (10130), 1622–1636.
- Torkildsen, O., Brunborg, L.A., Myhr, K.M., Bø, L., 2008. The cuprizone model for demyelination. *Acta Neurol. Scand. Suppl.* 188, 72–76.
- Vizcaino, J.A., Csordas, A., Del-Toro, N., Dianas, J.A., Griss, J., Lavidas, I., Mayer, G., Perez-Riverol, Y., Reisinger, F., Ternent, T., Xu, Q.W., Wang, R., Hermjakob, H., 2016. 2016 update of the PRIDE database and its related tools. *Nucleic Acids Res.* 44 (22), 11033.
- Wergeland, S., Torkildsen, O., Myhr, K.M., Mork, S.J., Bø, L., 2012. The cuprizone model: regional heterogeneity of pathology. *APMIS* 120 (8), 648–657.
- Werner, S.R., Saha, J.K., Broderick, C.L., Zhen, E.Y., Higgs, R.E., Duffin, K.L., Smith, R.C., 2010. Proteomic analysis of demyelinated and remyelinating brain tissue following dietary cuprizone administration. *J. Mol. Neurosci.* 42 (2), 210–225.
- Wiśniewski, J.R., A. Z., Nagaraj, N., Mann, M., 2009. Universal sample preparation method for proteome analysis. *Nat. Methods* 6 (5), 359–362.
- Yazdi, A., Baharvand, H., Javan, M., 2015. Enhanced remyelination following lysolecithin-induced demyelination in mice under treatment with fingolimod (FTY720). *Neuroscience* 311, 34–44.
- Yazdi, A., Ghasemi-Kasman, M., Javan, M., 2019. Possible regenerative effects of fingolimod (FTY720) in multiple sclerosis disease: an overview on remyelination process. *J. Neurosci. Res.* 00, 1–13.
- Zhang, J., Zhang, Z.G., Li, Y., Ding, X., Shang, X., Lu, M., Elias, S.B., Chopp, M., 2015. Fingolimod treatment promotes proliferation and differentiation of oligodendrocyte progenitor cells in mice with experimental autoimmune encephalomyelitis. *Neurobiol. Dis.* 76, 57–66.
- Zhang, Y., Li, X., Ciric, B., Ma, C.G., Gran, B., Rostami, A., Zhang, G.X., 2017. Effect of fingolimod on neural stem cells: a novel mechanism and broadened application for neural repair. *Mol. Ther.* 25 (2), 401–415.

Supporting information for paper I

The supporting information for this paper is printed in the following.

Table S1: Antibodies used for immunohistochemistry specified.

Table S2: Pooling strategy for the proteomics experiment.

Table S3: Proteins significantly different ($p < 0.01$, \log_2 FC Fingolimod - Placebo $> 20\%$) after 6 weeks of demyelination.

Table S4: Proteins significantly different ($p < 0.01$, \log_2 FC Fingolimod – Placebo $> 20\%$) after 1 week of remyelination.

Table S5: Proteins significantly different ($p < 0.01$, \log_2 FC Fingolimod – Placebo $> 20\%$) after 3 weeks of remyelination.

Table S6A: Histochemistry and immunohistochemistry data from the midline of corpus callosum. Controls

Table S6B: Histochemistry and immunohistochemistry data from the midline of corpus callosum. 6 weeks of cuprizone exposure

Table S6C: Histochemistry and immunohistochemistry data from the midline of corpus callosum. 1 week of remyelination

Table S6D: Histochemistry and immunohistochemistry data from the midline of corpus callosum. 3 weeks of remyelination

Table S7A: Histochemistry and immunohistochemistry data from the secondary motor cortex
Controls

Table S7B: 6 weeks of cuprizone exposure

Table S7C: 1 week of remyelination

Table S7D: 3 weeks of remyelination

Figure S1A: Study design.

Figure S1B: Regional sampling sites for histochemistry and immunohistochemistry in the mouse brain.

Figure S2: Distribution of the average protein \log_2 abundances prior to statistical analysis in limma.

Figure S3: The average \log_2 abundances based on three pools, each containing two biological replicates and their standard deviation. (IHC markers)

Figure S4. CD3 immunopositivity

Figure S4. CD3 immunoreactivity

Supplementary methods

Supplementary tables

Table S1. Antibodies used for immunohistochemistry specified.

Target antigen	Species, type	Working dilution	Incubation time/ Temperature	Demasking	Provider
PLP	Mouse, monoclonal	1:1000	24h/4°C	Citrate	Serotec
GFAP	Rabbit, monoclonal	1:2000	½h/ RT	Tris-EDTA	Dako (Agilent)
NOGO-A	Rabbit, polyclonal	1:1000	1h/RT	Citrate	Chemicon, Temecula
MAC-3	Rat, monoclonal	1:200	24h/RT	Citrate	BD Biosciences
CD3	Rabbit, polyclonal	1:500	½h/RT	Tris-EDTA	Dako
APP	Mouse, monoclonal	1:2000	24h/4°C	Citrate	Merck
NFL	Mouse, monoclonal	1:1600	1h/RT	Tris-EDTA	Merck

RT = room temperature

PLP: anti-Proteolipid Protein

GFAP: anti-Glial Fibrillary Acidic Protein

NOGO-A: anti-Neurite Outgrowth Inhibitor Protein A

CD3: cluster of differentiation 3

APP: anti-Alzheimer Precursor Protein A4, clone 22C11

NFL: anti-phosphorylated Neurofilament light

Table S2.
Pooling strategy for the proteomics experiment.

	Fingolimod			Placebo		Reference
DM	1RM	3RM	DM	1RM	3RM	
2 biological samples TMT 126	2 biological samples TMT 127N	2 biological samples TMT 128N	2 biological samples TMT 129N	2 biological samples TMT 130C	2 biological samples TMT 130N	36 samples TMT 131
2 biological samples TMT 127C	2 biological samples TMT 128C	2 biological samples TMT 129C	2 biological samples TMT 128C	2 biological samples TMT 129C	2 biological samples TMT 130C	36 samples TMT131
2 biological samples TMT 126	2 biological samples TMT 127C	2 biological samples TMT 127N	2 biological samples TMT 128N	2 biological samples TMT 129N	2 biological samples TMT 130N	

The brain samples (n=6 in each condition) were randomized and divided into 3 mini-pools. Each condition was represented in both TMT 10 plex experiment 1 (White) and 2 (Blue). One reference pool containing equal amounts of each brain lysate was included in each TMT 10-plex to enable comparison in the post analysis.

Table S3.
Proteins significantly different ($p < 0.01$ \log_2 FC Fingolimod - Placebo $> 20\%$) after 6 weeks of demyelination.

Accession	Description	Gene short	\log_2 FC	p-value
O08530	Sphingosine 1-phosphate receptor 1	S1pr1	-0.54	0.0000005
Q7M6Z0	Reticulon-4 receptor-like 2	Rtn4rl2	0.21	0.0002
Q80SZ7	Guanine nucleotide-binding protein G(I)/G(S)/G(O) subunit gamma-5	Gng5	-0.45	0.0003
Q8CJ61	CKLF-like MARVEL transmembrane domain-containing protein 4	Cmtm4	-0.29	0.0003
Q6PGG6	Guanine nucleotide-binding protein-like 3-like protein	Gnl3l	-0.43	0.0005
Q8BUV8	Protein GPR107	Gpr107	-0.47	0.001
Q922W5	Pyrroline-5-carboxylate reductase 1, mitochondrial	Pycr1	-0.35	0.001

Q8K209	G-protein coupled receptor 56	Gpr56	-0.39	0.002
E9Q5K9	YTH domain-containing protein 1	Ythdc1	-0.26	0.002
Q810B8	SLIT and NTRK-like protein 4	Slitrk4	-0.22	0.003
Q9CX11	rRNA-processing protein UTP23 homolog	Utp23	-0.29	0.003
O89020	Afamin	Afm	-0.68	0.003
P46662	Merlin	Nf2	-0.32	0.003
Q3UHF7	Transcription factor HIVEP2	Hivep2	-0.23	0.004
Q8BHR8	UPF0705 protein C11orf49 homolog	1 SV=1	-0.26	0.004
Q5RJH6	Protein SMG7	Smg7	-0.34	0.006
Q6PDY0	Coiled-coil domain-containing protein 85B	Ccdc85b	0.22	0.007
Q62313	Trans-Golgi network integral membrane protein 1	Tgoln1	-0.22	0.008
Q8CI11	Guanine nucleotide-binding protein-like 3	Gnl3	-0.23	0.009
Q91W92	Cdc42 effector protein 1	Cdc42ep1	-0.46	0.009
A2AV25	Fibrinogen C domain-containing protein 1	Fibcd1	-0.32	0.010

Table S4.
Proteins significantly different ($p < 0.01$, \log_2 FC Fingolimod – Placebo $> 20\%$) after 1 week of remyelination.

Accession	Description	Gene short	\log_2 FC	p-value
O08530	Sphingosine 1-phosphate receptor 1	S1pr1	-0.84	0.00000003
O35448	Lysosomal thioesterase PPT2	Ppt2	-0.49	0.000004
Q80SZ7	Guanine nucleotide-binding protein G(I)/G(S)/G(O) subunit gamma-5	Gng5	-0.47	0.0001
O55236	mRNA-capping enzyme	Rngtt	-0.21	0.002
Q8BHK1	Magnesium transporter NIPA1	Nipa1	-0.21	0.002
Q9QXN3	Activating signal cointegrator 1	Trip4	0.28	0.003
Q9D1G2	Phosphomevalonate kinase	Pmvk	-0.33	0.004
Q9CR24	Nucleoside diphosphate-linked moiety X motif 8, mitochondrial	Nudt8	0.28	0.004

Q3TRM8	Hexokinase-3	Hk3	-0.38	0.004
Q9WTQ8	Mitochondrial import inner membrane translocase subunit Tim23	Timm23	0.22	0.005
Q9DC04	Regulator of G-protein signaling 3	Rgs3	0.22	0.005
Q8BNA6	Protocadherin Fat 3	Fat3	0.25	0.005
Q69ZN7	Myoferlin	Myof	-0.28	0.006
Q00623	Apolipoprotein A-I	Apoa1	-0.24	0.007
Q8CFJ9	WD repeat-containing protein 24	Wdr24	-0.23	0.009
Q8BGS7	Choline/ethanolaminephosphotransferase 1	Cept1	0.20	0.009

Table S5.
Proteins significantly different ($p < 0.01$, \log_2 FC Fingolimod – Placebo $> 20\%$) after 3 weeks of remyelination.

Accession	Description	Gene short	\log_2 FC	p-value
O08530	Sphingosine 1-phosphate receptor 1	S1pr1	-0.87	0.000000002
Q9WVA4	Transgelin-2	Tagln2	0.21	0.0005
Q9JHK5	Pleckstrin	Plek	0.21	0.001
Q80SZ7	Guanine nucleotide-binding protein G(I)/G(S)/G(O) subunit gamma-5	Gng5	-0.39	0.001
P08207	Protein S100-A10	S100a10	0.58	0.001
O88878	AN1-type zinc finger protein 5	Zfand5	0.43	0.001
Q8CAM5	Ras-related protein Rab-36	Rab36	0.49	0.002
Q9CX11	rRNA-processing protein UTP23 homolog	Utp23	0.31	0.002
Q9JJR9	Nuclear receptor-interacting protein 3	Nrip3	0.26	0.002
Q8BWU8	Ethanolamine-phosphate phospho-lyase	Etnppl	0.27	0.002
Q8VCM7	Fibrinogen gamma chain	Fgg	0.28	0.002
P97433	Rho guanine nucleotide exchange factor 28	Arhgef28	-0.40	0.002
P31649	Sodium- and chloride-dependent GABA transporter 2	Slc6a13	0.44	0.003
Q8BFR6	AN1-type zinc finger protein 1	Zfand1	-0.30	0.003
Q9QXE0	2-hydroxyacyl-CoA lyase 1	Hac11	-0.26	0.003

Q8R5F3	O-acetyl-ADP-ribose deacetylase 1	Oard1	0.24	0.003
Q08091	Calponin-1	Cnn1	0.62	0.003
Q9CQ28	Diphthine--ammonia ligase	Dph6	0.31	0.004
Q63959	Potassium voltage-gated channel subfamily C member 3	Kcnc3	0.21	0.004
Q8VC16	Leucine-rich repeat-containing protein 14	Lrrc14	0.20	0.004
Q64339	Ubiquitin-like protein ISG15	Isg15	-0.23	0.005
Q9D658	Protein tyrosine phosphatase type IVA 3	Ptp4a3	-0.29	0.006
Q64345	Interferon-induced protein with tetratricopeptide repeats 3	Ifit3	-0.25	0.006
Q9EP71	Ankyrin	Rai14	0.23	0.006
P28653	Biglycan	Bgn	0.46	0.006
Q8K353	Cysteine-rich and transmembrane domain-containing protein 1	Cystm1	0.27	0.007
Q9CZE3	Ras-related protein Rab-32	Rab32	0.40	0.008
P37804	Transgelin	Tagln	0.71	0.009
Q8BHG9	CGG triplet repeat-binding protein 1	Cggbp1	0.22	0.009
Q9ES52	Phosphatidylinositol 3,4,5-trisphosphate 5-phosphatase 1	Inpp5d	-0.27	0.009

Table S6A
Histochemistry and immunohistochemistry data from the midline of corpus callosum.

Controls

	Healthy Control			Cuprizone Control			<i>p</i>
	Mean	Median	SD	Mean	Median	SD	
LFB	0.3	0.0	0.5	1.5	1.5	0.5	0.036
PLP	90.2	91.9	5.5	71.3	64.1	13.7	0.13
GFAP	0.7	0.5	0.3	1.8	1.5	0.6	0.024
MAC-3	0.0	0.0	0.0	14.0	15.0	6.6	0.018
NOGO-A	29.8	29.5	16.4	15.5	15.5	12.0	0.21
NFL	90.9	91.0	2.6	63.2	64.9	24.9	0.041
APP	0.0	0.0	0.0	29.0	28.5	17.1	0.002
CD3	0.5	0.0	1.2	1.0	1.0	1.0	0.46

p = Sig. (2-tailed), Exact. Sig. (2-tailed) when Mann-Whitney is used.

Table S6B**Histochemistry and immunohistochemistry data from the midline of corpus callosum.****6 weeks of cuprizone exposure**

	Fingolimod		SD	Placebo		SD	<i>p</i>
	Mean	Median		Mean	Median		
LFB	1.8	2.0	0.5	2.0	2.5	0.7	0.38
PLP	64.3	66.7	16.4	57.1	65.2	22.9	0.64
GFAP	1.8	1.8	0.7	1.8	2.0	0.8	0.93
MAC-3	21.8	22.0	4.0	12.1	10.0	7.3	0.058
NOGO-A	10.0	5.0	9.5	6.4	7.0	1.5	0.58
NFL	80.7	84.4	13.1	78.9	82.2	12.4	0.81
APP	18.8	18.5	1.9	22.5	20.5	8.1	0.80
CD3	0.0	0.0	0.0	0.2	0.0	0.4	1.00

p = Sig. (2-tailed), Exact. Sig. (2-tailed) when Mann-Whitney is used.

Table S6C**Histochemistry and immunohistochemistry data from the midline of corpus callosum.****1 week of remyelination**

	Fingolimod			Placebo			<i>p</i>
	Mean	Median	SD	Mean	Median	SD	
LFB	2.2	2.0	0.3	2.1	2.0	0.4	1.00
PLP	50.8	39.5	28.4	51.8	54.8	23.8	0.96
GFAP	2.1	2.0	0.6	1.8	2.0	0.5	0.36
MAC-3	14.0	12.5	9.1	10.0	9.0	5.8	0.42
NOGO-A	24.2	22.0	9.2	30.0	29.0	8.5	0.31
NFL	79.9	81.6	8.5	85.1	85.2	7.9	0.30
APP	7.0	5.0	5.2	13.5	15.5	8.3	0.25
CD3	0.8	0.0	1.5	0.5	0.5	0.6	0.79

p = Sig. (2-tailed), Exact. Sig. (2-tailed) when Mann-Whitney is used.

Table S6D**Histochemistry and immunohistochemistry data from the midline of corpus callosum.****3 weeks of remyelination**

	Fingolimod		SD	Placebo		SD	<i>p</i>
	Mean	Median		Mean	Median		
LFB	1.7	1.5	0.3	1.3	1.3	0.7	0.40
PLP	71.6	70.9	4.8	62.6	57.6	12.0	0.28
GFAP	1.8	1.5	0.5	1.8	2.0	0.3	0.81
MAC-3	5.4	5.0	3.5	10.4	9.0	5.0	0.10
NOGO-A	30.0	32.5	9.9	31.4	29.0	7.5	0.90
NFL	84.7	85.5	4.4	88.6	90.9	4.0	0.26
APP	5.7	5.0	3.9	4.2	2.0	3.5	0.35
CD3	0.4	0.0	0.6	1.0	0.5	1.4	0.76

p = Sig. (2-tailed), Exact. Sig. (2-tailed) when Mann-Whitney is used.

Table S7A
Histochemistry and immunohistochemistry data from the secondary motor cortex

Controls

	Healthy Control		Cuprizone Control		(SD)	<i>p</i>	
	Mean	Median	Mean	Median			
LFB	1.4	1.5	1.3	3.0	3.0	0.0	0.15
PLP	7.9	7.3	5.9	0.9	1.1	0.4	0.053
GFAP	0.0	0.0	0.0	2.0	2.0	0.0	0.008
MAC-3	0.0	0.0	0.0	14.0	5.0	6.6	0.018
NOGO-A	10.3	9.0	4.3	4.5	4.5	6.4	0.004
NFL	16.2	5.5	16.0	13.1	12.6	9.6	0.697

p = Sig. (2-tailed), Exact. Sig. (2-tailed) when Mann-Whitney is used.

Table S7B**6 weeks of cuprizone exposure**

	Fingolimod			Placebo			<i>p</i>
	Mean and Median		(SD)	Mean and Median		(SD)	
LFB	3.0	3.0	0.0	2.9	3.0	0.2	1.0
PLP	1.0	1.0	0.3	2.9	1.8	2.7	0.128
GFAP	2.4	2.5	0.6	1.7	1.5	0.8	0.160
MAC-3	21.8	5.5	4.0	12.2	4.0	7.5	0.530
NOGO-A	0.7	0.0	1.2	7.2	8.0	5.8	0.084
NFL	9.4	8.7	4.3	19.9	19.2	5.2	0.005

p = Sig. (2-tailed), Exact. Sig. (2-tailed) when Mann-Whitney is used.

Table S7C**1 week of remyelination**

	Fingolimod			Placebo			<i>p</i>
	Mean	Median	(SD)	Mean	Median	(SD)	
LFB	2.5	3.0	0.9	2.8	3.0	0.3	0.773
PLP	2.1	2.3	0.8	4.7	4.9	3.7	0.481
GFAP	1.6	1.5	0.3	1.9	2.0	0.5	0.171
MAC-3	14.0	4.5	9.1	10.0	2.5	5.8	0.065
NOGO-A	4.2	3.0	2.7	4.5	4.5	2.6	0.749
NFL	21.1	19.7	12.0	16.1	16.9	8.2	0.419

p = Sig. (2-tailed), Exact. Sig. (2-tailed) when Mann-Whitney is used.

Table S7D**3 weeks of remyelination**

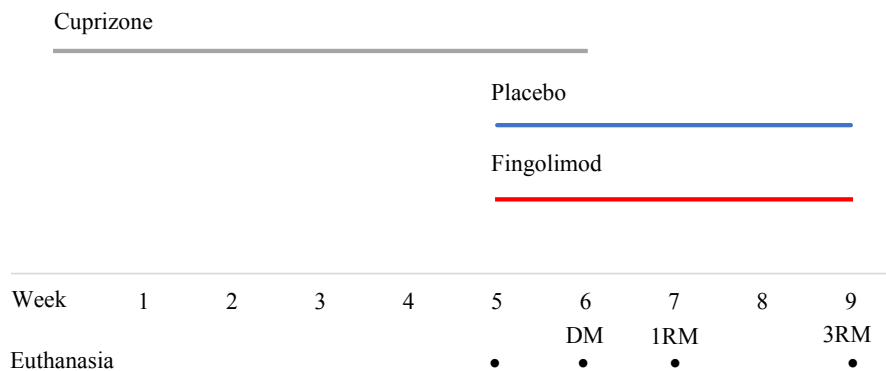
	Fingolimod			Placebo			<i>p</i>
	Mean and Median		(SD)	Mean and Median		(SD)	
LFB	2.4	2.5	0.7	2.5	2.5	0.6	1.0
PLP	3.3	2.0	3.2	3.8	2.6	2.6	0.662
GFAP	1.2	1.0	0.3	1.0	1.0	0.5	0.643
MAC-3	5.4	1.0	3.5	10.4	0.0	5.0	0.784
NOGO-A	5.2	3.5	4.3	1.6	2.0	0.6	0.032
NFL	14.0	13.4	7.1	12.9	13.7	3.8	0.824

p = Sig. (2-tailed), Exact. Sig. (2-tailed) when Mann-Whitney is used.

Supplementary figures

Figure S1A

Study design.

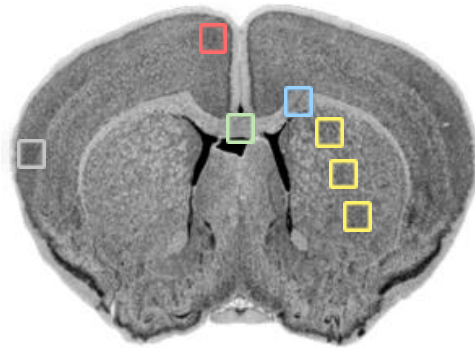


Supplementary figure 1.

The figure shows the timeline for the experiment, including cuprizone exposure. Fingolimod or placebo was given by gavage daily from week five until euthanasia. Cuprizone controls and healthy controls were euthanized after 5 and 9 weeks, respectively. Brain samples for cuprizone mice treated with fingolimod or placebo were prepared for immunohistochemistry and proteomics at three different time points, 6 weeks of demyelination (DM), 1 week of remyelination (1RM) and 3 weeks of remyelination (3RM).

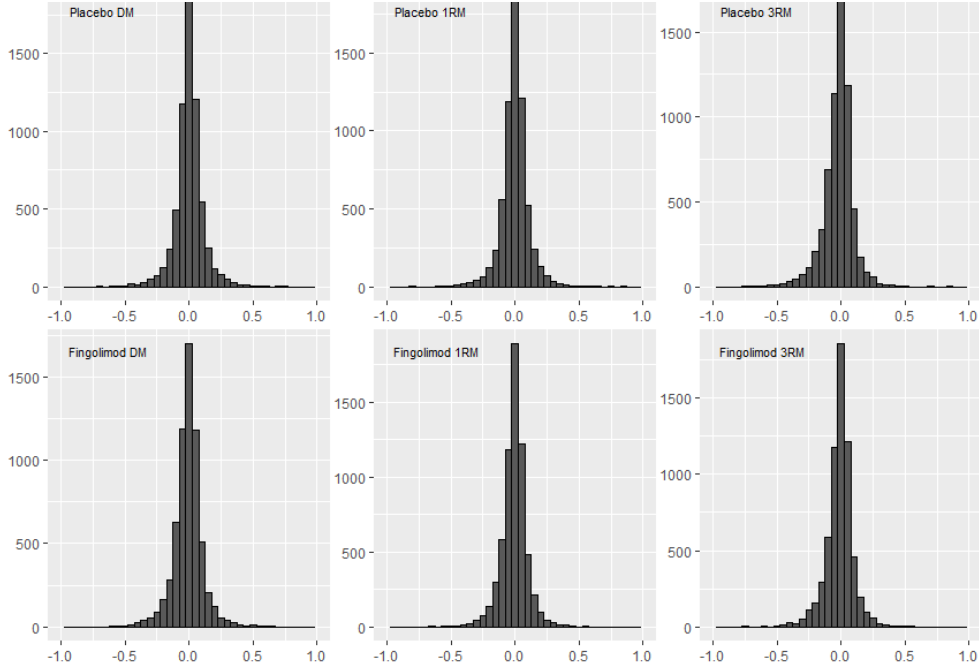
Figure S1B

Regional sampling sites for histochemistry and immunohistochemistry in the mouse brain.



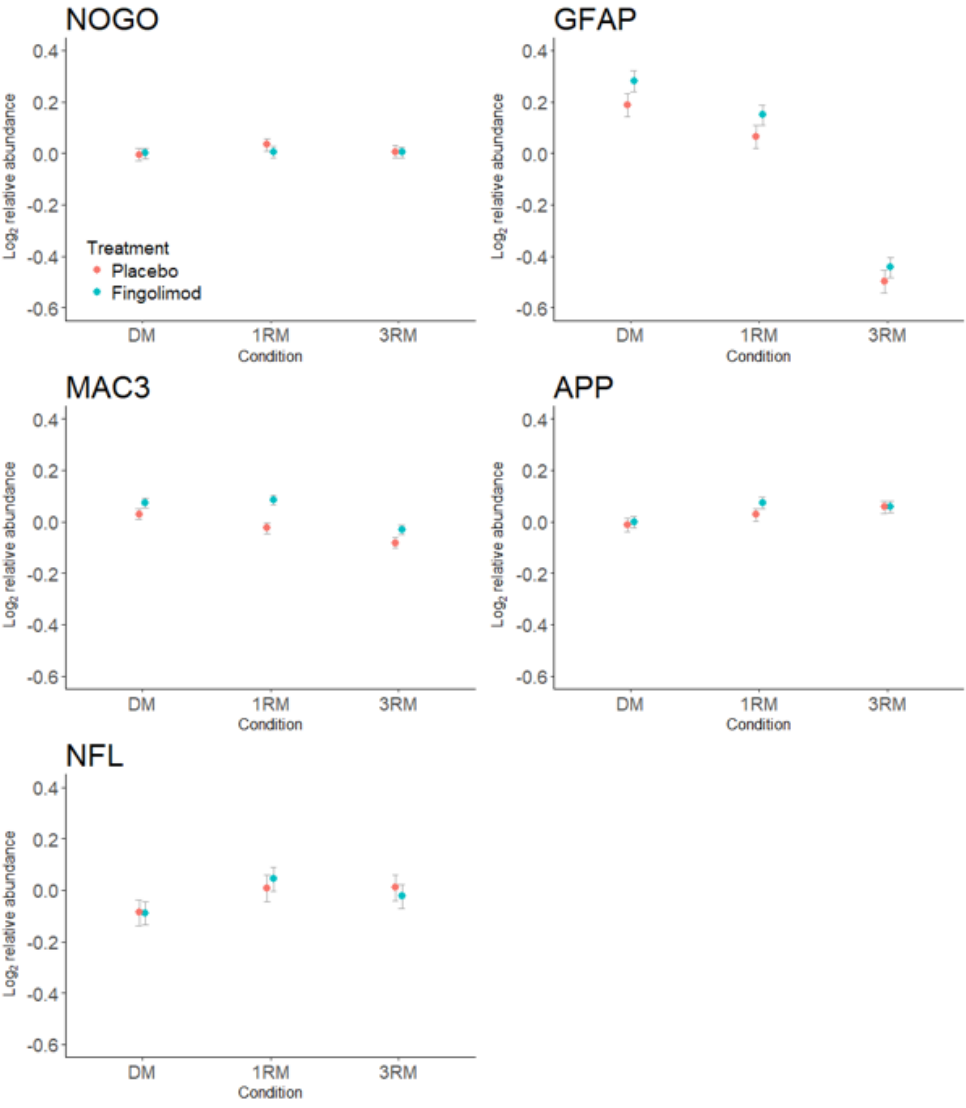
Red: Supplementary motor cortex (M2), green: Medial corpus callosum (cc), blue: Lateral corpus callosum (cingulum, cg), yellow: Deep gray matter –striatum (CPu), grey: 2nd somatosensory cortex (S2).

Figure S2



Supplementary figure 2: Distribution of the average protein \log_2 abundances prior to statistical analysis in limma. The averages are based on three pools, each containing two biological replicates. DM= six weeks of demyelination, 1RM= one week of remyelination, 3RM = three weeks of remyelination.

Figure S3

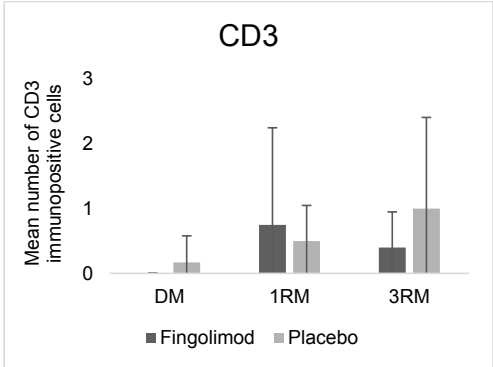


Supplementary figure 3: The average log₂ abundances based on three pools, each containing two biological replicates and their standard deviation. NOGO-A: Neurite Outgrowth Inhibitor Protein A, GFAP: Glial Fibrillary Acidic Protein, MAC-3: macrophages and microglia, APP: amyloid precursor

protein A4, NFL: phosphorylated neurofilament light. DM= six weeks of demyelination, 1RM= one week of remyelination, 3RM= three weeks of remyelination.

Figure S4. CD3 immunopositivity

A)

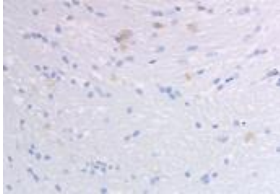
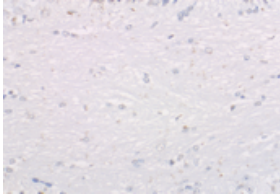


B)

CD3

Healthy control

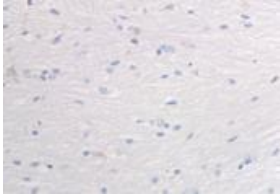
Cuprizone control



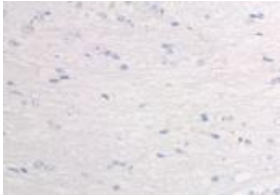
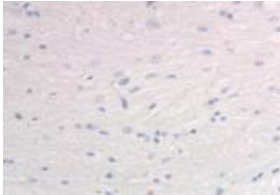
Fingolimod

Placebo

DM



1RM



3RM

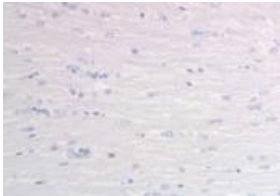
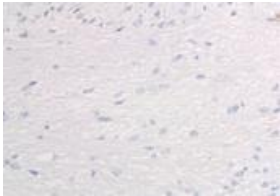


Figure S4. CD3 immunoreactivity

A) Number of CD3 immunopositive cells in the fingolimod and placebo group after 6 weeks of demyelination, 1 week of remyelination and 3 weeks of remyelination. We did not find a difference between the fingolimod and the placebo group at any time point. Cell counts are provided as mean number of cells per 0.0625 mm^2 , in the midline of the corpus callosum. Error bars: $\pm 1 \text{ SD}$.

B) CD3 and hematoxyline stained sections. DM= six weeks of demyelination, 1RM= one week of remyelination, 3RM= three weeks of remyelination. All images at 40x.

Supplementary methods

LC-MS analysis of TMT-labeled samples

About 0.5 µg tryptic peptides were injected into an Ultimate 3000 RSLC system (Thermo Scientific, Sunnyvale, California, USA) connected to a Q-Exactive HF equipped with a nanospray Flex ion source (Thermo Scientific, Bremen, Germany). The sample was loaded and on a pre-column Acclaim PepMap 100, 2cm x 75µm i.d. nanoViper column, packed with 3µm C18 beads at a flow rate of 3µl/min for 5 min with 0.1% TFA (trifluoroacetic acid, vol/vol). Peptides were separated during a biphasic ACN gradient from two nanoflow UPLC pumps (flow rate of 0.250 µl/min) on a 25 cm analytical column (Easy-Spray 802, 25cm x 75µm i.d. PepMap RSLC column, packed with 2µm C18 beads (Thermo Scientific). Solvent A was 0.1% FA (vol/vol) in water, and solvent B was 100% ACN. The fractions were applied different LC-methods depending on their elution from the mixed mode column.

LC-gradients for the TMT-labeled fractions in the LC-MS analysis

The mixed mode fractions were applied different LC-gradients depending on their elution from the mixed mode column, solvent A was 0.1% FA (vol/vol) in water and solvent B was 100% ACN. Fraction 1-6 had a gradient of 5 % B 0-5 min, then 5-12 % B 5-65 min, 12-30 % B from 65-87 min, 30-90 % B from 87-92 min, 90 % B from 92-102 min, 90-5 % B from 102-105 min and held at 5% B until the end. Fractions 7-36 had a gradient of 5 % B from 0-5 min, 5-7 % B from 5-5,5 min, 7-22 % B from 5.5-65 min, 22-35% B from 65-87 min, 35-90 % B from 87-92 min, 90 % B from 92-102 min, 90-5 % B from 102-105 min, 5 % B from 108-120. Fractions 37-60 had a gradient of 5 % B 0-5 min, 5-7 % B from 5-5,5 min, 7-40 % B from 5,5-87 min, 40-90 % B from 87-92 min, 90 % B from 92-102 min, 90-5 % B from 102-105 min, and 5% from 105-120 min.

Mass spectrometer settings

The mass spectrometer was operated in the data-dependent-acquisition mode to automatically switch between full scan MS¹ and MS² acquisition. The instrument was controlled through Q-Exactive HF Tune 2.4 and Xcalibur 3.0. MS¹ spectra were acquired to detect precursors in the scan range 375-1500 m/z with resolution R = 60,000 at 200 m/z. The automatic gain control (AGC) had an ion target of 3e6 and a maximum injection time (IT) of 50 milliseconds (ms). The 15 most intense precursors with charge states 2 or higher and above intensity threshold 5e4 were sequentially isolated. The target AGC value for MS² was 1e5, acquired at R = 30,000. The ions were collected with IT 45 ms and fragmented with a normalized collision energy of 32 %. The precursor isolation window was 1.6 m/z, and with isolation offset of 0.3 Da. A dynamic exclusion of 30 seconds was used to prevent precursor re-sampling and to maximize the number of sampled precursors. Lock-mass internal calibration was used, and isotope exclusion was on.

Quantification of TMT data in Proteome Discoverer

Following LC-MS analysis, data from the two TMT-10 plex experiments were collected and analyzed in Proteome Discoverer 2.0 (Thermo Scientific), using Sequest HT, and MS Amanda (version 1.4.4.2822) and the SwissProt *Mus musculus* downloaded 15.10.2015 (canonical sequences not including isoforms) and the cRAP contaminants database from 30.01.2015 (<ftp://ftp.thegpm.org/fasta/cRAP/>). The following settings were used for both search engines. Trypsin was set as the enzyme, and maximum two missed cleavages were allowed. TMT tagging of N-terminals and lysines were established as a fixed modification, in addition to carbamidomethylation of cysteine. Oxidation of methionine was set as a variable modification. The fragment mass tolerance was set to 0.01 Da for MS Amanda and 0.02 for Sequest HT. The identification deviance was set to 10 ppm for MS1 precursors. The PSM validation from all search engines was performed using Percolator, with a strict and relaxed target FDR of 0.01 and 0.05, respectively. TMT 10-plex was set as the quantification method with the integration tolerance 20 ppm and the integration method most

confident centroid. All samples were normalized to the reference sample within each TMT 10-plex using Proteome Discoverer. Unique peptides were used for quantification.

The two 10-plexes were merged globally by search engine type, and PSMs with low confidence were discarded. The reporter ion isotopic distribution provided with the TMT kit was used to minimize cross-contamination in the TMT channels. The co-isolation threshold was set to 50%. The reporter abundance was based on a signal to noise values when available, if not intensities were used. The average signal to noise threshold was set to 10 s/n. Only proteins identified with unambiguously identified high confidence peptides (FDR <1%) were used. The datasets were normalized to the total peptide amount. The resulting quantified proteins were filtered so that only master proteins were exported for analysis.

Statistical analysis in R

Prior to data upload to R, contaminants and proteins containing missing values were removed. The dataset was analyzed by the statistical software limma (Ritchie et al., 2015), where the batch effect was taken into account. Specifically, a linear model with the function $\text{abundance} = \text{condition} + \text{batch}$ (condition = Placebo DM, Placebo 1RM, Placebo 3RM, Fingolimod DM, Fingolimod 1RM, Fingolimod 3RM) (batch = 0 or 1 depending on the TMT experiment) was generated before empirical Bayes statistics (Smyth, 2004) on the resulting values for condition. Proteins with a p-value <0.01 and a $\log_2 \text{FC} > 0.2$ or < -0.2 was considered significant. Benjamini Hochberg correction was used to adjust the p-values for multiple comparisons (q-value <0.05). The graphics package ggplot2 (H. Wickham. ggplot2: Elegant Graphics for Data Analysis. Springer-Verlag New York, 2009) was used to generate figures. Gene Ontology Biological process enrichment analysis was carried out for the proteins considered to be significantly different in Panther (Mi, Muruganujan, Ebert, Huang, & Thomas, 2019; Thomas et al., 2006). The R script used for statistical analysis and graphics is publicly available at <https://github.com/RagnhildRLereim/Fingolimod>.

References

- Mi, H., Muruganujan, A., Ebert, D., Huang, X., & Thomas, P. D. (2019). PANTHER version 14: more genomes, a new PANTHER GO-slim and improvements in enrichment analysis tools. *Nucleic Acids Res*, 47(D1), D419-D426. Retrieved from <https://www.ncbi.nlm.nih.gov/pubmed/30407594>
<https://www.ncbi.nlm.nih.gov/pmc/articles/PMC6323939/pdf/gky1038.pdf> doi:10.1093/nar/gky1038
- Ritchie, M. E., Phipson, B., Wu, D., Hu, Y., Law, C. W., Shi, W., & Smyth, G. K. (2015). limma powers differential expression analyses for RNA-sequencing and microarray studies. *Nucleic Acids Res*, 43(7), e47. Retrieved from <https://www.ncbi.nlm.nih.gov/pubmed/25605792>
<https://www.ncbi.nlm.nih.gov/pmc/articles/PMC4402510/pdf/gkv007.pdf> doi:10.1093/nar/gkv007
- Smyth, G. K. (2004). Linear models and empirical bayes methods for assessing differential expression in microarray experiments. *Stat Appl Genet Mol Biol*, 3, Article3. Retrieved from <https://www.ncbi.nlm.nih.gov/pubmed/16646809>
<https://www.degruyter.com/view/j/sagmb.2004.3.issue-1/sagmb.2004.3.1.1027/sagmb.2004.3.1.1027.xml> doi:10.2202/1544-6115.1027
- Thomas, P. D., Kejariwal, A., Guo, N., Mi, H., Campbell, M. J., Muruganujan, A., & Lazareva-Ulitsky, B. (2006). Applications for protein sequence-function evolution data: mRNA/protein expression analysis and coding SNP scoring tools. *Nucleic Acids Res*, 34(Web Server issue), W645-650. Retrieved from <https://www.ncbi.nlm.nih.gov/pubmed/16912992>
<https://www.ncbi.nlm.nih.gov/pmc/articles/PMC1538848/pdf/gkl229.pdf>.

Paper II

RESEARCH

Open Access



Development of robust targeted proteomics assays for cerebrospinal fluid biomarkers in multiple sclerosis

Astrid Guldbrandsen^{1,2} , Ragnhild Reehorst Lereim^{1,2}, Mari Jacobsen¹, Hilde Garberg³, Ann Cathrine Kroksveen³, Harald Barsnes^{1,2} and Frode S. Berven^{1*}

Abstract

Background: Verification of cerebrospinal fluid (CSF) biomarkers for multiple sclerosis and other neurological diseases is a major challenge due to a large number of candidates, limited sample material availability, disease and biological heterogeneity, and the lack of standardized assays. Furthermore, verification studies are often based on a low number of proteins from a single discovery experiment in medium-sized cohorts, where antibodies and surrogate peptides may differ, thus only providing an indication of proteins affected by the disease and not revealing the bigger picture or concluding on the validity of the markers. We here present a standard approach for locating promising biomarker candidates based on existing knowledge, resulting in high-quality assays covering the main biological processes affected by multiple sclerosis for comparable measurements over time.

Methods: Biomarker candidates were located in CSF-PR (proteomics.uib.no/csf-pr), and further filtered based on estimated concentration in CSF and biological function. Peptide surrogates for internal standards were selected according to relevant criteria, parallel reaction monitoring (PRM) assays created, and extensive assay quality testing performed, i.e. intra- and inter-day variation, trypsin digestion status over time, and whether the peptides were able to separate multiple sclerosis patients and controls.

Results: Assays were developed for 25 proteins, represented by 72 peptides selected according to relevant guidelines and available literature and tested for assay peptide suitability. Stability testing revealed 64 peptides with low intra- and inter-day variations, with 44 also being stably digested after 16 h of trypsin digestion, and 37 furthermore showing a significant difference between multiple sclerosis and controls, thereby confirming literature findings. Calibration curves and the linear area of measurement have, so far, been determined for 17 of these peptides.

Conclusions: We present 37 high-quality PRM assays across 21 CSF-proteins found to be affected by multiple sclerosis, along with a recommended workflow for future development of new assays. The assays can directly be used by others, thus enabling better comparison between studies. Finally, the assays can robustly and stably monitor biological processes in multiple sclerosis patients over time, thus potentially aiding in diagnosis and prognosis, and ultimately in treatment decisions.

Keywords: Proteomics, Parallel reaction monitoring, Cerebrospinal fluid, Multiple sclerosis, Biomarker, Assay development, Neurological diseases

Background

There are currently only a few biomarkers for multiple sclerosis (MS) in clinical use, including MRI (T2-weighted lesions), oligoclonal bands and IgG ratio,

*Correspondence: frode.berven@uib.no

¹ Proteomics Unit, PROBE, Department of Biomedicine, University of Bergen, Bergen, Norway

Full list of author information is available at the end of the article



© The Author(s) 2020. This article is licensed under a Creative Commons Attribution 4.0 International License, which permits use, sharing, adaptation, distribution and reproduction in any medium or format, as long as you give appropriate credit to the original author(s) and the source, provide a link to the Creative Commons licence, and indicate if changes were made. The images or other third party material in this article are included in the article's Creative Commons licence, unless indicated otherwise in a credit line to the material. If material is not included in the article's Creative Commons licence and your intended use is not permitted by statutory regulation or exceeds the permitted use, you will need to obtain permission directly from the copyright holder. To view a copy of this licence, visit <http://creativecommons.org/licenses/by/4.0/>. The Creative Commons Public Domain Dedication waiver (<http://creativecommons.org/publicdomain/zero/1.0/>) applies to the data made available in this article, unless otherwise stated in a credit line to the data.

JC viral antibody titers and neurofilament light, as summarized in a recent review [1]. However, both in-house discovery studies and available literature suggest numerous additional biomarkers representing several of the processes and pathways active in MS, such as inflammation and neurodegeneration [2–5]. Such findings however require further verification via robust targeted assays, e.g. through parallel reaction monitoring (PRM) using high-quality stable isotope labelled heavy peptides [6–8].

The process of developing robust targeted assays in turn requires the consideration of a multitude of factors in order to ensure the quality and relevance of the assays, especially when the goal is to provide absolute protein measurements that would allow the consecutive analyses of proteins both across different labs and over time. This will make it possible to monitor specific pathological processes occurring in individual MS patients and thereby gain a deeper insight into the processes active at the various stages of the disease, which in turn would be a valuable tool in diagnosis, prognosis and treatment decisions.

Cerebrospinal fluid (CSF) is a commonly used body fluid in studies of neurological diseases, such as MS. Although not as easily accessible as serum/plasma, it is likely to better reflect ongoing neurological processes as it is in direct contact with the central nervous system [9]. However, large scale biomarker verification of discovery experiments has proven difficult in CSF and results are rarely consistent between studies. Likely reasons for this are methodological differences, large individual variations in total CSF protein concentrations [10] as well as significant heterogeneity in neurological diseases [11–13]. As a consequence, the quantitative data from individual biomarker discovery and verification studies do not always overlap and cannot directly and easily be compared and combined [14]. The large dynamic range of proteins in CSF also leads to challenges when measuring small disease-related changes in low abundant proteins [13, 15], especially vulnerable to small methodological variations and inaccuracies. Combined with relatively low patient numbers in most studies, it becomes almost impossible to conclude regarding a biomarker's potential, and thus move from the biomarker discovery phase to clinically useful biomarkers. It is therefore crucial to create robust targeted assays for accurate measurements of biomarker candidates.

Here we describe a suggested standard approach for the selection of candidate biomarkers in CSF for MS, and detail the required validation of PRM assays for absolute quantification of 25 proposed biomarker candidates. The validation includes (i) intra- and inter-day variation, (ii) the effect of trypsin digestion time, and (iii) verification of the separation capability between MS and controls

observed from the literature [14]. Additionally, the linearity around the typical concentration of target peptides was determined and corresponding response curves determined. The validated assays are ready to be used in large-scale analysis of patient samples and the presented standard approach for PRM assay development can also be applied for other neurological diseases.

Results—from biomarker candidates to high-quality PRM assays

The following sections describes the steps from potential literature-based biomarker candidates from CSF-PR (proteomics.uib.no/csf-pr), to the list of the most promising proteins and peptides to include in robust high-quality PRM biomarker assays for MS (Fig. 1).

Selection of proteins and peptides

Literature curation using CSF-PR

The recently published CSF-PR 2.0 [14] contains structured and searchable quantitative data for thousands of CSF-proteins from close to 100 datasets related to MS, Alzheimer's disease (AD) and Parkinson's disease (PD). The data in CSF-PR comes from mass spectrometry studies that have passed certain filters notably related to (i) methodology (bottom-up shotgun or targeted proteomics for main experiment; ELISA for verification), (ii) number of patients ($n \geq 5$ in each disease group; if using pools, ≥ 3 pools for each disease group and $n \geq 20$ total), and (iii) sample type (CSF from living subjects).

The biomarker selection was conducted by merging relevant datasets from MS and control subcategories in CSF-PR and extracting the proteins found to be significantly different in abundance in the majority of studies, according to certain criteria. See “Materials and methods” section for more details. The CSF-PR data extraction resulted in an initial list of 133 proteins (Additional file 1: Table S1), representing promising biomarker candidates for MS quantified in several experiments where various degree of fractionation had been used. Separately, we also collected a list of proteins that were changed between MS and control, but quantified in only one study in CSF-PR (Additional file 2: Table S2). Most of the latter were proteins from our recent discovery study [5], where both depletion and extensive peptide fractionation was performed, and they are therefore likely the lowest abundant proteins possible to quantify by current mass spectrometry proteomics technology.

Identifying proteins within the suitable dynamic range of CSF

An important condition for assay development is to be able to perform PRM quantitation in crude CSF without high-abundant protein depletion or peptide

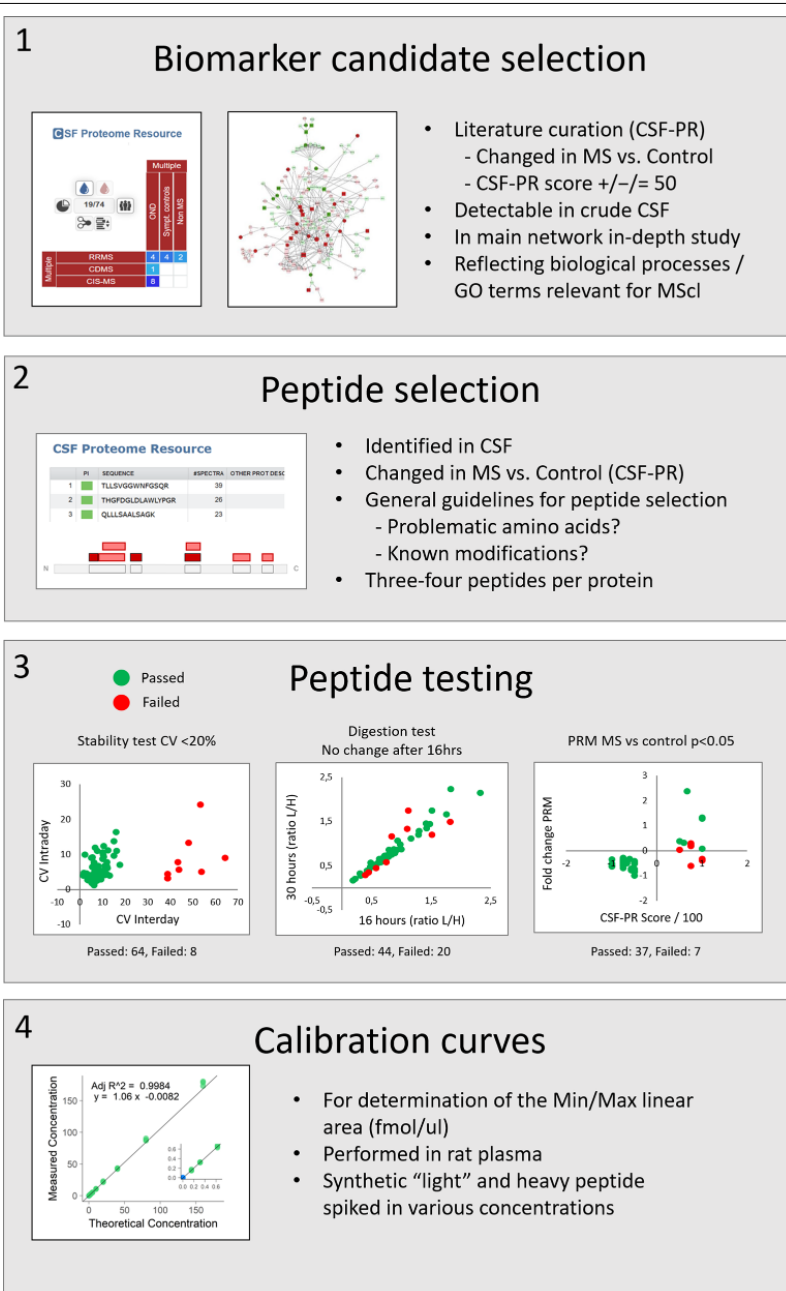


Fig. 1 The main steps in developing robust PRM assays for CSF biomarkers related to MS

fractionation. In order to find the proteins most likely fulfilling this condition, a CSF fractionation test was carried out, where the trypsin digested CSF-proteome was separated into eleven fractions and analysed by data-dependent acquisition (DDA) MS/MS, resulting in 1194 proteins. We estimate that PRM can be ten times more sensitive than what can be identified in a regular DDA shotgun experiment [16]. Therefore, the identification of a protein in a 20 µg un-depleted sample, fractionated into 11 fractions (first fraction usually does not contain peptides), indicates that the protein can be quantified by PRM in crude CSF. A total of 120 of the 132 proteins extracted from CSF-PR were identified in the DDA analysis (Additional file 3: Table S3) and passed on to the next steps in the assay development. All of the proteins identified in the DDA analysis can be found in Additional file 4: Table S4.

Biological processes and categories

A closer inspection of the 120 proteins revealed several groups of related proteins with similar names, functions and abundance relationship between MS and control, e.g. immunoglobulin proteins, cadherin proteins, receptor-type tyrosine-protein phosphatases, and SLIT and NTRK-like proteins. These proteins are likely to be involved in the same biological processes, and therefore developing individual PRM assays for all these proteins is probably not necessary, as recent studies indicate that such related proteins are most-often affected in the same manner [4, 5].

A representative selection of the 120 proteins from Additional file 3: Table S3 was made based on available information from CSF-PR, i.e. the number and proportion of studies where changes between MS and Non-MS was observed. Additionally, the large network of interacting and significantly changed proteins between MS and other neurological diseases (OND) generated in our recent publication [5] was utilized to select one or two proteins as representatives of the various biological processes likely to be affected in MS. These processes include e.g. (i) inflammation—a hallmark of the MS disease, (ii) extracellular matrix organization proteins—providing structure and support for developing neurons (e.g. collagens and proteoglycans), (iii) ephrin proteins—involved in neuron development, myelination and axonal guidance, and (iv) cadherins—cell adhesion proteins known

to be involved in de- and re-myelination. Additional proteins found especially interesting based on keywords in UniProt [17] or our own previous experiments were also included. All the steps in the protein selection process is outlined in Fig. 2, and the 25 selected proteins are shown in Table 1.

Peptide selection

Selecting peptides to represent the proteins under investigation, so-called surrogate or signature peptides, is a crucial step in the development of a targeted proteomics assay, and a number of criteria determines if a peptide is suitable [19, 20]. Here, the initial peptide selection was done mainly based on peptide data available from CSF-PR combined with general guidelines for selecting peptides for targeted proteomics [6, 19–21]. As a rule, three- to four peptides were selected per protein and the corresponding isotopically heavy labelled versions were ordered. However, not all peptides were found with an acceptable signal in the MS/MS analysis, hence, some of the proteins are only represented by a single peptide. For one protein (chitinase-3-like protein 1), more than three heavy peptides were ordered given that this protein has been reported as particularly interesting in relation to MS [22–28], and we had previously experienced that this protein could be challenging to quantify (data not shown). In total, 72 peptides were selected to represent the 25 proteins (Table 2). Further testing was performed to determine whether they were truly suitable as protein surrogates, as outlined below.

Peptide stability testing

PRM assays ought to have low intra- and inter-day variation in order to allow comparable quantitative measurements over time. To test this, PRM experiments with two replicates were processed each day across 5 days, and the intra- and inter-day coefficient of variation (CV) was calculated for all the 72 peptides. Most of the peptides displayed an intra- and inter-day CV of less than 20% (Fig. 3). Only eight of the initial 72 peptides had a CV above 20%, with seven from chitinase-3-like protein 1 (CH3L1), failing only the inter-day CV, and one from Seizure 6-like protein 2 (SEZ6L2), failing both intra- and inter-day CV. Notably, none of the peptides from CH3L1 showed an acceptable inter-day CV. Peptides not fulfilling the intra- and inter-day CV limits were discarded,

(See figure on next page.)

Fig. 2 The main steps in the identification and selection of biomarker candidate proteins for inclusion in the PRM assays. Screenshots are from CSF-PR [14], PPI network is from [5] and other figures are from Servier Medical Art licensed under a Creative Commons Attribution 3.0 Unported License. TMT = tandem mass tag, DDA = data dependent acquisition, MM-RP AX = mixed-mode reversed-phase anion exchange [18], GO = gene ontology, ECM = Extracellular matrix

1

CSF-PR candidate extraction

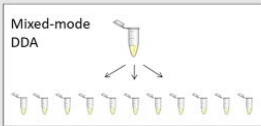


- MS vs. non-inflammatory Controls
- Changed in the same direction in ≥ 2 studies
- Regulation CSF-PR score (x) of ≥ 0.5 or ≤ -0.5

$$x = \frac{\text{(number of studies that found the protein increased - number of studies that found the protein decreased)}}{\text{number of studies that quantified the protein}}$$

2

Suitable dynamic range for PRM



- Proteins detectable by PRM in crude CSF
- DDA experiment with crude CSF peptide fractionated in 11 fractions
→ comparable sensitivity to PRM

3

Further selection criteria

- In main network in-depth TMT study
 - Reflecting biological processes and Gene Ontology (GO) terms relevant for MS
- Keywords: neuron, axon, synapse, signal transmission, myelination, immune response, inflammation, complement system, cell binding, adhesion, ECM organization

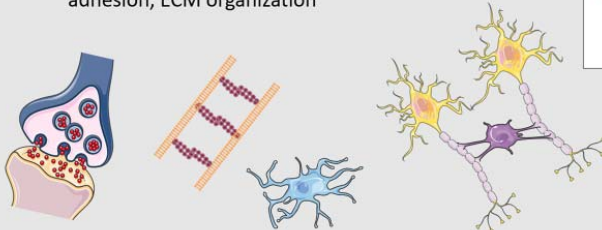
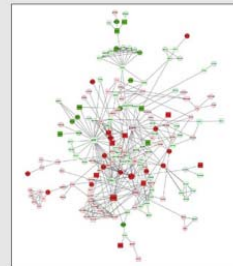


Table 1 The 25 proteins selected for assay development

Accession	Name	Network*	CSF-PR score**	Datasets***	Selected keywords from UniProt and Gene Ontology
P51693	Amyloid-like protein 1	Yes	-50	1 ↑ [56] 1 - [57] 4 ↓ [4, 5, 56]	Postsynaptic function, neurite outgrowth, neuronal apoptosis
P61769	Beta-2-microglobulin	Yes	60	3 ↑ [4, 5] 2 - [25, 57]	Component of the class I MHC, antigen presentation, innate immune response
P55290	Cadherin-13	Yes	-75	3 ↓ [4, 5] 1 - [25]	Cell adhesion, negative regulator of neural cell growth
P16070	CD44 antigen	Yes	75	3 ↑ [4, 5] 1 - [25]	Mediates cell-cell and cell-matrix interactions, cell migration
P36222	Chitinase-3-like protein 1		70	8 ↑ [4, 5, 24, 25, 56] 1 - [22] 1 ↓ [56]	Lectin that binds glycans, no chitinase activity, inflammatory response, macrophage differentiation
Q15782	Chitinase-3-like protein 2		100	6 ↑ [4, 5, 25]	Lectin that binds glycans, no chitinase activity, carbohydrate metabolic process
P10645	Chromogranin-A		-50	4 ↓ [4, 5, 22] 4 - [2, 25, 57]	Innate immune response, defence response (fungus, bacterium), negative regulation of neuron death
P12111	Collagen alpha-3(VI) chain	Yes	50	2 ↑ [4, 5] 2 - [4, 25]	Cell binding/adhesion, extracellular matrix organization
P02747	Complement C1q subcomponent subunit C	Yes	100	3 ↑ [4, 5]	Complement system, immune response
P00736	Complement C1r subcomponent	Yes	75	3 ↑ [4, 5] 1 - [25]	Complement system, immune response
P54764	Ephrin type-A receptor 4	Yes	-100	5 ↓ [4, 5, 56]	RTK signalling, promiscuous, prevents axonal regeneration, cell adhesion, cell signalling, repair after injury in the nervous system, axonal guiding
Q6MZW2	Follistatin-related protein 4		-75	3 ↓ [4, 5] 1 - [25]	Negative regulation of dendritic spine development and collateral sprouting
P48058	Glutamate receptor 4	Yes	-50	2 ↓ [4, 5] 2 - [4, 25]	Excitatory synaptic transmission
P01591	Immunoglobulin J chain		67	2 ↑ [4], 1 - [5]	Links monomers of IgM or IgA, antigen binding, immune response
Q92876	Kallikrein-6	Yes	-60	1 ↑ [56] 2 - [-2, 25] 7 ↓ [2, 4, 5, 22, 56, 57]	Serine protease, Indicated in AD, regulation of axon outgrowth after injury, myelination
P32004	Neural cell adhesion molecule L1	Yes	-75	3 ↓ [4, 5] 1 - [25]	Nervous system development, neuron-neuron adhesion, neuronal migration, axonal growth, synaptogenesis
Q9ULB1	Neurexin-1		67	2 ↓ [4, 5] 1 - [4]	Cell surface protein, cell-cell interactions, axon guidance, signal transmission, neurotransmitter release
Q9P2S2	Neurexin-2		-75	3 ↓ [4, 5] 1 - [25]	Neuronal cell surface protein, cell recognition, adhesion, signalling
Q92823	Neuronal cell adhesion molecule		-75	3 ↓ [4, 5] 1 - [25]	Neurite outgrowth, cell-cell contacts between Schwann cells and axons, formation and maintenance of the nodes of Ranvier on myelinated axons.
Q99983	Osteomodulin	Yes	75	3 ↑ [4, 5] 1 - [25]	Biominaleralization processes, cell adhesion, extracellular matrix
Q9UHG2	ProSAAS	Yes	-75	3 ↓ [4, 5] 1 - [25]	Control of the neuroendocrine secretory pathway.
P23468	Receptor-type tyrosine-protein phosphatase delta	Yes	-100	2 ↓ [4, 5]	Phosphatase, pre- and post-synaptic differentiation of neurons
O00584	Ribonuclease T2		100	3 ↑ [4, 5]	Lysosomal degradation of ribosomal RNA
P13521	Secretogranin-2		-57	4 ↓ [4, 5, 22] 3 - [2, 25]	Neuroendocrine secretory granule protein

Table 1 (continued)

Accession	Name	Network*	CSF-PR score**	Datasets***	Selected keywords from UniProt and Gene Ontology
Q6UXD5	Seizure 6-like protein 2		−50	2 ↓ [4, 5] 2 − [4, 25]	Specialized ER function in neurons?

Relevant details for the selected proteins, such as whether or not they were found in the main protein–protein interaction network in our recent in-depth discovery study [5], their CSF-PR score, studies that found them increased or decreased in MS vs. Non-MS and selected gene ontology terms and keywords related to their function. Arrows pointing down: decreased abundance in MS; arrows pointing up: increased abundance in MS; Dash: no change in abundance between MS and Non-MS

* Proteins found in the main protein interaction network from [4]

** The score for MS vs. Non-MS calculated by CSF-PR according to the equation described in “Materials and methods” section

*** Multiple datasets can be from the same paper

resulting in 64 peptides from 24 proteins retained. Detailed results from this experiment can be found in Additional file 5: Table S5.

Peptide digestion testing

In order to create assays for absolute protein concentrations in CSF samples, it is important to investigate how the trypsin incubation time affects the quantitative results. The main question is whether the detected amount of a peptide continues to increase after completing a standard trypsin digestion protocol with 16 h digestion time (see “Materials and methods” section), as then the absolute concentration of the corresponding protein cannot be determined via such a standard digestion protocol using the given peptide.

The experiment investigated five different digestion times (1, 5, 16, 24 and 30 h), each with three replicates, and was repeated three times. A peptide was considered stably digested after 16 h if the percentage change from 16 to 24 h and from 16 to 30 h was both less than 20%. In addition, the resulting peaks had to be satisfactory with regards to intensity, interference and shape, evaluated through the Skyline [29] data analysis. A total of 44 peptides, with at least one peptide from each of the 24 proteins, passed the digestion test. In other words, 20 peptides, but no proteins, were discarded based on this test.

How the peptides changed (ratio light/heavy) after 16 h is illustrated in Fig. 4a, b, where red dots represent the peptides who failed the test. Examples of observed peptide profiles for two selected proteins are shown in Fig. 5a, b.

As can be seen from Fig. 5a, all of the three peptides from neuronal cell adhesion molecule show limited increase after 16 h of digestion, i.e. they all passed the test. However, some proteins demonstrated an increase in peptide amount after 16 h and/or a varying digestion profile for the different peptides. As an example, we see that peptide SLPSEASEQYLTK in Fig. 5a appears to be readily digested already after 1 h. Other proteins had

some peptides passing and some failing the digestion test. In Fig. 5b, we see that one peptide for the protein Seizure-6-like protein 2 increase in amount up to 16 h of digestion, and then no increase beyond 20% is found (peptide passed), while a different peptide from the same protein continue to increase after 16 h, thereby failing the test, notably with a high variation in the minimum and maximum values.

All the data from this experiment is available in Additional file 6: Table S6 and the complete digestion profile for all peptides can be found in Additional file 7: Fig. S1 and peptide abundance change at all measured time points are in Additional file 8: Fig. S2.

RRMS vs non-inflammatory controls

To test whether the changes indicated in CSF-PR between MS and Non-MS could be reproduced, a small PRM study was conducted using six pools of CSF from MS (three pools of seven RRMS patients) and control (three pools of seven OND patients) patients. These pools have previously been analysed in-depth by shotgun TMT-based proteomics [5], and were selected to test how well the optimized PRM assays reflect the differences between the two patient categories.

The majority of the 44 tested peptides showed similar regulation trends as previously reported in the literature (Fig. 6), but a couple of the peptides were not found significantly changed in this study (Osteomodulin—two peptides, Complement C1q subcomponent subunit C—one peptide, Collagen alpha-3(VI) chain—one peptide, CD44 antigen—one peptide), and two peptides showed the opposite direction of regulation compared to CSF-PR (Complement C1q subcomponent subunit C—one peptide, Complement C1r subcomponent—one peptide). These were therefore discarded from further assay development. In conclusion, seven of 44 tested peptides failed this test.

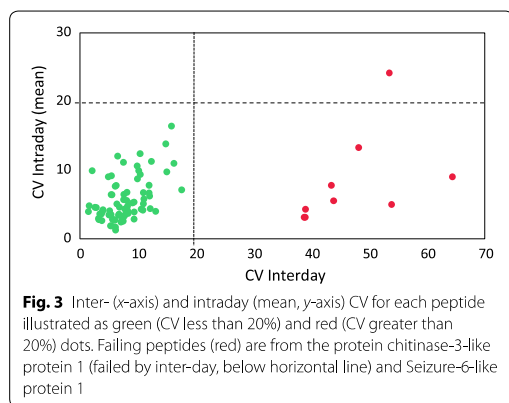
We concluded that the remaining 37 peptides were suitable to reflect the previously reported regulations, and therefore represent the most promising biomarkers

Table 2 The 72 signature peptides selected for the 25 proteins

Accession	Protein name	# Peptides	Peptide sequence(s)
P51693	Amyloid-like protein 1	3	WEPDPQR FQVHHLQVIEER GPPFHSSEIQR
P61769	Beta-2-microglobulin	2	VEHSDLSFSK VNHVTLTSQPK
P55290	Cadherin-13	3	YEVSSPYFK VNSDGGGLVALR INENTGSVSVTR
P16070	CD44 antigen	3	FAGVFHVEK ALSIGFETCR YGFIEGHVMPR
P36222	Chitinase-3-like protein 1	7	EGDGSCFPDALDR TLLSVGGWNFGSQR GTTGHHSPFLR EAGTLAYEICDFLR ILGQQVPYATK GNQWVGYYDDQESVK FPLTNAIK
Q15782	Chitinase-3-like protein 2	2	LVCYFTNWSQDR LLLTAGVSAGR
P10645	Chromogranin-A	3	ILSILR SGELEQEEER EDSLEAGLPLQVR
P12111	Collagen alpha-3(VI) chain	2	EVYTFASEPNDVFFK WYYDPNTK
P02747	Complement C1q subcomponent subunit C	3	QTHQPAPNSLIR FNAVLTNPQGDYDTSTGK TNQVNSGGVLLR
P00736	Complement C1r subcomponent	4	TLDEFTIQNLQPQYQFR NLPNGDFR ESEQGVTCTAQGIWK LPVANPQACENWLR
P54764	Ephrin type-A receptor 4	3	VYPANEVTLLDSR NLAQFPDITIGADTSSLVEVR GLNPLTSYVFHVR
Q6MZW2	Follistatin-related protein 4	3	GPDVGVGESQAEPR FDDYNSDSSLTLR VLQSIGVDPLPAK
P48058	Glutamate receptor 4	3	NTDQEYAFR LQNILEQIVSVGK EYPGSETPPK
P01591	Immunoglobulin J chain	2	SSEDPNEDIVER IIVPLNNR
Q92876	Kallikrein-6	3	LSELIQPLPLER TADGDFPDTIQCAYIHLVSR DSCQGDSSGGLVCGDHLR
P32004	Neural cell adhesion molecule L1	3	INGIPVEELAK AQLLVGSPGPVPR EGPGEAIR

Table 2 (continued)

Accession	Protein name	# Peptides	Peptide sequence(s)
Q9ULB1	Neurexin-1	3	DLFIDGQSK SDLYGGVAK LPDLISDALFCNGQIER
Q9P2S2	Neurexin-2	3	LSALTLSTVK GATADPLCAPAR AIVADPVTFK
Q92823	Neuronal cell adhesion molecule	3	AETYEGVYQCTAR SLPSEASEQYLTK VFNTPEGVPSAPSSLK
Q99983	Osteomodulin	2	IDYGVFAK LLLGYNEISK
Q9UHG2	ProSAAS	1	ALAHLLAEAR
P23468	Receptor-type tyrosine-protein phosphatase delta	3	SPQGLGASTAEISAR ILYDDGK SYSFVLNTR
O00584	Ribonuclease T2	2	ELDLNSVLLK VYGVIPK
P13521	Secretogranin-2	3	DQLSDDVSK TSYFPNPYNQEK VLEYLNQEK
Q6UXD5	Seizure 6-like protein 2	3	VSLDEDNDR FEAFEEDR TASDAGFPVGVSHVQYR



for MS. The complete results from this test is found in Additional file 9: Table S7.

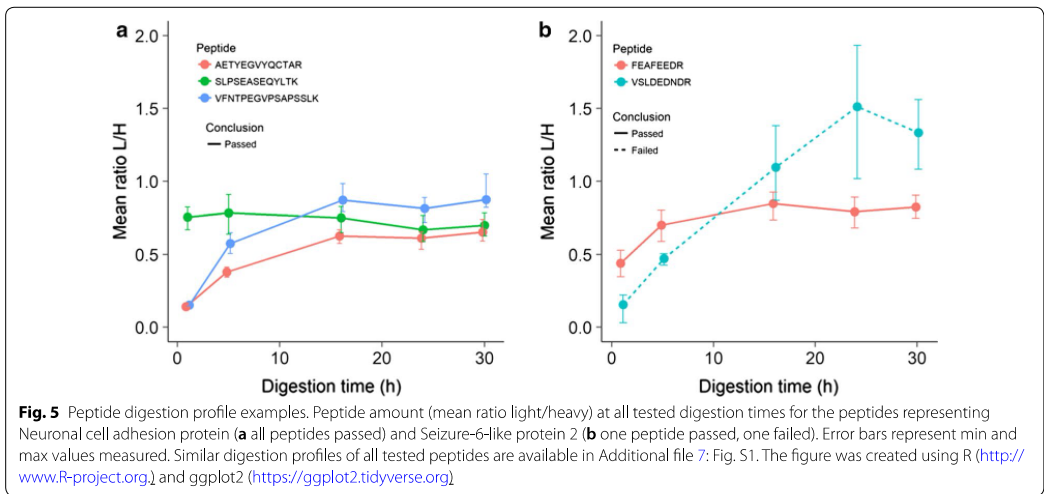
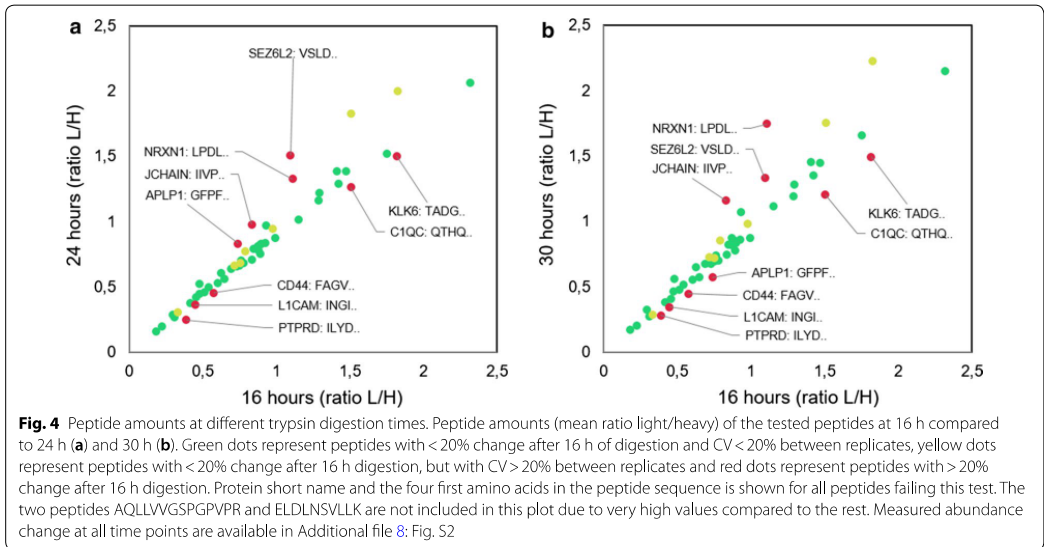
Final assay peptides

After all the steps detailed above, we finally arrived at a list of 37 peptides from 21 proteins for which promising absolute quantitative PRM assays could be developed

(Table 3). These represent the best surrogates to precisely and reproducibly quantitate proteins affected by MS. A complete table of all the tested peptides, important results and data from each experiment is collected in Additional file 10: Table S8, and a protein level overview of the number of peptides passing the various tests can be found in Additional file 11: Table S9.

Calibration curves

To ensure that the peptides could be accurately quantified by PRM mass spectrometry around the level of its observed concentration in CSF, calibration curves determining the linear areas of quantification have to be determined. Calibration curves have so far been generated for 17 of the peptides passing the initial testing and the work is ongoing. Rat plasma was used as matrix with varying amounts of synthetic light peptide and stable spike-in of heavy surrogate peptide. The linear area was determined by weighed least squares regression. For further details see “Materials and methods” section. An example of a calibration curve is shown in Fig. 7 and all of the calibration curves developed so far are provided in Additional file 12: Fig. S3 and additional details related to slope, intercept and linear areas are in Additional file 10: Table S8.



Discussion

The verification of biomarker candidates in CSF from discovery studies has been challenging due to the many issues pointed out in the introduction. One of the major bottlenecks has been to simultaneously measure a larger number of proteins in a high number of samples in a reproducible fashion and over time. In our view there is a need to develop well-described high-quality assays able to generate reproducible data over time, and ideally also

between laboratories, in order to achieve efficient biomarker verification in CSF.

Recently, there has been at least two publications going in the direction of generating high-quality PRM assays for CSF-proteins; one describing assays for 30 brain proteins [30], and another assays for monitoring a set of defined biological process [31]. In our study, we have contributed towards this idea by developing 37 well-described high-quality PRM peptide assays representing 21 proteins

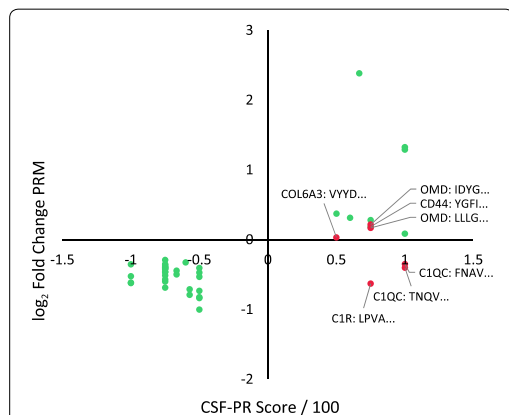


Fig. 6 CSF-PR score (MS vs. Non-MS) compared to fold change from PRM comparison study (RRMS vs. OND). Comparison of the score found from CSF-PR (x-axis, score/100), representing the direction of change between MS and Non-MS in the literature, and the fold change (y-axis, \log_2 transformed) found in our PRM study. Green dots represent peptides that were found significantly changed in the same direction in the literature and in the PRM study (passed) and red dots represent peptides that either were not significant or were significantly changed, but in opposite direction compared to the literature (failed). Protein short name and the four first amino acids in the peptide sequence is shown for all peptides failing this test

found to be affected in multiple sclerosis across multiple studies. Our goal is that these assays can be used to generate comparable data over time and provide the possibility to analyse and compare the protein levels in a large number of patient samples in a long-term perspective.

An important aspect of this work is that the biomarker candidates have been selected based on data from several studies using the online database CSF-PR. This approach is likely to provide less false positive candidates as more data, most often from several research groups, is used in the selection. Furthermore, the surrogate peptides have been selected based on quantitative information available from CSF-PR (when available), indicating that the particular peptide is actually regulated in the target protein. In sum, we argue that our approach is a step forward in increasing the effectiveness of verifying biomarker candidates in CSF.

Selection of proteins and peptides—what is important to consider?

Using CSF-PR as a starting point for selecting proteins affected by MS differs substantially from using a single experiment as the basis for selection, and the 133 proteins initially identified thus represents the proteins collectively reported to be affected by MS from the

mass spectrometry proteomics literature. In our view, this approach increase the chance of including the most relevant proteins and those more likely affected by MS, compared to basing the selection on a single study.

Next, we wanted to make sure that all of the proteins included in the assay development was possible to quantify in a PRM experiment without the need for protein depletion or peptide fractionation, as these steps both have their drawbacks. Targeted immunoaffinity depletion of high-abundant proteins is a useful way to increase the chance of measuring low-abundant proteins. Depletion is however a debated approach in biomarker studies, given that proteins not targeted by the depletion column may be co-depleted due to unspecific binding and protein interactions, potentially introducing a bias already at an early stage in the sample preparation [32–34]. As for peptide fractionation, this step will increase the analysis time, cost and complexity, and is therefore not desirable.

To arrive at a more manageable number, and as a demonstration of our suggested workflow, we selected 25 proteins. These proteins will of course not reflect all off the disease-affected processes represented by the complete list of 120 proteins, nor are they meant to represent a final list of biomarker candidates for multiple sclerosis. However, they do cover a range of functions and processes relevant in the MS disease as summarized in Table 1.

Creating PRM assays for all peptides from all potentially interesting CSF-proteins would be preferable, but as there will always be a cost vs. benefit consideration this is not realistic

Using the peptide level quantitative information available in CSF-PR as part of the surrogate peptide selection was also considered important. For the disease-affected proteins we observed that not all of the peptides were regulated in the discovery data, and that some peptides were also regulated in the opposite direction (Fig. 8). We suggest inspecting and using the peptide level data available in CSF-PR to select peptides that are observed as significantly changed, thus increasing the chance of the peptide actually representing the regulation reported at the protein level.

Different peptides from the same protein may show different (relative) abundance due to: (i) peptides mapping to multiple proteins or proteoforms with different regulation status, (ii) some peptides can be less suitable for mass spectrometry or in too low amounts for stable and accurate quantitation, and (iii) certain peptides have varying degrees of post-translational modifications, resulting in unstable concentration for the unmodified form. In addition, it is important to consider the general

Table 3 The most promising biomarker candidate proteins and peptides

Accession	Protein name	Peptide sequence(s)	Highest in	Cal.curve	MinLin (fmol/μl)	MaxLin (fmol/μl)
P51693	Amyloid-like protein 1	WEPDPQR	Control	Yes	0.525	560
		FQVHHLQVIEER	Control	No		
P61769	Beta-2-microglobulin	VNHVTLSQLPK	MS	No		
P55290	Cadherin-13	YEVSSPYFK	Control	Yes	0.15	160
		INENTGSVSVTR	Control	No		
P16070	CD44 antigen	ALSIGFETCR	MS	Yes	0.105	112
Q15782	Chitinase-3-like protein 2	LVCYFTNWSQDR	MS	Yes	0.045	48
		LLLTAGVSAGR	MS	Yes	0.045	48
P10645	Chromogranin-A	ILSLIR	Control	No		
		SGELEQEEER	Control	Yes	0.75	800
		EDSLEAGLPLQVR	Control	No		
P12111	Collagen alpha-3(VI) chain	EVYTFASEPNDVFFK	MS	No		
P54764	Ephrin type-A receptor 4	VYPANEVTLDSR	Control	Yes	0.075	80
		NLAQFPDTITGADTSSLVEVR	Control	No		
Q6MZW2	Follistatin-related protein 4	GPDVGVGSEQAEEPR	Control	No		
		FDDYNSDSSLTLR	Control	No		
		VLQSIGVDPLPAK	Control	Yes	0.045	48
P48058	Glutamate receptor 4	NTDQEYAFR	Control	Yes	0.09	96
P01591	Immunoglobulin J chain	SSEDPNEDIVER	MS	No		
Q92876	Kallikrein-6	DSCQGDSSGGPLVCGDHLR	Control	Yes	0.15	160
P32004	Neural cell adhesion molecule L1	AQLLVVGSPPVPR	Control	Yes	0.045	48
		EGPGEAIVR	Control	No		
Q9ULB1	Neurexin-1	DLFIDGQSK	Control	No		
		SDLYIGGVAK	Control	Yes	0.045	48
Q9P2S2	Neurexin-2	LSALTLSTVK	Control	Yes	0.045	48
		GATADPLCAPAR	Control	No		
		AIVADPVTFK	Control	No		
Q92823	Neuronal cell adhesion molecule	AETYEYVQCTAR	Control	No		
		SLPSEASEQYLTK	Control	Yes	0.15	160
		VFNTPEGVPSAPSSLK	Control	No		
Q9UHG2	ProSAAS	ALAHILLEAER	Control	No		
P23468	Receptor-type tyrosine-protein phosphatase delta	SPQGLGASTAEISAR	Control	No		
		SYSFVLNTR	Control	Yes	0.045	48
O00584	Ribonuclease T2	VYGVIPK	MS	No		
P13521	Secretogranin-2	DQLSDDVSK	Control	Yes	0.045	48
		VLEYLNQEK	Control	Yes	0.18	192
Q6UXD5	Seizure 6-like protein 2	FEAFEDR	Control	No		

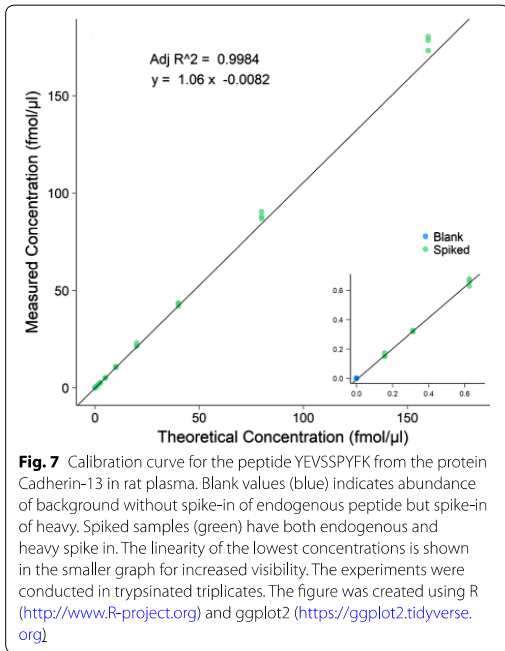
Proteins and peptides passing all quality controls described in this study, thereby representing the most promising biomarker candidates for PRM assays. The table also shows if the protein is highest in MS or control, if calibration curves have been developed, and, if so, its linear area

Cal.curves: Calibration curves. MinLin: Lowest theoretical concentration that will be used for quantitation. MaxLin: Maximum theoretical concentration that will be used for quantitation

guidelines for peptide selection in targeted proteomics, i.e. to avoid non-unique peptides and peptides prone to mis-cleavages.

Peptide stability testing—most peptides are stable across runs

A large majority of the tested peptides passed our stability test, indicating that they are suitable for PRM monitoring robustly over time. We can conclude that they are in the appropriate concentration range in CSF for the



method to consistently provide a sufficient signal for stable measurements.

Chitinase-3-like protein 1 peptides give unstable measurements over time

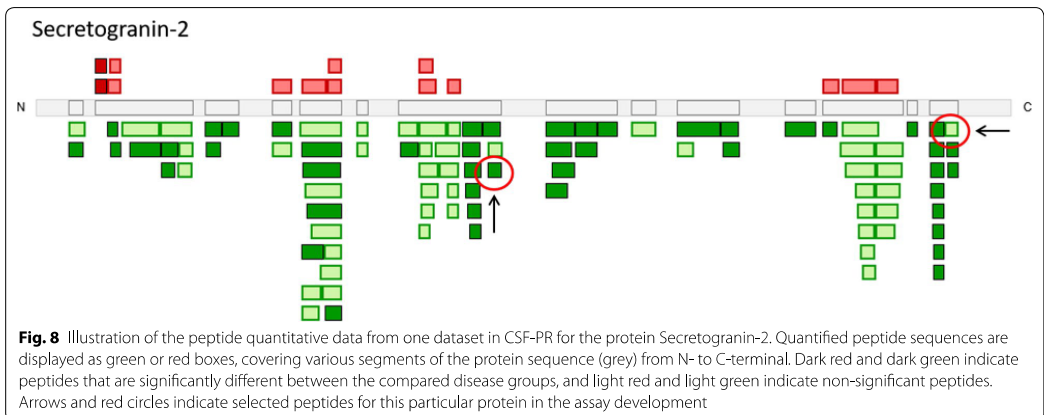
Chitinase-3-like protein 1 (CH3L1) has been linked to several neurological diseases [23, 26, 35–39], including MS [22, 24, 25, 27, 28]. However, it seems that this

protein is not ideal for an absolute targeted assay, due to the unstable peptide measurements across runs. One explanation is that CH3L1 is low-abundant in many patient categories used in testing and as controls, but more abundant in MS patients. This may explain why several discovery studies have found it regulated [5, 24, 25, 28] compared to controls and why we find high variations in this stability test using CSF from Control (OND) patients. Some peptides for CH3L1 were not far from being acceptable in terms of variation, having inter-day CV values between 20 and 30%. Due to the potential importance of this protein one could consider including PRM assays for these peptides, but then taking into account that the variation in the data is larger.

Peptide digestion testing—most peptides show no increase after 16 h

Considering our goal of creating PRM assays able to measure absolute protein amounts, we found that it was crucial to examine the digestion status after the standard 16 h of trypsin incubation. This is not a standard test for PRM assays, but in order for an assay to come as close as possible to reflect the absolute protein amount, we found it essential. For most proteins, digestion times of 16 h were sufficient, in that no significant increase (or decrease) in peptide amount was observed after prolonged incubation. But there were a couple of peptides increasing also after 16 h of digestion, and nine proteins having some peptides passing and some failing the digestion test (Fig. 4b).

When examining the full profile of peptide amount (L/H) measured after various trypsin incubation times (Additional file 7: Fig. S1), we also note that certain peptides show a decrease already before 16 h of digestion. Although, no decrease beyond 20% was observed before



16 h, this may still indicate that some undesired peptide degradation is occurring already before 16 h. Such “fast digesting” peptides should ideally have shorter trypsin incubation times. For the peptides where the digestion was not completed after 16 h, one could envision longer digestion times in order to reach complete digestion, or consider testing other digestion conditions. However, applying individual trypsin digestion times and conditions for a large number of peptides in assays run over time is tedious and unrealistic. The peptides where the digestion was not complete after 16 h are not suitable for absolute quantification, but the assays could still be used for relative quantitation if trypsin incubation times are equally long between experiments. An alternative would be to search for other peptides better representing these proteins when using 16 h digestion time.

The overall results from the digestion testing show that each peptide can have specific physiochemical properties affecting the digestion process and demonstrate the necessity of obtaining peptide digestion profiles for each individual peptide. Another approach could be to use isotopically labelled proteins as internal standards, instead of peptides, in which case digestion variability would be adjusted for by the internal standard. This is however a quite costly approach.

PRM RRMS vs control—confirmation of previously found changes

This small PRM study was designed to investigate whether the selected peptides could reproduce the previously reported quantitative differences between MS and controls. As we had merged some of the disease sub-categories when performing the initial CSF-PR search, it was not possible to find identical MS and control groups. We concluded that using relapsing–remitting MS (RRMS) and OND controls, was a good choice for this experiment.

Most of the peptides also passed this test, but seven peptides did not show the same significant difference between RRMS and OND as reported between MS and Non-MS in the CSF-PR publications [14], either because the difference was not significant or they showed the opposite change. One reason may be that the number of patients included in both the PRM study described here and the studies in CSF-PR is not large enough to eliminate the biological variation as a factor, creating false positive biomarker candidates. The patient groups used were also not identical, which could result in variation in differentially abundant proteins.

Another reason for the discrepancy may be that many of the studies in CSF-PR used depletion of high-abundant proteins, which on purpose was not performed in our PRM pilot experiment. Depletion could potentially affect

the protein quantitation and thereby the resulting differentially abundant proteins as variation is introduced, as discussed above. This is particularly relevant if the number of patients is low. Even though the seven rejected peptides did not pass this test, they could still prove valuable upon more thorough testing with larger patient numbers. In the current study, the 37 peptides displaying similar differential abundance as previously reported were prioritized.

Development of calibration curves—linearity down to the highest dilution point

Calibration curves were generated in rat plasma as it is a somewhat similar matrix to CSF and from a different species (non-human CSF was not possible to obtain), so that there would be no endogenous presence of analyte signal in the matrix, which would add to the spiked signal [40]. The calibration curves displayed a high degree of linearity down to the highest dilution point, with adjusted R^2 values all over 0.99. Ideally, the calibration curves would include endogenous analyte concentrations so that the signal would be indistinguishable from the background, yielding a hockey-stick shape of the curve. The % CV of the replicates of the lowest endogenous peptide concentrations was less than 20% for all but one peptide, indicating that the limit of quantification (LOQ) was not reached for these. As the analyte concentrations rarely varies more than the span covered by the linear curve, the assays were deemed sufficient for our purposes, and the concentration span between the lowest and highest measured endogenous concentration will be used for absolute quantitation.

Relevance for multiple sclerosis and other neurological disorders

The assays have been developed to monitor processes affected by MS, but through CSF-PR, we find that several of the protein candidates are also found changed in Alzheimer’s and Parkinson’s disease. This is the case for nine of the 21 proteins having peptides that passed all test (CD44 [41], Follistatin-related protein 4 [41], Secretogranin-2 [31, 42] ProSAAS [42], Neurexin-1 [31], Cadherin-13 [43], Kallikrein-6 [44], Amyloid-like protein 1 [44] and Ephrin type-A receptor 4 [44]). It indicates, not surprisingly, that many of the processes affected by MS are also affected by other neurological disorders, and are thus not specific to MS. Which in turn can mean that the diagnostic value of these particular proteins is limited, however they could still be very valuable as biomarkers for disease status, treatment effect and prognosis.

Validation in larger cohorts using the developed assays is necessary to determine the value of the proteins as biomarkers in a clinical setting. After validation of a subset

Table 4 Overview of cerebrospinal fluid pools used in the various experiments

Name	#Patients each pool	Female/Male	Disease category	Average age	Used in experiment
Pool 1	3	2/1	OIND	35.3	Peptide digestion test
Pool 2	N/A	N/A	OND	N/A	DDA + peptide stability test
Pool 3–5	7	18/3	RRMS	36.8	PRM RRMS vs. control
Pool 6–8	7	18/3	OND	35.4	PRM RRMS vs. control

RRMS: Relapsing-remitting multiple sclerosis; OIND: Other inflammatory neurological diseases; OND: Other neurological diseases; DDA: data-dependent acquisition

of the proteins using PRM, one likely way to implement the measurement of the proteins into the clinic would be to develop ELISA-assays for the most valuable proteins. In the future the PRM-assays could perhaps also be used directly in the clinic.

It is also expected that these assays will be useful in shedding light on the disease status for other diseases where similar processes are affected. The remaining 12 proteins with peptides that passed all tests are however only changed in the MS categories in CSF-PR. These proteins may therefore be the most useful for diagnostic purposes and monitoring of processes occurring specifically in MS patients. For more details, the proteins can be searched and available data investigated in CSF-PR.

Conclusion

In this study, we have developed 37 robust PRM peptide assays for 21 CSF proteins likely affected by MS. The selected proteins cover many of the pathways and processes recently reported to be affected in MS, but also in other neurological diseases such as Alzheimer's and Parkinson's disease. The peptides chosen as protein surrogates are quantifiable without the need for depletion, fractionation or enrichment prior to mass spectrometry. Due to the documented inter- and intra-day stability of the assays and the digestion stability, comparable quantitative values over time is expected. This allows for large-scale analyses of patient samples to reveal the relationship between the monitored MS-affected processes, disease progression and treatment response, and results from future large-scale patient analyses using these assays are expected to aid in treatment decisions.

These well-documented absolute quantitative assays could also be adopted by other laboratories and have the potential to generate comparable quantitative measurements between laboratories. To explore this potential future, inter-laboratory comparisons must be conducted.

We recommend that the presented workflow should be used as a general guideline for the development of targeted PRM biomarker assay in CSF, and consider this work to be a contribution towards standardizing CSF protein quantification allowing us to move from non-comparable data between single experiments to accumulation of

reproducible quantitative data over time. In our view this is essential in order to enable the analyses of large enough patient cohorts to reveal disease-related changes in the CSF proteome related to disease status and progression.

Materials and methods

Biological material

Cerebrospinal fluid

Human cerebrospinal fluid (CSF) was obtained by diagnostic lumbar puncture, according to the standardized protocol for collection and biobanking [45]. Patients gave written consent and the study was approved by the Regional Committee for Medical Research Ethics of Western Norway. Various pools of CSF were used in the experiments described in this paper, mainly due to the limited availability of CSF samples to use for assay optimization and testing. Details about the pools can be found in Table 4 and in [5]. The same pools as in [5] were used for the MS vs. Control PRM study (MS and OND pools, here: Pools 3–8). The pool used for the DDA proteome depth and peptide stability experiment consisted of various OND patients (Pool 2), the pool used in the digestion test consisted of 3 OIND patients (Pool 1, all with myelitis).

Rat plasma

Rat plasma (P2516, Sigma Aldrich) was used to construct calibration curves for high-purity peptides. The purchased rat plasma contained lyophilized material derived from 1 ml pooled and filtrated rat blood with the addition of anticoagulant, 3.8% trisodium citrate. The concentration of the rat plasma was estimated by BCA, and diluted in 1xPBS to a final concentration of 0.5 µg/µl prior to trypsination.

Literature curation using CSF-PR

We used CSF-PR (<https://proteomics.uib.no/csf-pr>) to extract biomarker candidates between MS and non-inflammatory control patients (Non-MS) as of August 2017. To specifically extract quantitative data relevant to this comparison, we first merged certain MS and control subcategories listed in CSF-PR as follows: RRMS (relapsing-remitting MS), CDMS (clinically

definite MS) and CIS-MS (clinically isolated syndrome with conversion to MS) were merged to the general category “MS” and the subcategories OND (other neurologically controls), symptomatic controls, Non-MS, healthy and healthy controls were all merged to the general category “Non-MS”. In this way we identified protein data from all papers in the resource comparing MS to non-inflammatory controls. The protein table with the quantitative data from these studies contained thousands of proteins, so we applied some selection criteria by using the table filtering options in CSF-PR before exporting the protein list: (i) proteins quantified in at least two studies and (ii) having a CSF-PR score () of ≥ 0.5 (50%) or ≤ -0.5 (–50%) according to the equation used in CSF-PR for summarizing overall reported protein regulation (see below, $\times 100$ for %), indicating that each protein was increased or decreased in at least 50% when averaging the results from all studies.

This resulted in 194 proteins, which were exported from CSF-PR, and further analysis was performed using Excel. To identify the most consistently changed proteins, we applied an additional criterion that (iii) proteins were found changed in the same direction (up or down) in at least two studies. This reduced the list to 133 proteins (Additional file 1: Table S1), representing the most promising and consistently reported biomarker candidates for MS. A separate list of proteins that were significantly changed between MS and Non-MS, but quantified in only one study in CSF-PR was also created (Additional file 2: Table S2).

CSF sample preparation—general

Protein concentration in the CSF pools was measured by the Qubit™ fluorometer (Invitrogen™, Thermo Scientific) and the Qubit™ protein assay kit (Invitrogen™, Thermo Scientific), following the manufacturers protocol. CSF samples were lyophilised at 30 °C in an Acid-Resistant CentriVap™ Concentrator System (Labconco™), and dissolved in 20 μ l freshly made Urea solution (8 M Urea/20 mM methylamine (Sigma Aldrich)). All CSF samples were in-solution digested as previously described [4] using trypsin porcine (Promega, art. V5111) added to samples in a 1:50 relationship, and desalted using OASIS® HLB μ Elution plates 30 μ m (Waters Corp, Millford, MA, USA) according to the manufacturer’s instructions. Samples were vacuum dried following desalting, and dissolved in 2% ACN, 0.1% TFA to a concentration of approximately 0.5 μ g/ μ l for the MS analysis. About 0.5 μ g were injected if not otherwise stated.

Preparation and spike-in of synthetic peptides

All isotopic labelled peptides (IS peptides) used as internal standards were purchased from Thermo Scientific at crude (unknown purity) and AQUA Ultimate (>95% purity) quality for peptide testing and AQUA Ultimate quality only for calibration curves, whilst synthetic light peptides (SpikeTides) were acquired from JPT. Heavy labelled peptides have been C-terminally modified with ¹³C and ¹⁵N isotope arginine or lysine. The synthetic heavy peptides were added to the samples before the desalting step, and the synthetic light peptides from JPT used to make calibration curves were added prior to digestion as they contain a tag that needs to be enzymatically released. Heavy peptides were spiked to the samples in an approximate 1:1 relationship between the heavy IS peptide and the endogenous analyte, which was estimated from initial peptide tests (data not shown). Notably, the lowest endogenous concentration was adjusted to 3 fmol/ μ g. Spike-in for calibration curve development is described under “calibration curve” section.

PRM mass spectrometry—general for all PRM experiments

The separation of peptides was performed by an Ultimate™ 3000 RSLCnano System (Thermo Fisher Scientific™) with an Acclaim PepMap™ 100 trap column (diameter width at 75 μ m \times 2 cm nanoviper C18 column, with particle size 3 μ m and length at 100 A) and 5 μ l 0.1% TFA solution. Peptides were separated on an analytical column PepMap™ RSLC C18 (diameter width 75 μ m \times 50 cm, particle size at 2 μ m and 100 A in length) with the combination of 95% solvent A (0.1% FA) and 5% solvent B (100% ACN, 0.1% FA) with a flow rate of 200 μ l/min. The column gradient for peptide elution went from 0 to 5 min with 5% solvent B, then an increase at 5–5.5 min to 8% of solvent B, 5.5–140 min 35% B, 140–155 min 90% B and 155–170 min 90% B. At 170–175 min solvent B decreased to 5% B and held at 5% solvent B from 175 to 190 min. Column temperature was specified to be 35 °C, whilst the auto sampler had a temperature of 4 °C. Ionization of samples occurred with an Easy-Spray™ (Thermo Scientific) ion source, with a spray voltage at 1.8 kV. The capillary temperature was set at 250 °C, heater temperature at 350 °C, whilst the S-lens RF value were at 60. Sheath and auxiliary gases were not used. As a result of the ion source, samples were obtained in a positive ionization mode.

Mass spectrometry analysis

The method duration was 195 min (runtime 10–175 min). The mass spectrometer was operated in PRM scheduled mode and switched between full scan MS1 between every 12th PRM MS2 scan. The instrument

was controlled through Q Exactive HF Tune 2.4 and Xcalibur 3.0. MS1 spectra were acquired in profile mode in the scan range of 375–1500 m/z with resolution of 15,000, automatic gain control (AGC) target of $3e6$, and a maximum injection time (IT) of 15 ms. The target peptides on the inclusion list were sequentially isolated for higher-energy collision dissociation (HCD) fragmentation and MS2 acquisition to a normalized HCD collision energy of 28%, target AGC value of $1e5$, resolution $R=15\,000$, and IT of 100 ms. The precursor isolation window was set to 1.6 m/z with no isolation offset or dynamic exclusion. Lock-mass (445.12003 m/z) internal calibration was used.

Skyline analysis

Skyline [29] was used for the creation of inclusion lists prior to PRM-mass spectrometry analysis and for data refinement of the PRM-mass spectrometry data. Skyline settings were overall kept at default, or updated depending on the parameters in the mass spectrometry analysis used to acquire data. Notably, structural modifications were specified with carbamidomethyl (C) and isotope modification “label: 13C(6) 15 N(2) (C-term K)” and label: “13C(6) 15 N(4) (C-term R)”. Both 2+ and 3+ charged precursors and b- and y-ions were investigated in the stability test experiment, while in the following (digestion, MS vs. OND and calibration curves), only 2+ precursors and y-ions were used, as these most often gave the best signal. Detailed Skyline settings for each experiment, e.g. the peptide and transition settings and filters, can be inspected in the Skyline documents uploaded to Panorama Public (https://panoramaweb.org/PRM_Assay_CSF.url).

The peak signal for each peptide was determined by the Skyline peak picking algorithm, and manually verified or re-integrated based on the fragment pattern of the peptide, elution profile and simultaneous retention time of the endogenous and the IS peptide. Spectral libraries from CSF samples generated on the same Q Exactive HF instrument were used as a reference to make sure the correct peak for the various peptides were chosen. The three fragments with the highest intensity, low interference, and mass error less than 10 ppm was selected for quantitation. Additional file 13: Fig. S4A and B shows examples of typical transitions used in the assay. All other transitions can be inspected in Panorama Public (https://panoramaweb.org/PRM_Assay_CSF.url) where the Skyline documents from all experiments can be downloaded.

Notably, for most peptides, one to three of the transitions were significantly more intense compared to the rest, only the top three where therefore chosen for quantification. A typical example of this is illustrated in Additional file 13: Fig. S4C and D. For some peptides

in certain tests or replicates, only two transitions were used for quantitation, due to missing data or bad peaks in specific replicates. These were mainly from very low abundant proteins and/or from peptides with only low intensity transitions. The area under the curve, excluding background, were summed to give one peak area value for each peptide.

Furthermore, the endogenous peak area was divided by the peak area of the heavy internal standard peptide to generate a ratio to standard which was used for quantitation. From Skyline, a.csv file was exported containing the quantitative data needed for follow-up processing in Microsoft Excel or R. To determine the difference between the two patient groups in the final PRM experiment, an unpaired two tailed, homoscedastic student's *t* test was performed using Microsoft Excel. A *p*-value of ≤ 0.05 was used to determine a significant difference.

CSF protein depth investigation

We tested the identification of CSF proteins from a 20 μg un-depleted CSF sample (pool 2) subjected to peptide fractionation into 11 fractions following trypsin digestion (as described above). Peptide fractionation was performed by mixed mode reversed phase-anion exchange chromatography (MM) [18] on a Promix MP column (MP10.250.0530, 1.0×250 mm, 5 μm , 300 \AA , Sielc Technologies), as previously described [33].

Data dependent acquisition mass spectrometry analysis

Approximately 0.5 μg of peptides from each fraction was injected into the same LC system, trap column and mass spectrometer as described above. However, a 25 cm analytical column (PepMap RSLC, 25 cm \times 75 μm i.d. EASY-spray column, packed with 2 μm C18 beads (Thermo Scientific) was used (flow rate of 0.250 $\mu\text{L}/\text{min}$). Solvent A and B was the same as above as was the other MS general instrumental parameters related to ionization, voltage, temperature etc.

The mass spectrometer was operated in data-dependent acquisition mode to automatically switch between full scan MS1 and MS2 acquisition. The method duration was 120 min (runtime 8–105 min). The instrument was controlled through Q Exactive HF Tune 2.4 and Xcalibur 3.0. MS spectra were acquired in the scan range of 375–1500 m/z with resolution of 60 000, automatic gain control (AGC) target of $3e6$, and a maximum injection time (IT) of 25 ms. The 12 most intense eluting peptides above intensity threshold $5e4$, and charge states two or higher, were sequentially isolated for higher-energy collision dissociation (HCD) fragmentation and MS2 acquisition to a normalized HCD collision energy of 28%, target AGC value of $1e5$, resolution $R=60,000$, and IT of 110 ms. The precursor isolation window was set to 1.6 m/z with

an isolation offset of 0.3 m/z and a dynamic exclusion of 20 s. Lock-mass (445.12003 m/z) internal calibration was used and isotope exclusion was active.

Data processing

All raw files were converted to mgf using ProteoWizard [46] and searched using X! Tandem [47], MyriMatch [48] and MS Amanda [49] via SearchGUI (v2.1.3) [50] against the homo sapiens complement of the UniProt/SwissProt reviewed database downloaded October 2015 (20 196 entries) [17] with the reversed version of every sequence added as decoys. The search settings were: carbamidomethylation of C; oxidation of M as variable modification; trypsin as enzyme with a maximum of two missed cleavages; precursor charge 2–5; peptide length 6–30; precursor mass tolerance 10 ppm and fragment mass tolerance 0.005 Dalton. All other settings were left as the defaults. The search engine results were combined and assembled in PeptideShaker [51] (v1.1.2). Hits were thresholded to retain only the best scoring until a false discovery rate (FDR) of 1% was reached, estimated using the distribution of target and decoy hits [52].

Peptide stability test

To test the intra- and inter-day variability of measurements for the peptides, we analysed aliquots from the same CSF samples (pool of OND patients) at two different time points at the same day across 5 days. Two 10 µg aliquotes of CSF-pool 2 were in-solution digested, spiked, desalted, dried and stored in –20 °C. This was repeated on five different days, and all samples were analysed by PRM MS as described above. Data was inspected and refined in Skyline as described above, and in Excel, the intra- and inter-day variation for each peptide (2+ and 3+ separately) was calculated on the exported total area ratio (light/heavy). This value for each peptide was compared between samples prepared on the same day (intra-day) and between each of the three sample sets (inter-day). Peptides with intra- and inter-day CV less than 20% was considered reproducible.

Peptide digestion test

Fifteen 10 µg aliquots of CSF-pool 1 was in-solution digested, spiked, and desalted as described above. Trypsination was however, stopped at five different time points (1, 5, 16, 24 and 30 h), and three replicates was stopped at each time point. This experiment was repeated three times (across three different weeks). Data was refined in Skyline, as described above and the percentage change in ratio to standard was calculated for each peptide between 16 to 24 h and 16 to 30 h. A peptide was considered stably trypsinated after 16 h if the percentage change from 16 to 14 h, and 16 to 30 h was less than 20%. Individual protein

plots showing ratios at all time points for all peptides were generated using R (<http://www.R-project.org>). The plots were generated using the graphics package ggplot2 (<https://ggplot2.tidyverse.org>) (Additional file 7: Fig. S1).

PRM RRMS vs control

Samples from six CSF-pools were used in this experiment. The samples were crude 100 µg aliquotes from the experiment described in [5], which was three pools of MS patients and three pools of OND patients (pools 3-8). The samples were purified and concentrated using 3 kDa ultracentrifugation filters as described in [53], before in-solution digestion and Oasis desalting as described above, except a 10 mg plate was used, as in [53], due to the high protein amount (100 µg). The eluate after the desalting was divided to 5 µg aliquots and two aliquots (replicates) from each pool was used for this experiment. The aliquots were spiked with heavy peptides, dried and dissolved in 2% ACN, 0.1% TFA to approximately 0.5 µg/µL. Approximately 1 µg sample was injected for MS analysis and analysed by PRM as described, except MS2 resolution was 30,000. The ratio to standard was used to calculate fold change and significance between groups.

Development of calibration curves

Calibration curve generation in rat plasma

The calibration curves were made in rat plasma by preparing a dilution series of synthetic normal mass (light) peptides based on the estimated endogenous concentration of each peptide in CSF Pool 2. An 11-point dilution curve was centered around this estimate, so that the varying analyte spanned 32 times the endogenous concentration and 32 times less than the estimated endogenous concentration. The dilution series was prepared for the synthetic light peptides for analysis in rat plasma (dilutions prepared in 8 M Urea/20 mM methylamine directly prior to trypsination). Additionally, a mix of heavy AQUA peptides in levels 1:1 with endogenous peptide was generated in 5% ACN. Eleven 10 µg aliquots of rat plasma were added synthetic light peptides in different dilutions. In addition, one sample without added light peptides and was used as a blank. The twelve samples were in-solution trypsin digested, and equal amounts of the AQUA heavy peptides mix were added to each sample prior to desalting. This procedure was performed in trypsinated triplicates.

Mass spectrometry analysis

For the calibration curve experiment, some optimized parameters were used in the PRM analysis. Peptides were separated on an analytical column PepMap™ RSLC C18 (diameter width 75 µm × 25 cm, particle size at 2 µm and 100 Å in length) with the combination of 95%

solvent A (0.1% FA) and 5% solvent B (100% ACN, 0.1% FA) with a flow rate of 250 μ l/min. The column gradient for peptide elution went from 0 to 5 min with 5% solvent B, then an increase at 5–5.5 min to 7% of solvent B, 5.5–65 min 22% B, 65–87 min 35% B, 87–92 min 90% B and 92–102 min with 90% B. At 102–105 min solvent B decreased to 5% solvent B and held a 5% solvent B from 105 to 120 min. The method duration for calibration curve runs was 120 min (runtime 10–110 min). The mass spectrometer was operated and MS spectra acquired as described above for PRM analysis, except MS2 spectra were acquired with optimized collision energies, resolution $R=60,000$ at 200 m/z , IT of 118 ms, AGC target value at 2e5 and precursor isolation window was set to 0.7 m/z . All other parameters related to the LC and MS instrumentation and settings were as described above for general PRM experiments.

Calibration curve development in R

Following data refinement in Skyline, the ratio to standard values were exported for analysis in the programming language R (<http://www.R-project.org>). For the peptides measured in rat plasma, the measured ratio to standard was multiplied with the spike-in level to give the measured concentration at each dilution point and was plotted against the theoretical concentration. Notably, as more variation is common in the high concentration measurements, the linear regression was weighted with $1/sd^2$ to limit the impact of the points with the highest variability on the regression equation [40]. The slope, intercept and the lowest and highest theoretical concentration points of the linear curve was exported. The plots were generated using the graphics package ggplot2 (<https://ggplot2.tidyverse.org>).

Supplementary information

Supplementary information accompanies this paper at <https://doi.org/10.1186/s12014-020-09296-5>.

Additional file 1: Table S1. 133 proteins significantly changed ($\geq \pm 50\%$) between MS and Non-MS from CSF-PR. Quantified in minimum two studies, and changed in same direction in minimum two studies.

Additional file 2: Table S2. 287 proteins significantly changed between MS and Non-MS, but that were quantified in only one study in CSF-PR.

Additional file 3: Table S3. 120 proteins from Table S1 found in the DDA protein depth experiment.

Additional file 4: Table S4. All 1194 identified proteins from DDA protein depth experiment.

Additional file 5: Table S5. Data from the peptide stability experiment.

Additional file 6: Table S6. Data from the trypsin digestion experiment.

Additional file 7: Fig. S1. Digestion profile plot across all time points for all peptides.

Additional file 8: Fig. S2. Scatter plots comparing peptide amount (ratio L/H) at all time points tested in the digestion experiment.

Additional file 9: Table S7. Data from the PRM RRMS vs. OND experiment.

Additional file 10: Table S8. Full table of all tested peptides with essential results from each test and whether they passed or failed the tests.

Additional file 11: Table S9. Overview of the tests for stability, digestion and MS vs. OND experiments, for the 25 proteins. The colours and numbers refer to the peptides passing the specific test. Green: protein passed with two or more peptides; yellow: passed with one peptide; and, red: either no peptides passed (0) or none were tested (-).

Additional file 12: Fig. S3. Calibration curves for 17 assay peptides that passed all quality control tests.

Additional file 13: Fig. S4. Representative transition peaks from the Skyline analysis. **A** and **B** show typical examples of used transitions. The transition intensity, integration limits, retention time and mass error (ppm) is illustrated. **C** and **D** show examples of how 1-3 transitions were often much higher than the rest. Peak smoothing (Savitzky-Golay) was used in Skyline, which notably does not affect the quantification.

Abbreviations

ACN: Acetonitrile; AD: Alzheimer's disease; AGC: Automatic gain control; CDMS: Clinically definite multiple sclerosis; CH3L1: Chitinase-2-like protein 2; CIS-MS: Clinically isolated syndrome with conversion to multiple sclerosis; CSF: Cerebrospinal fluid; CSF-PR: CSF Proteome Resource; CV: Coefficient of variation; DDA: Data dependent acquisition; FDR: False discovery rate; HCD: Higher-energy collision induced dissociation; IS: Internal standard; IT: Injection time; LC: Liquid chromatography; LOQ: Limit of quantitation; MM: Mixed-mode reversed phase anion exchange; MS: Mass spectrometry; MS: Multiple sclerosis; OIND: Other inflammatory neurological diseases; OND: Other neurological diseases; PD: Parkinson's disease; PRM: Parallel reaction monitoring; RRMS: Relapsing–remitting multiple sclerosis; SRM: Selected reaction monitoring.

Acknowledgements

Not applicable.

Authors' contributions

FB, AG, HB and ACK designed the study. AG, ACK and FB performed literature investigations and the protein and peptide selection. HG, MJ, ACK and RRL performed the wet lab experiments. AG, RRL, MJ and HB made the figures and tables. AG, RRL, MJ, ACK, HG and FB analysed the results. AG, RRL, MJ, FB and HB wrote the paper. All authors read and approved the final manuscript.

Funding

A.G. and H.B. are supported by the Research Council of Norway (251235). H.B. and R.R.L. are supported by the Trond Mohn Foundation (BFS2016REK02). FB is supported by the Western Norway Regional Health Authority (912166).

Data availability

The mass spectrometry proteomics data from the DDA experiment have been deposited to the ProteomeXchange Consortium via the PRIDE [54] partner repository with the dataset identifier PXD013449 and <https://doi.org/10.6019/pxd013449>. All other mass spectrometry data are targeted PRM data, and Skyline documents and raw files are available through Panorama Public [55] at https://panoramaweb.org/PRM_Assay_CSF.url and at ProteomeXchange with dataset identifier PXD017281.

Availability of data and materials

The raw files and datasets supporting the conclusions of this article are available in the PRIDE repository (ID: PXD013449 and PXD017281) and in Panorama Public (https://panoramaweb.org/PRM_Assay_CSF.url).

Consent for publication

Not applicable.

Competing interests

The authors declare that they have no competing interests.

Author details

¹ Proteomics Unit, PROBE, Department of Biomedicine, University of Bergen, Bergen, Norway. ² Computational Biology Unit, CBU, Department of Informatics, University of Bergen, Bergen, Norway. ³ Biobank Haukeland, Haukeland University Hospital, Bergen, Norway.

Received: 5 July 2019 Accepted: 8 September 2020

Published online: 18 September 2020

References

- Paul A, Comabella M, Gandhi R. Biomarkers in multiple sclerosis. *Cold Spring Harb Perspect Med*. 2019;9(3):a029058.
- Kroksveen AC, Aasebø E, Vethe H, Van Pesch V, Franciotta D, Teunissen CE, et al. Discovery and initial verification of differentially abundant proteins between multiple sclerosis patients and controls using iTRAQ and SID-SRM. *J Proteomics*. 2013;78:312–25.
- Kroksveen AC, Jaffe JD, Aasebø E, Barsnes H, Bjørlykke Y, Franciotta D, et al. Quantitative proteomics suggests decrease in the secretogranin-1 cerebrospinal fluid levels during the disease course of multiple sclerosis. *Proteomics*. 2015;15(19):3361–9.
- Opsahl JA, Vaudel M, Guldbrandsen A, Aasebø E, Van Pesch V, Franciotta D, et al. Label free analysis of human cerebrospinal fluid addressing various normalization strategies and revealing protein groups affected by multiple sclerosis. *Proteomics*. 2016;16(7):1154–65.
- Kroksveen AC, Guldbrandsen A, Vaudel M, Lereim RR, Barsnes H, Myhr KM, et al. In-depth cerebrospinal fluid quantitative proteome and deglycoproteome analysis: presenting a comprehensive picture of pathways and processes affected by multiple sclerosis. *J Proteome Res*. 2017;16(1):179–94.
- Lange V, Picotti P, Dorn B, Aebersold R. Selected reaction monitoring for quantitative proteomics: a tutorial. *Mol Syst Biol*. 2008;4:222.
- Bourmaud A, Gallien S, Dorn B. Parallel reaction monitoring using quadrupole-orbitrap mass spectrometer: principle and applications. *Proteomics*. 2016;16(15–16):2146–59.
- Peterson AC, Russell JD, Bailey DJ, Westphall MS, Coon JJ. Parallel reaction monitoring for high resolution and high mass accuracy quantitative, targeted proteomics. *Mol Cell Proteomics*. 2012;11(11):1475–88.
- Bridel C, Eijlers AJC, van Wieringen WN, Koel-Simmellink M, Leurs CE, Schoonheim MM, et al. No pathologic proteomic signature at clinical disease onset associated with 11 year clinical, cognitive and MRI outcomes in relapsing-remitting multiple sclerosis patients. *Front Mol Neurosci*. 2018;11:371.
- Schilde LM, Kosters S, Steinbach S, Schork K, Eisenacher M, Galozzi S, et al. Protein variability in cerebrospinal fluid and its possible implications for neurological protein biomarker research. *PLoS ONE*. 2018;13(11):e0206478.
- Disanto G, Berlanga AJ, Handel AE, Para AE, Burrell AM, Fries A, et al. Heterogeneity in multiple sclerosis: scratching the surface of a complex disease. *Autoimmune Dis*. 2010;2011:932351.
- Hensiek AE, Sawcer SJ, Compston DA. Searching for needles in haystacks—the genetics of multiple sclerosis and other common neurological diseases. *Brain Res Bull*. 2003;61(3):229–34.
- Zhang J. Proteomics of human cerebrospinal fluid - the good, the bad, and the ugly. *Proteomics Clin Appl*. 2007;1(8):805–19.
- Guldbrandsen A, Farag Y, Kroksveen AC, Oveland E, Lereim RR, Opsahl JA, et al. CSF-PR 2.0: an interactive literature guide to quantitative cerebrospinal fluid mass spectrometry data from neurodegenerative disorders. *Mol Cell Proteomics*. 2017;16(2):300–9.
- Huhner AF, Biringier RG, Amato H, Fonteh AN, Harrington MG. Protein analysis in human cerebrospinal fluid: physiological aspects, current progress and future challenges. *Dis Markers*. 2006;22(1–2):3–26.
- Bauer M, Ahrne E, Baron AP, Glatzer T, Fava LL, Santamaria A, et al. Assessment of current mass spectrometric workflows for the quantification of low abundant proteins and phosphorylation sites. *Data Brief*. 2015;5:297–304.
- Apweiler R, Bairoch A, Wu CH, Barker WC, Boeckmann B, Ferro S, et al. UniProt: the universal protein knowledgebase. *Nucleic Acids Res*. 2004;32(Database issue):D115–9.
- Phillips HL, Williamson JC, van Elburg KA, Snijders AP, Wright PC, Dickman MJ. Shotgun proteome analysis utilising mixed mode (reversed phase-anion exchange chromatography) in conjunction with reversed phase liquid chromatography mass spectrometry analysis. *Proteomics*. 2010;10(16):2950–60.
- Chiva C, Sabido E. Peptide selection for targeted protein quantitation. *J Proteome Res*. 2017;16(3):1376–80.
- Pan S, Aebersold R, Chen R, Rush J, Goodlett DR, McIntosh MW, et al. Mass spectrometry based targeted protein quantification: methods and applications. *J Proteome Res*. 2009;8(2):787–97.
- Rauniyar N. Parallel reaction monitoring: a targeted experiment performed using high resolution and high mass accuracy mass spectrometry. *Int J Mol Sci*. 2015;16(12):28566–81.
- Borras E, Canto E, Choi M, Maria Villar L, Alvarez-Cermeno JC, Chiva C, et al. Protein-based classifier to predict conversion from clinically isolated syndrome to multiple sclerosis. *Mol Cell Proteomics*. 2016;15(1):318–28.
- Coffman FD. Chitinase 3-Like-1 (CH3L1): a putative disease marker at the interface of proteomics and glycomics. *Crit Rev Clin Lab Sci*. 2008;45(6):531–62.
- Comabella M, Fernández M, Martin R, Rivera-Vallvé S, Borrás E, Chiva C, et al. Cerebrospinal fluid chitinase 3-like 1 levels are associated with conversion to multiple sclerosis. *Brain*. 2010;133(Pt 4):1082–93.
- Hinsinger G, Galeotti N, Nabholz N, Urbach S, Rigau V, Demattei C, et al. Chitinase 3-like proteins as diagnostic and prognostic biomarkers of multiple sclerosis. *Mult Scler*. 2015;21(10):1251–61.
- Johansen JS, Jensen BV, Roslind A, Nielsen D, Price PA. Serum YKL-40, a new prognostic biomarker in cancer patients? *Cancer Epidemiol Biomarkers Prev*. 2006;15(2):194–202.
- Modvig S, Degn M, Roed H, Sorensen TL, Larsson HB, Langkilde AR, et al. Cerebrospinal fluid levels of chitinase 3-like 1 and neurofilament light chain predict multiple sclerosis disease development and disability after optic neuritis. *Mult Scler*. 2015;21(14):1761–70.
- Stoop MP, Singh V, Stingl C, Martin R, Khademi M, Olsson T, et al. Effects of natalizumab treatment on the cerebrospinal fluid proteome of multiple sclerosis patients. *J Proteome Res*. 2013;12(3):1101–7.
- MacLean B, Tomazela DM, Shulman N, Chambers M, Finney GL, Frewen B, et al. Skyline: an open source document editor for creating and analyzing targeted proteomics experiments. *Bioinformatics*. 2010;26(7):966–8.
- Begcevic I, Brinc D, Dukic L, Simundic AM, Zavoreo I, Basic Kes V, et al. Targeted mass spectrometry-based assays for relative quantification of 30 brain-related proteins and their clinical applications. *J Proteome Res*. 2018;17(7):2282–92.
- Brinkmalm G, Sjodin S, Simonsen AH, Hasselbalch SG, Zetterberg H, Brinkmalm A, et al. A parallel reaction monitoring mass spectrometric method for analysis of potential CSF biomarkers for Alzheimer's Disease. *Proteomics Clin Appl*. 2018;12(11):1700131.
- Koutroukides TA, Guest PC, Leveke FM, Bailey DM, Rahmoune H, Bahn S, et al. Characterization of the human serum depleteome by label-free shotgun proteomics. *J Sep Sci*. 2011;34(13):1621–6.
- Guldbrandsen A, Vethe H, Farag Y, Oveland E, Garberg H, Berle M, et al. In-depth characterization of the cerebrospinal fluid (CSF) proteome displayed through the CSF proteome resource (CSF-PR). *Mol Cell Proteomics*. 2014;13(11):3152–63.
- Ramström M, Hagman C, Mitchell JK, Derrick PJ, Håkansson P, Bergquist J. Depletion of high-abundant proteins in body fluids prior to liquid chromatography fourier transform ion cyclotron resonance mass spectrometry. *J Proteome Res*. 2005;4(2):410–6.
- Houston DR, Recklies AD, Krupa JC, van Aalten DM. Structure and ligand-induced conformational change of the 39-kDa glycoprotein from human articular chondrocytes. *J Biol Chem*. 2003;278(32):30206–12.
- Bereman MS, Beri J, Enders JR, Nash T. Machine learning reveals protein signatures in CSF and plasma fluids of clinical value for ALS. *Sci Rep*. 2018;8(1):16334.
- Wildsmith KR, Schauer SP, Smith AM, Arnott D, Zhu Y, Haznedar J, et al. Identification of longitudinally dynamic biomarkers in Alzheimer's disease cerebrospinal fluid by targeted proteomics. *Mol Neurodegener*. 2014;9:22.
- Kester MI, Teunissen CE, Sutphen C, Herries EM, Ladenson JH, Xiong C, et al. Cerebrospinal fluid VILIP-1 and YKL-40, candidate biomarkers to diagnose, predict and monitor Alzheimer's disease in a memory clinic cohort. *Alzheimers Res Ther*. 2015;7(1):59.

39. Llorens F, Thune K, Tahir W, Kanata E, Diaz-Lucena D, Xanthopoulos K, et al. YKL-40 in the brain and cerebrospinal fluid of neurodegenerative dementias. *Mol Neurodegener*. 2017;12(1):83.
40. Mani DR, Abbatiello SE, Carr SA. Statistical characterization of multiple-reaction monitoring mass spectrometry (MRM-MS) assays for quantitative proteomics. *BMC Bioinform*. 2012;13(Suppl 16):S9.
41. Barucker C, Sommer A, Beckmann G, Eravci M, Harmeier A, Schipke CG, et al. Alzheimer amyloid peptide abeta42 regulates gene expression of transcription and growth factors. *J Alzheimers Dis*. 2015;44(2):613–24.
42. Spellman DS, Wildsmith KR, Honigberg LA, Tuefferd M, Baker D, Raghavan N, et al. Development and evaluation of a multiplexed mass spectrometry based assay for measuring candidate peptide biomarkers in Alzheimer's Disease Neuroimaging Initiative (ADNI) CSF. *Proteomics Clin Appl*. 2015;9(7–8):715–31.
43. Ebers GC. Randomised double-blind placebo-controlled study of interferon beta-1a in relapsing/remitting multiple sclerosis. PRISMS (Prevention of Relapses and Disability by Interferon beta-1a Subcutaneously in Multiple Sclerosis) Study Group. *Lancet*. 1998;352(9139):1498–504.
44. Shi M, Movius J, Dator R, Aro P, Zhao Y, Pan C, et al. Cerebrospinal fluid peptides as potential Parkinson disease biomarkers: a staged pipeline for discovery and validation. *Mol Cell Proteomics*. 2015;14(3):544–55.
45. Teunissen CE, Petzold A, Bennett JL, Berven FS, Brundin L, Comabella M, et al. A consensus protocol for the standardization of cerebrospinal fluid collection and biobanking. *Neurology*. 2009;73(22):1914–22.
46. Kessner D, Chambers M, Burke R, Agus D, Mallick P. ProteoWizard: open source software for rapid proteomics tools development. *Bioinformatics*. 2008;24(21):2534–6.
47. Craig R, Beavis RC. TANDEM: matching proteins with tandem mass spectra. *Bioinformatics*. 2004;20(9):1466–7.
48. Tabb DL, Fernando CG, Chambers MC. MyriMatch: highly accurate tandem mass spectral peptide identification by multivariate hypergeometric analysis. *J Proteome Res*. 2007;6(2):654–61.
49. Dorfer V, Pichler P, Stranzl T, Stadlmann J, Taus T, Winkler S, et al. MS Amanda, a universal identification algorithm optimized for high accuracy tandem mass spectra. *J Proteome Res*. 2014;13(8):3679–84.
50. Barsnes H, Vaudel M. SearchGUI: a highly adaptable common interface for proteomics search and de Novo engines. *J Proteome Res*. 2018;17(7):2552–5.
51. Vaudel M, Burkhardt JM, Zahedi RP, Oveland E, Berven FS, Sickmann A, et al. PeptideShaker enables reanalysis of MS-derived proteomics data sets. *Nat Biotechnol*. 2015;33(1):22–4.
52. Elias JE, Gygi SP. Target-decoy search strategy for increased confidence in large-scale protein identifications by mass spectrometry. *Nat Methods*. 2007;4(3):207–14.
53. Guldbrandsen A, Barsnes H, Kroksveen AC, Berven FS, Vaudel M. A simple workflow for large scale shotgun glycoproteomics. *Methods Mol Biol*. 2016;1394:275–86.
54. Vizcaino JA, Csordas A, Del-Toro N, Dianas JA, Griss J, Lavidas I, et al. 2016 update of the PRIDE database and its related tools. *Nucleic Acids Res*. 2016;44(D1):D447–56.
55. Sharma V, Eckels J, Schilling B, Ludwig C, Jaffe JD, MacCoss MJ, et al. Panorama public: a public repository for quantitative data sets processed in skyline. *Mol Cell Proteomics*. 2018;17(6):1239–44.
56. Schutzer SE, Angel TE, Liu T, Schepmoes AA, Xie F, Bergquist J, et al. Gray matter is targeted in first-attack multiple sclerosis. *PLoS ONE*. 2013;8(9):e66117.
57. Kroksveen AC, Guldbrandsen A, Vedeler C, Myhr KM, Opsahl JA, Berven FS. Cerebrospinal fluid proteome comparison between multiple sclerosis patients and controls. *Acta Neurol Scand Suppl*. 2012;195:90–6.

Publisher's Note

Springer Nature remains neutral with regard to jurisdictional claims in published maps and institutional affiliations.

Ready to submit your research? Choose BMC and benefit from:

- fast, convenient online submission
- thorough peer review by experienced researchers in your field
- rapid publication on acceptance
- support for research data, including large and complex data types
- gold Open Access which fosters wider collaboration and increased citations
- maximum visibility for your research: over 100M website views per year

At BMC, research is always in progress.

Learn more biomedcentral.com/submissions



Supporting information for paper II

The supporting information for this paper is printed in the following. Files that are too large/not suited for the format of this thesis are in **bold** below. These files are available for download via the journal home-page:

<https://link-springer-com.pva.uib.no/article/10.1186/s12014-020-09296-5#Sec43>

Table S1: 133 proteins significantly changed ($\approx \pm 50\%$) between MS and Non-MS from CSF-PR. Quantified in minimum two studies, and changed in same direction in minimum two studies.

Table S2: 287 proteins significantly changed between MS and Non-MS, but that were quantified in only one study in CSF-PR.

Table S3: 120 proteins from Table S1 found in the DDA protein depth experiment.

Table S4: All 1194 identified proteins from DDA protein depth experiment.

Table S5: Data from the peptide stability experiment.

Table S6: Data from the trypsin digestion experiment.

Table S7: Data from the PRM RRMS vs. OND experiment.

Table S8: Full table of all tested peptides with essential results from each test and whether they passed or failed the tests.

Table S9: Overview of the tests for stability, digestion and MS vs. OND experiments, for the 25 proteins. The colours and numbers refer to the peptides passing the specific test. Green: protein passed with two or more peptides; yellow: passed with one peptide; and, red: either no peptides passed (0) or none were tested (-).

Figure S1: Digestion profile plot across all time points for all peptides. – *Modified to include title and to be printed on fewer pages*

Figure S2: Scatter plots comparing peptide amount (ratio L/H) at all times points tested in the digestion experiment.

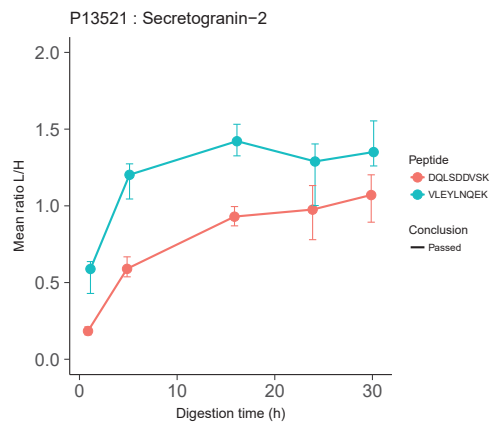
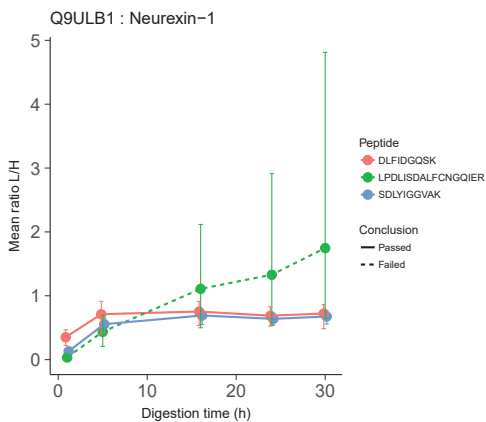
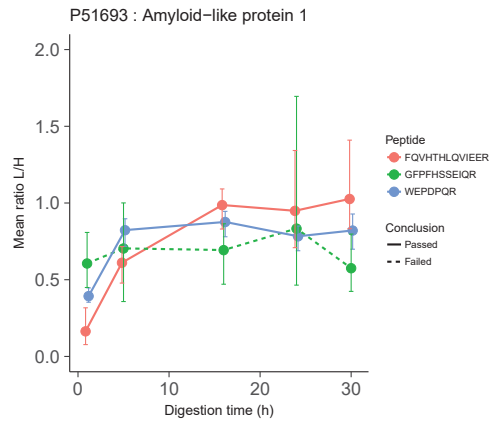
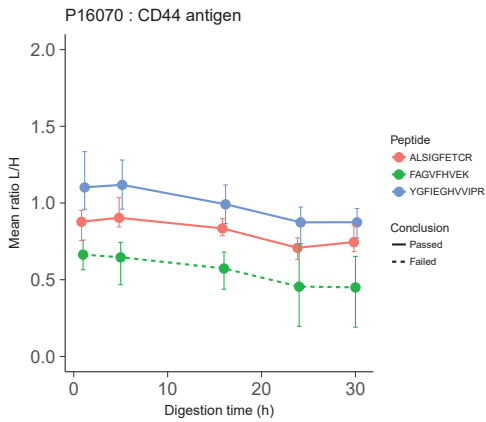
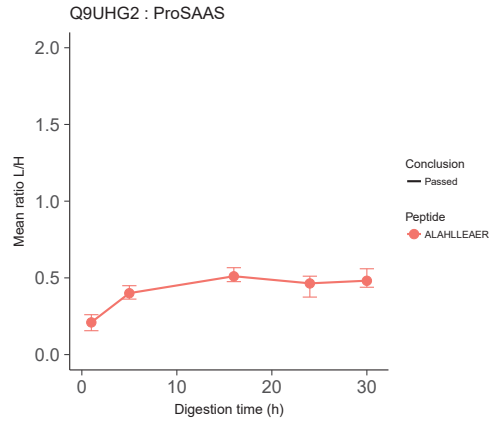
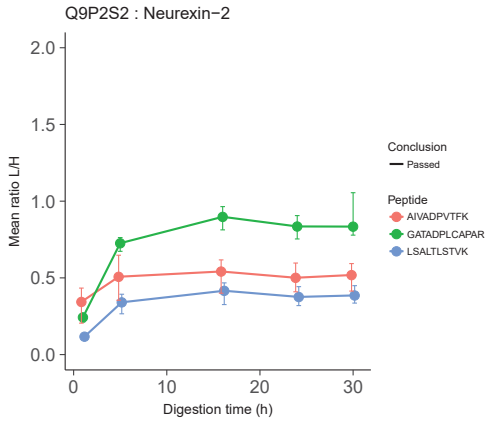
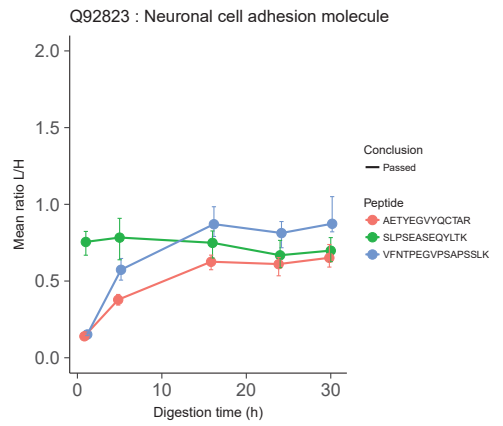
Figure S3: Calibration curves for 17 assay peptides that passed all quality control tests. – *Modified to include title and to be printed on fewer pages*

Figure S4: Representative transition peaks from the Skyline analysis. A and B show typical examples of used transitions. The transition intensity, integration limits, retention time and mass error (ppm) is illustrated. C and D show examples of how 1-3 transitions were often much higher than the rest. Peak smoothing (Savitzky-Golay) was used in Skyline, which notably does not affect the quantification.

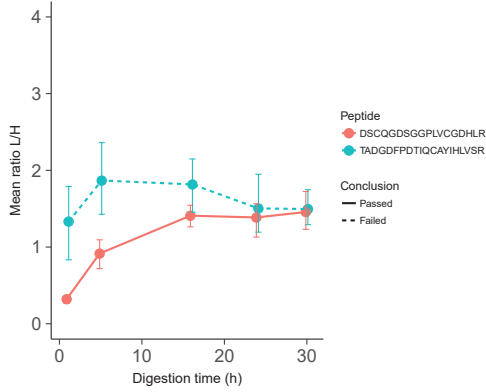
Accession	Protein Name	Stability	Digestion	MS vs. OND
P51693	Amyloid-like protein 1	3	2	2
P61769	Beta-2-microglobulin	2	1	1
P55290	Cadherin-13	3	2	2
P16070	CD44 antigen	3	2	1
P36222	Chitinase-3-like protein 1	0	-	-
Q15782	Chitinase-3-like protein 2	2	2	2
P10645	Chromogranin-A	3	3	3
P12111	Collagen alpha-3(VI) chain	3	3	1
P02747	Complement C1q subcomponent subunit C	3	2	0
P00736	Complement C1r subcomponent	4	1	0
P54764	Ephrin type-A receptor 4	3	2	2
Q6MZW2	Follistatin-related protein 4	3	3	3
P48058	Glutamate receptor 4	3	1	1
P01591	Immunoglobulin J chain	2	1	1
Q92876	Kallikrein-6	3	1	1
P32004	Neural cell adhesion molecule L1	3	2	2
Q9ULB1	Neurexin-1	3	2	2
Q9P2S2	Neurexin-2	3	3	3
Q92823	Neuronal cell adhesion molecule	3	3	3
Q99983	Osteomodulin	2	2	0
Q9UHG2	ProSAAS	1	1	1
P23468	Receptor-type tyrosine-protein phosphatase delta	3	2	2
O00584	Ribonuclease T2	2	1	1
P13521	Secretogranin-2	3	2	2
Q6UXD5	Seizure 6-like protein 2	2	1	1

Supplementary Table 9: Overview of the tests for stability, digestion and MS vs. OND experiments, for the 25 proteins. The colours and numbers refer to the peptides passing the specific test. Green: protein passed with two or more peptides; yellow: passed with one peptide; and, red: either no peptides passed (0) or none were tested (-).

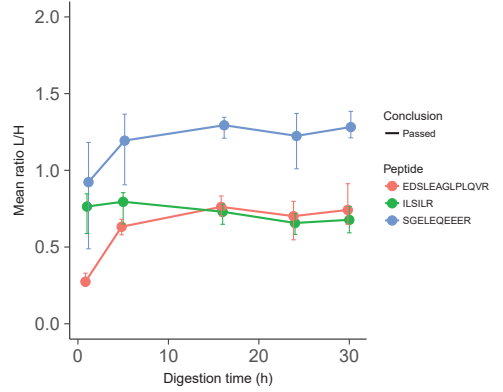
Figure S1:
Digestion profile plot
across all time points for all
peptides.



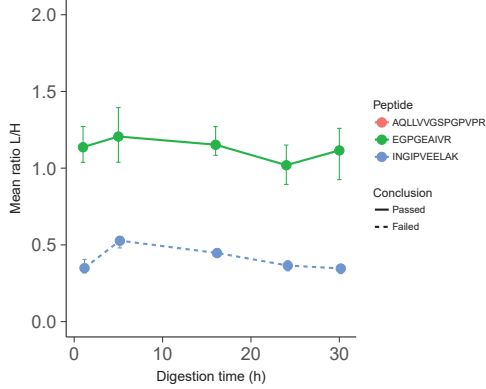
Q92876 : Kallikrein-6



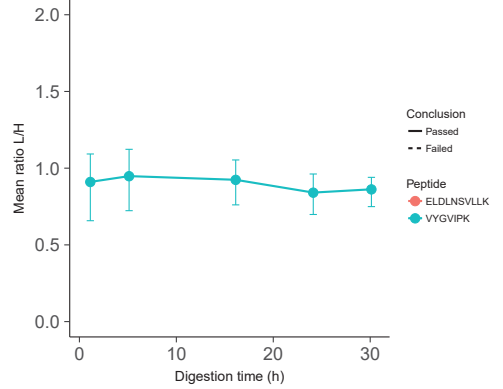
P10645 : Chromogranin-A



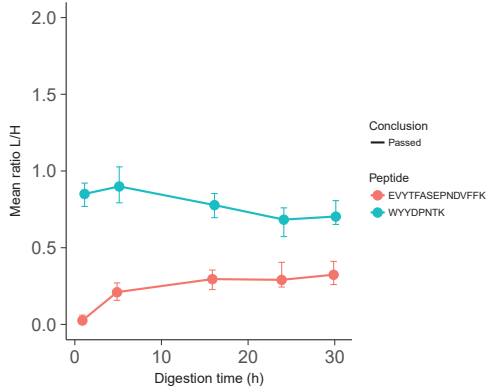
P32004 : Neural cell adhesion molecule L1



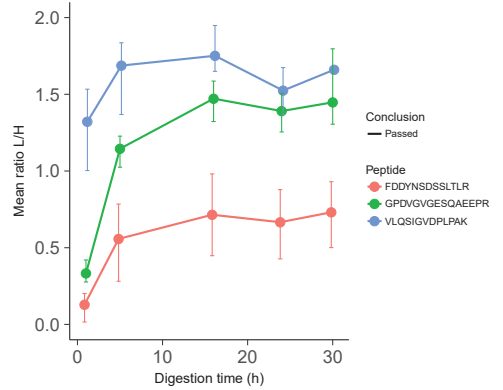
O00584 : Ribonuclease T2



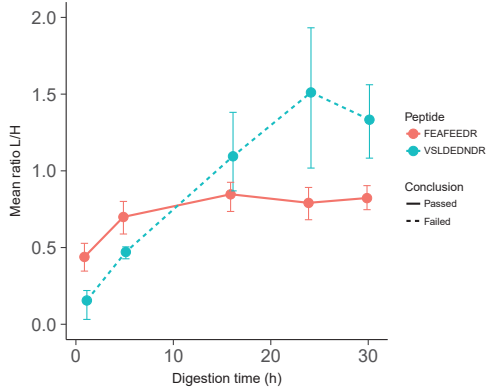
P12111 : Collagen alpha-3(VI) chain



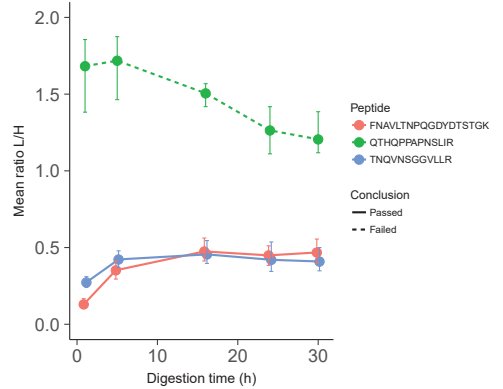
Q6MZW2 : Follistatin-related protein 4



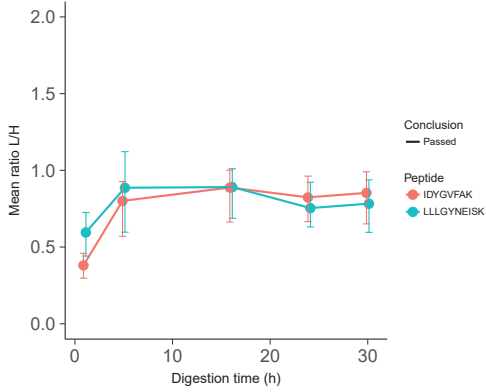
Q6UXD5 : Seizure 6-like protein 2



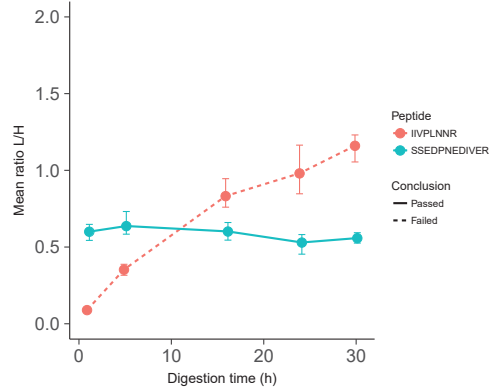
P02747 : Complement C1q subcomponent subunit C



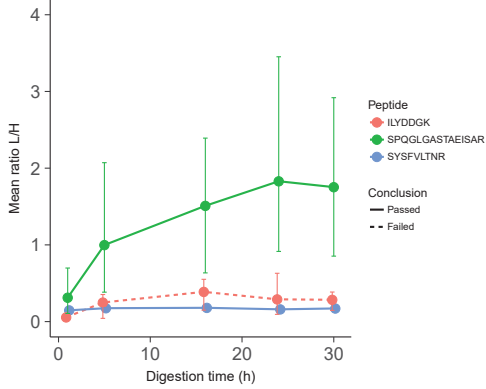
Q99983 : Osteomodulin



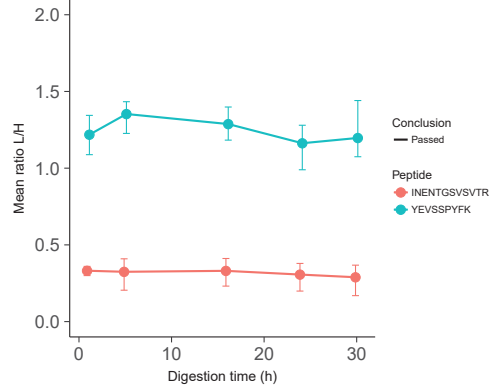
P01591 : Immunoglobulin J chain



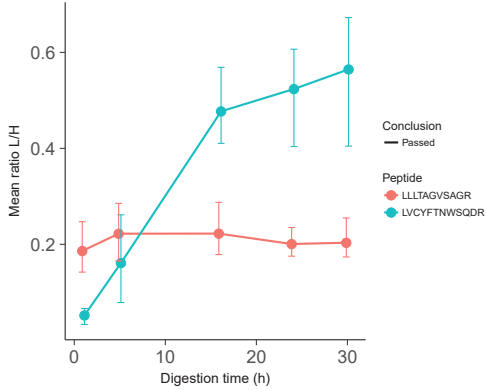
P23468 : Receptor-type tyrosine-protein phosphatase delta



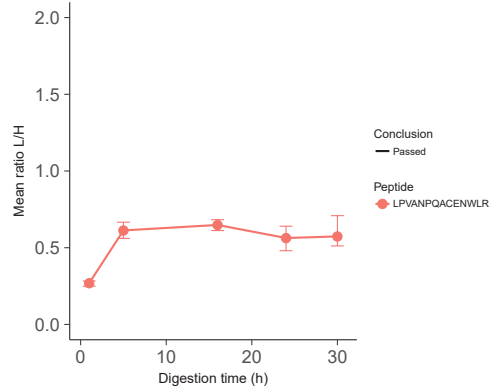
P55290 : Cadherin-13



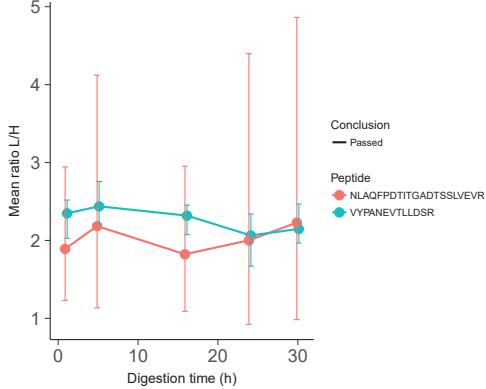
Q15782 : Chitinase-3-like protein 2



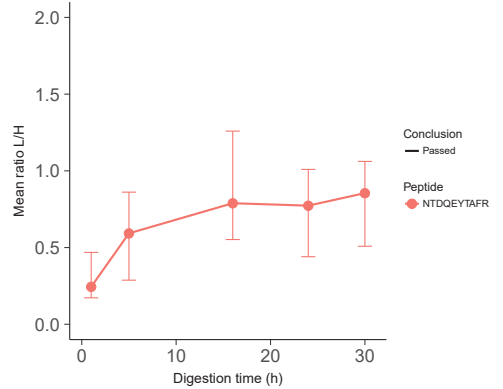
P00736 : Complement C1r subcomponent



P54764 : Ephrin type-A receptor 4



P48058 : Glutamate receptor 4



P61769 : Beta-2-microglobulin

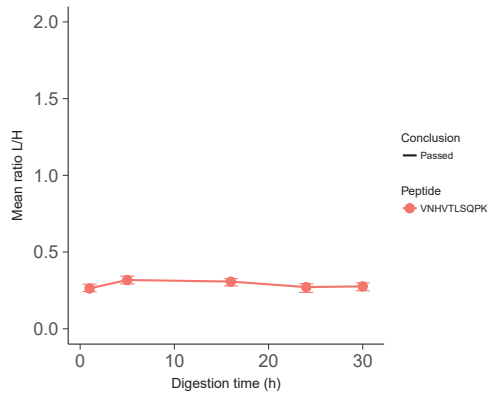


Figure S2. Scatter plots comparing peptide amount (ratio L/H) at all times points tested in the digestion experiment.

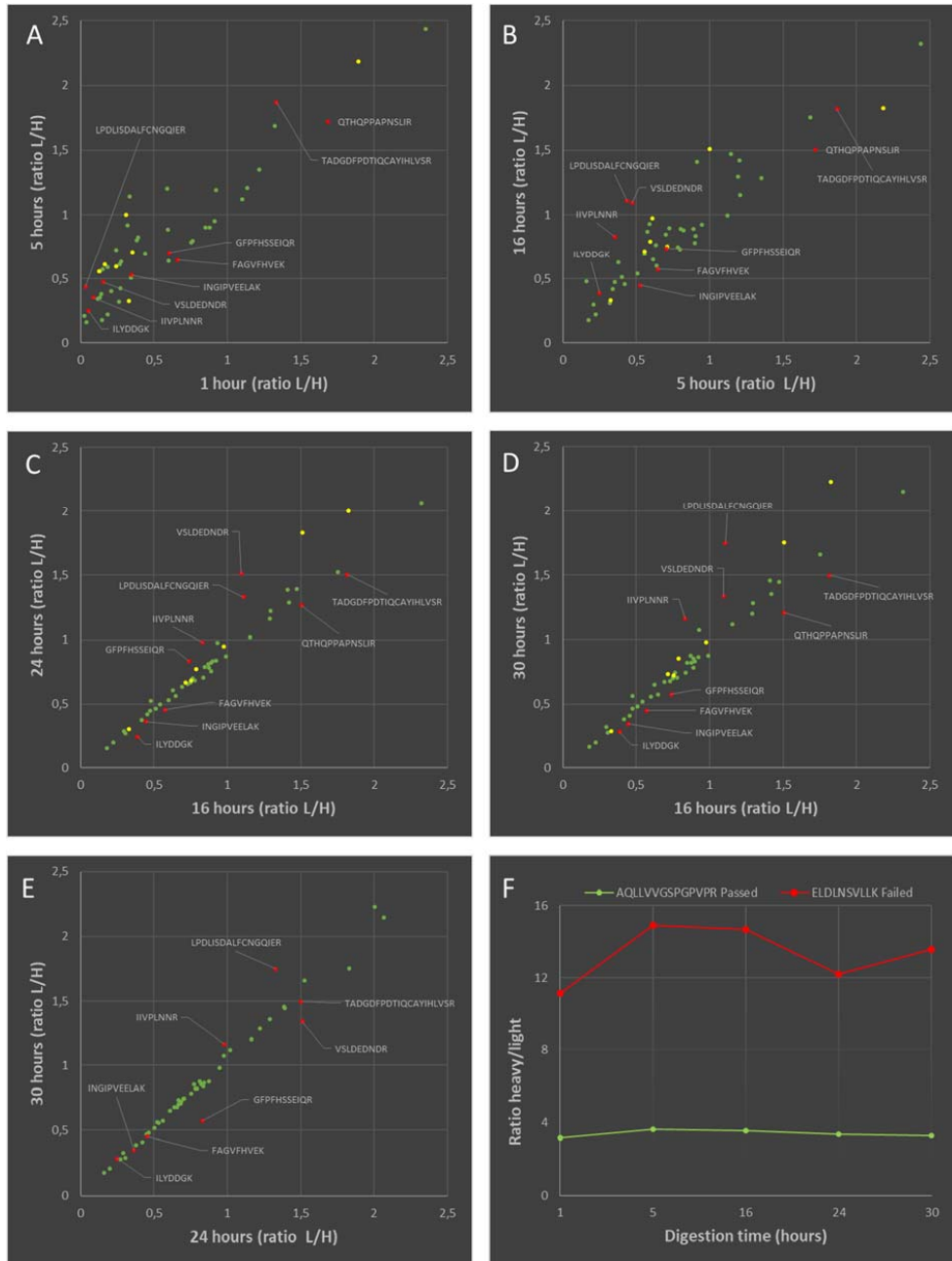
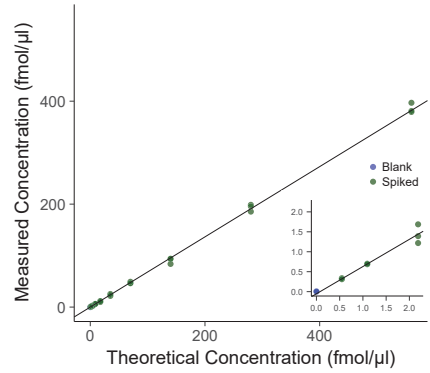


Figure S3:
Calibration curves for 17
assay peptides that passed all
quality control tests.

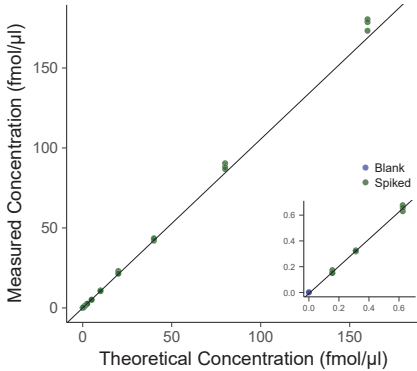
APLP1 : WEPDPQR

Adj R² = 0.9981 , y = 0.682 x -0.053



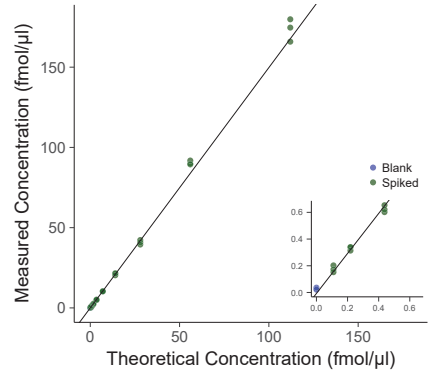
CAD13 : YEVSSPYFK

Adj R² = 0.9983 , y = 1.06 x -0.0082



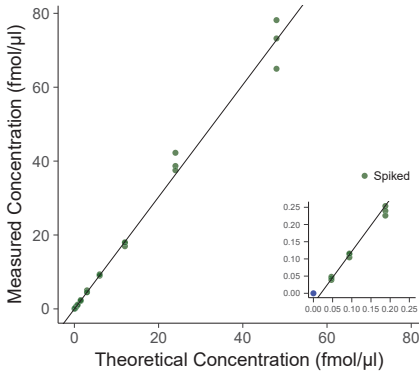
CD44 : ALSIGFETCR

Adj R² = 0.9982 , y = 1.5 x -0.0073



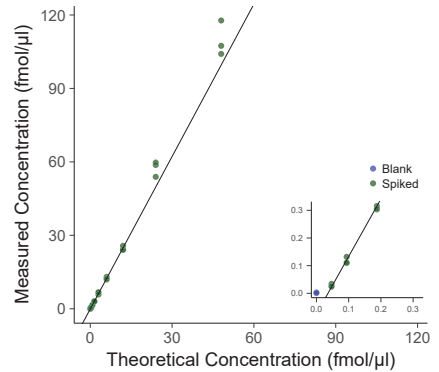
CH3L2 : LLLTAGVSAGR

Adj R² = 0.9974 , y = 1.52 x -0.03



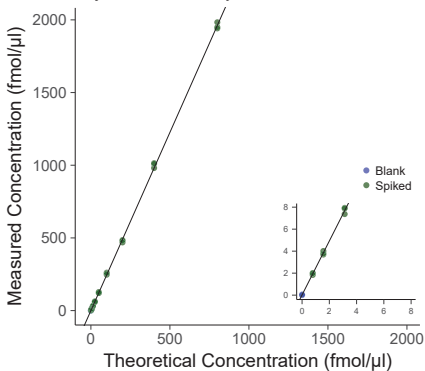
CH3L2 : LVCYFTNWSQDR

Adj R² = 0.9961 , y = 2.08 x -0.074



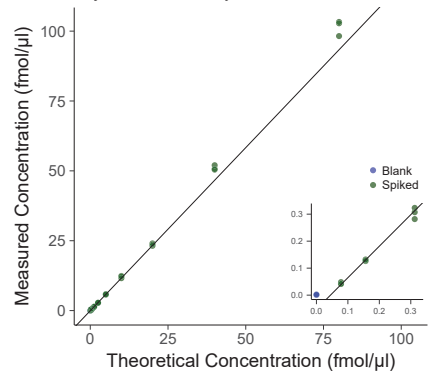
CMGA : SGELEQEEER

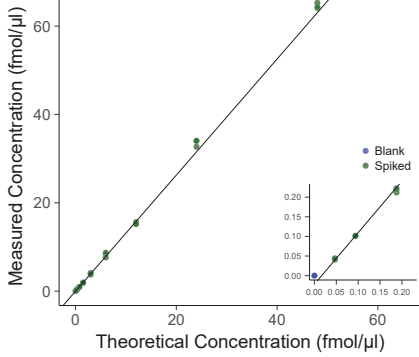
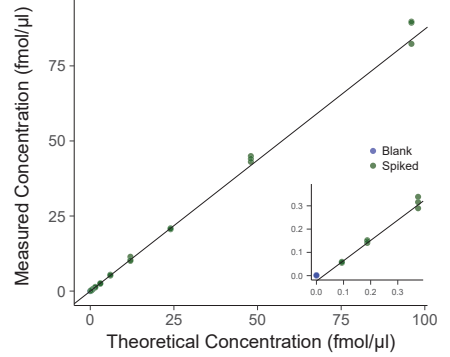
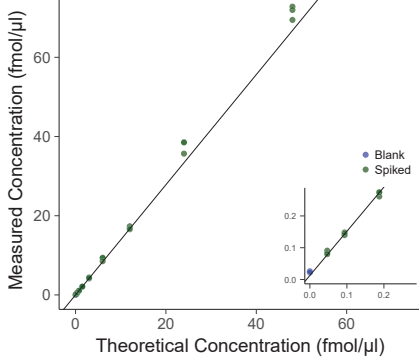
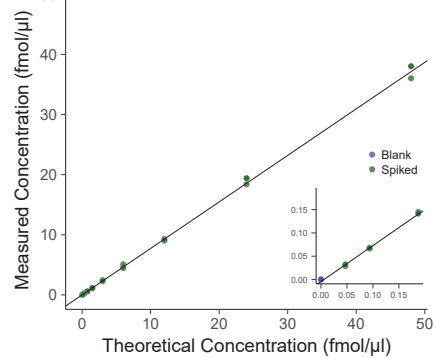
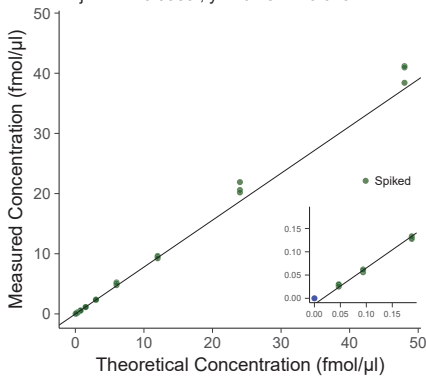
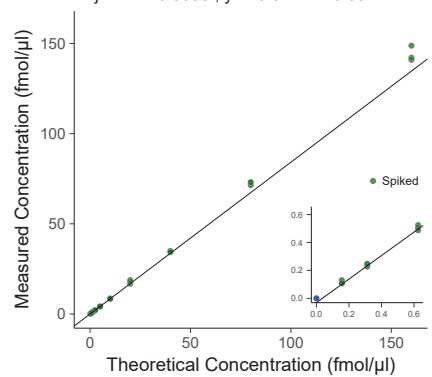
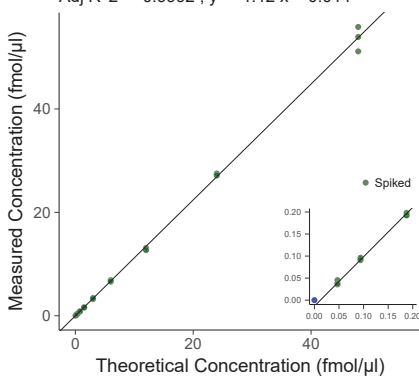
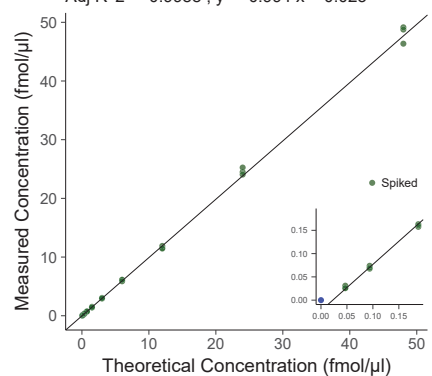
Adj R² = 0.9993 , y = 2.45 x + 0.021



EPHA4 : VYPANEVTLDSR

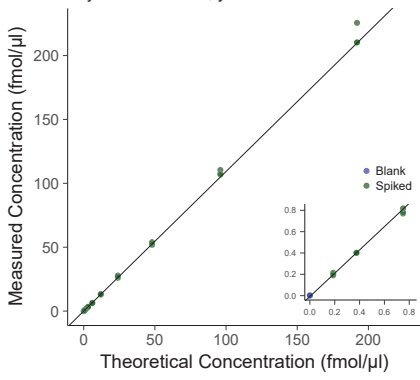
Adj R² = 0.9979 , y = 1.17 x -0.052



FSTL4 : VLQSIGVDPLPAKAdj R² = 0.9983 , y = 1.31 x -0.022**GRIA4 : NTDQEYTAFR**Adj R² = 0.9992 , y = 0.872 x -0.023**L1CAM : AQLLVGSPGPVPR**Adj R² = 0.9992 , y = 1.39 x + 0.013**NRX1A : SDLYIGGVAK**Adj R² = 0.9992 , y = 0.774 x -0.0046**NRX2A : LSALTSTVK**Adj R² = 0.9983 , y = 0.78 x -0.013**NRCAM : SLPSEASEQYLTK**Adj R² = 0.9995 , y = 0.842 x -0.031**PTPRD : SYSFVLTNR**Adj R² = 0.9992 , y = 1.12 x -0.014**SCG2 : DQLSDDVSK**Adj R² = 0.9988 , y = 0.994 x -0.023

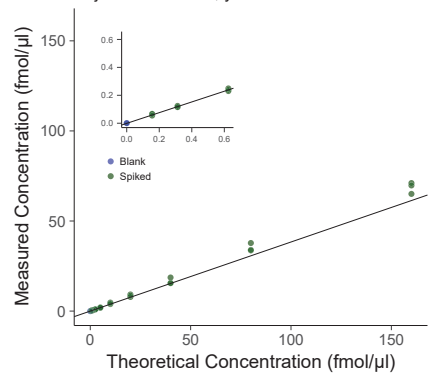
SCG2 : VLEYLNQEK

Adj R² = 0.9988 , y = 1.09 x -0.0084



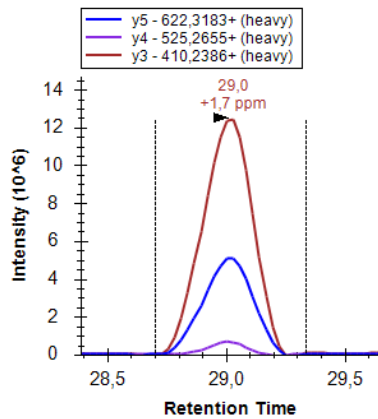
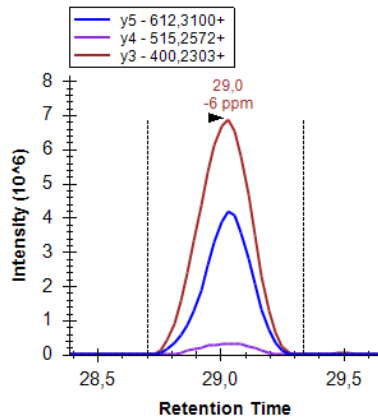
KLK6 : DSCQGDSGGPLVCGDHLR

Adj R² = 0.9981 , y = 0.383 x -0.00095

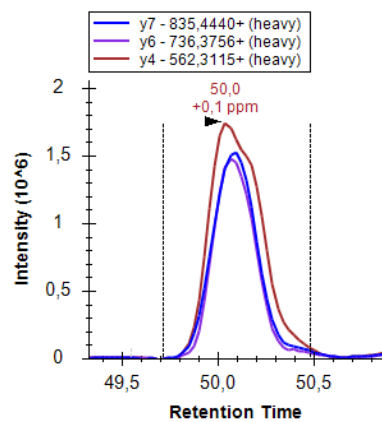
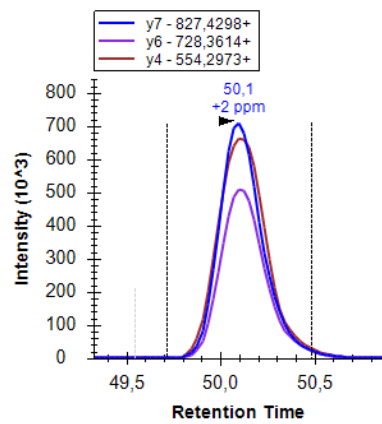


Supplementary Figure 4

A Amyloid-like protein 1
WEPDQQR

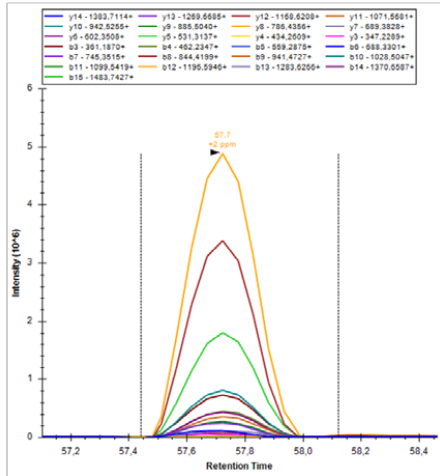


B Cadherin-13
YEVSSPYFK

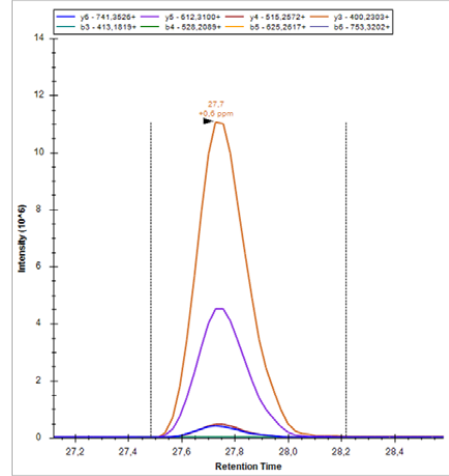


C

Neuronal cell adhesion molecule
VFNTPEGVPSAPSSLK

**D**

Amyloid-like protein 1
WEPDQR



Supplementary Figure 4: Representative transition peaks from the Skyline analysis. **A** and **B** show typical examples of used transitions. The transition intensity, integration limits, retention time and mass error (ppm) is illustrated. **C** and **D** show examples of how 1-3 transitions were often much higher than the rest. Peak smoothing (Savitzky-Golay) was used in Skyline, which notably does not affect the quantification.



Graphic design: Communication Division, UIB / Print: Skjipes Kommunikasjon AS



uib.no

ISBN: 9788230859995 (print)
9788230860694 (PDF)